UNIVERSITÀ
DEGLI STUDI
DI PADOVA

Sede Amministrativa: Università degli Studi di Padova

Dipartimento di Ingegneria Elettrica

SCUOLA DI DOTTORATO DI RICERCA IN : Ingegneria Industriale
INDIRIZZO: Energetica
CICLO XXII

Analyses and experimental tests for the development of the Quench Protection System for the superconducting magnets of the Satellite Tokamak JT-60SA

Direttore della Scuola : Ch.mo Prof. Paolo F. Bariani

Coordinatore d'indirizzo: Ch.mo Prof. Alberto Mirandola

Supervisori : Ch.mo Prof. Giorgio Rostagni
Dr. Ing. Elena Gaio

Dottorando : Luca Novello

Table of Contents

Abstract

The energy production by fusion in magnetically confined plasmas is an ambitious and important goal, which could contribute to solve the problem of a sustainable energy source for mankind. Present available technologies do not allow for the construction of a commercial thermonuclear fusion reactor, and important progresses are needed toward the realization of a demonstrative fusion reactor, named DEMO. In this direction the International Thermonuclear Experimental Reactor (ITER) project has been supported by the international community. However, in Japan and Europe it has been recognized that not all the necessary information for the development of DEMO can be gathered by ITER alone and that other complementary facilities would accelerate the development of magnetic fusion. Consequently, a Japanese-European Broader Approach Agreement has been signed, which includes the joint design, construction and exploitation of the Satellite Tokamak JT-60SA.

The JT-60SA maximum plasma current is foreseen to be 5.5 MA, with a flat top duration up to 100 s thanks to the additional heating provided by neutral beam injection and Electron Cyclotron Radio Frequency (ECRF). JT-60SA is characterized by the employment of superconducting toroidal and poloidal magnets, which require the installation of a protection system, able to rapidly remove the magnet current in case of loss of superconductive status (quench). Italian National Research Council (CNR) acting through Consorzio RFX is in charge of designing and providing the Quench Protection Circuits (QPC) for the superconducting magnets of JT-60SA.

The design of QPC requires the definition of the maximum current that under different conditions can flow in the superconducting magnets. The JT-60SA poloidal circuit is quite complex due to the mutual coupling among the superconducting magnets and the other active and passive conductors, and it is possible that in case of rapid variation of current in one of the circuits, overcurrent is induced in other mutual coupled circuits. Therefore, to derive the information needed for the QPC design, a complete model of the circuits has been set up, capable of taking into account all the mutually coupled elements. The model has been used to analyze plasma disruption

and QPC intervention in a large variety of conditions, to identify the possible magnet overcurrents.

After having defined the ratings of the QPC, it has been possible to develop a conceptual design for these devices, which core is represented by a dc Circuit Breaker able to commutate the current into a dump resistor. It is difficult to find a single device able to carry in steady state high values of dc current with reduced power losses and then to safely interrupt it with a reapplied voltage of some kilo-volts. Therefore, large emphasis is laid on the feasibility study of a hybrid mechanical-static dc Circuit Breaker, based on a mechanical By-Pass Switch connected in parallel to a static circuit breaker composed of Integrated Gate Commutated Thyristor (IGCT). The integration of mechanical and static devices allows combining the benefits of both employed technologies. The sizing of the static part of the circuit breaker has been carried out considering two different types of IGCTs; a comparison with the sizing obtained with the use of a fully static circuit breaker has been performed, proving the saving in terms of static devices' number and power dissipation allowed by the hybrid solution.

The proposed hybrid mechanical-static circuit breaker represents an innovative solution never employed for the interruption of high dc current values, thus it needs to be carefully investigated both in terms of feasibility and reliability. One of the main feasibility issues, regarding the possibility of turn-on of many paralleled IGCTs with low voltage applied, has been positively faced by means of experimental tests, proving the practicability of the proposed solution.

In order to gain experience on the current commutation from the mechanical BPS to the Static CB, and to assess its reliability, a prototype of the QPC Hybrid CB has been developed and tested at Consorzio RFX. More than one hundred current commutations and interruptions up to 7 kA have been successfully performed with the prototype, and the positive experimental results have proven the feasibility and the reliability of the hybrid mechanical-static solution proposed for the QPC circuit breaker of JT-60SA.

The thesis is organized as follows:

Chapter 1 - The international path for the research and development of a thermonuclear fusion reactor based on magnetic confined plasma is outlined, including ITER and DEMO devices. The reasons leading to the signature of the Broader Approach agreement are highlighted and the main characteristics of the Satellite Tokamak JT-60SA are described.

Chapter 2 - The chapter is focused on the analyses performed for the definition of the maximum current that the JT-60SA QPC shall be able to interrupt. A detailed description of the model of poloidal circuits developed and used for the simulation of plasma disruption and QPC intervention is given. The analyses performed in a large variety of different conditions are shown and the results commented.

Chapter 3 - The conceptual design of the QPC for the superconducting magnets of JT-60SA is described. Most of the chapter is focused on the QPC dc circuit breaker: the feasibility of the hybrid mechanical-static solution for the dc circuit breaker is deeply investigated, including the experimental results of turn-on of static devices with low voltage applied. The sizing of the number of static devices is also reported.

Preliminary considerations on the other QPC components (pyrobreaker and dump resistor) are included.

Chapter 4 - The hybrid dc circuit breaker prototype is described. The experimental results obtained performing more than one hundred current interruptions are illustrated and commented.

Chapter 5 – Conclusions and results are summarized in this chapter.

Prefazione

La produzione di energia per mezzo della fusione termonucleare in plasmi confinati magneticamente è un obiettivo ambizioso e importante, che potrebbe contribuire a risolvere il problema delle fonti energetiche per l'umanità. Le tecnologie attualmente disponibili non permettono ancora la realizzazione di un reattore a fusione commerciale, e notevoli progressi sono necessari per la costruzione di un reattore a fusione dimostrativo, denominato DEMO. In questa direzione il progetto del reattore sperimentale internazionale (ITER) è stato promosso e supportato dalla comunità internazionale. Tuttavia in Giappone e in Europa è stato riconosciuto che non tutte le informazioni necessarie per lo sviluppo di DEMO possono essere ottenute solamente da ITER, e che altre strutture complementari accelererebbero lo sviluppo della fusione. Conseguentemente è stato stipulato un accordo giapponese – europeo (Broader Approach Agreement) che include la progettazione, la costruzione e l'operazione congiunta del Tokamak Satellite JT-60SA.

La massima corrente di plasma di JT-60SA sarà di circa 5.5MA, con una durata di flat-top di circa 100s, grazie all'ignizione di potenza per mezzo di neutral beam e radio frequenza ciclotronica elettronica (ECRF). L'esperimento JT-60SA è caratterizzato dall'impiego di magneti superconduttori toroidali e poloidali, che richiedono l'installazione di un sistema di protezione atto a rimuovere rapidamente la corrente dai magneti in caso di perdita dello stato di superconduttività (quench). Il Consiglio Nazionale della Ricerca (CNR) italiano, per mezzo del Consorzio RFX, ha il compito di progettare e fornire i circuiti di protezione in caso di quench (QPC) per i magneti superconduttori di JT-60SA.

La progettazione delle QPC richiede la definizione della massima corrente che può circolare nei magneti superconduttori in diverse condizioni. Il circuito poloidale di JT-60SA è particolarmente complesso, anche a causa dei mutui accoppiamenti tra i magneti superconduttori e gli altri conduttori attivi e passivi, ed è possibile che, in caso di variazione rapida della corrente in uno dei circuiti, si manifestino sovracorrenti indotte negli altri circuiti mutuamente accoppiati.

Per ottenere le informazioni utili alla progettazione delle QPC, è stato necessario sviluppare un modello completo dei circuiti, in grado di tenere in considerazione tutti gli elementi mutuamente accoppiati. Il modello è stato utilizzato per analizzare la disruzione di plasma e l'intervento delle QPC in numerose e varie condizioni, per determinare le possibili sovracorrenti nei magneti.

Dopo aver definito le specifiche delle QPC, è stato possibile sviluppare un progetto concettuale di questi dispositivi, il cui elemento principale è rappresentato da un interruttore in corrente continua in grado di commutare la corrente in una resistenza di scarica.

Non è semplice individuare un singolo dispositivo in grado di portare un'elevata corrente dc in steady state con ridotte perdite di potenza e di essere poi affidabile nell'effettuare un'interruzione di corrente con tensione applicata di alcuni kilo-volts. Di conseguenza è dedicato ampio spazio allo studio di fattibilità di un interruttore dc ibrido meccanico-statico, basato sull'impiego di un interruttore meccanico di by-pass (BPS) collegato in parallelo a un interruttore statico composto da Integrated Gate Commutated Thyristor (IGCT). L'integrazione di dispositivi meccanici e statici permette di combinare i benefici di entrambe le tecnologie impiegate. Il dimensionamento della parte statica dell'interruttore è stato eseguito prendendo in considerazione due diversi tipi di IGCT; si è operato un confronto con il dimensionamento ottenuto nel caso di utilizzo di un interruttore completamente statico, dimostrando così il risparmio ottenuto con la soluzione ibrida in termini di numero di componenti statici e di dissipazione di potenza.

L'interruttore ibrido meccanico-statico proposto rappresenta una soluzione innovativa mai utilizzata per l'interruzione di elevate correnti continue, di conseguenza deve essere attentamente analizzato sia in termini di fattibilità che di affidabilità. Uno dei principali aspetti concernenti la fattibilità, ovvero la possibilità di accendere più IGCT collegati in parallelo con una bassa tensione applicata, è stato affrontato con successo per mezzo di test sperimentali che hanno dimostrato la praticabilità della soluzione proposta.

Per acquisire esperienza sulla commutazione di corrente tra il BPS meccanico e l'interruttore statico, e per valutarne l'affidabilità, si è sviluppato e testato un prototipo dell'interruttore ibrido per le QPC presso il Consorzio RFX. Con questo prototipo sono state eseguite con successo più di cento commutazioni e interruzioni di corrente fino al valore di 7 kA, e i positivi risultati sperimentali hanno dimostrato la fattibilità e l'affidabilità della soluzione ibrida meccanico-statica proposta per l'interruttore delle QPC di JT-60SA.

Il lavoro presentato in questa tesi è così organizzato:

Capitolo 1 – Viene riassunto il percorso internazionale per la ricerca e lo sviluppo di un reattore a fusione termonucleare basato su plasmi a confinamento magnetico, includendo gli esperimenti ITER e DEMO. Vengono illustrate le motivazioni che hanno portato alla sottoscrizione dell'accordo Broader Approach e sono descritte le caratteristiche principali del Tokamak Satellite JT-60SA.

Capitolo 2 – Il capitolo è incentrato sulle analisi effettuate per la definizione della massima corrente che le QPC di JT-60SA dovranno essere in grado di interrompere. Viene data una descrizione dettagliata del modello dei circuiti poloidali usati per la simulazione delle disruzioni di plasma e dell'intervento delle QPC. Vengono illustrate le analisi effettuate in numerose condizioni e sono commentati i risultati ottenuti.

Capitolo 3 – Viene descritto il progetto concettuale delle QPC per i magneti superconduttori di JT-60SA. Gran parte del capitolo è dedicato all'interruttore dc delle QPC: viene approfonditamente studiata la fattibilità di una soluzione ibrida meccanico-statica per l'interruttore dc, includendo i risultati sperimentali di accensione dei componenti statici con una bassa tensione applicata. Viene inoltre riportato il dimensionamento del numero di componenti statici. Sono infine incluse alcune considerazioni preliminari sugli altri componenti delle QPC (pyrobreaker e resistenza di scarica).

Capitolo 4 – Viene descritto il prototipo di interruttore dc ibrido realizzato e sono illustrati e commentati i risultati sperimentali ottenuti effettuando più di cento interruzioni di corrente.

Capitolo 5 – Sono qui riassunte le conclusioni e i risultati ottenuti del lavoro effettuato.

CHAPTER 1

1. The Broader Approach Agreement

1.1 Introduction

The world energy demand is increasing very rapidly. By the year 2050, it is expected that there will be nine billion people on earth, compared with the six billion now, and they will all need energy. People in developing countries will want to use as much energy as people in developed ones. For these reasons, it is expected that in 2050 the world energy demand will be at least twice what it is today. [1]. This increase of energy consumption requires the development of innovative systems for energy production.

Many energy sources alternative to fossil fuels – coal, oil and natural gas have been suggested and already implemented, including wind power, tidal power, geothermal power, combustion of wood and biomass, hydroelectric power and solar energy. These alternative or renewable energy sources are not too promising as long term energy options, certainly not for the energy requirements implied by projections of our level of consumption. Many of these alternative energy sources are restricted to particular geological or geographic sites (tidal, geothermal, hydroelectric) and/or tend to be least available when most needed (solar energy at night or in winter), and/or cannot be turned on and off at will to meet the power demand curve of an electric utility.

Among other possible energy resources, nuclear fusion is notable for its substantial advantages over other forms of energy generation in terms of safety, fuel availability and environmental protection. For reaching the conditions allowing the development of fusion reaction, two alternatives are under study: magnetic and inertial confinement.

The development of inertial fusion is strongly linked to military research, since it involves the use of high power lasers and it is partially covered by military secret, therefore European Union has always favored the other research line, based on plasma confinement obtained with magnetic fields.

Magnetic confinement fusion reactor is inherently safe and does not create high level radioactive waste, nor are global warming emissions a concern associated with the generation of fusion energy; moreover abundant supply of fuel and raw material required for nuclear fusion is available.

For these reasons worldwide effort in research and development has been continuing towards the practical utilization of fusion energy as a long-term ultimate energy source.

1.2 ITER

Seventy years ago some scientists understood the physics behind fusion, and proposed to reproduce, here on Earth, what was happening in the Universe, where Sun and stars transmute matter transforming Hydrogen nuclei into Helium atoms and releasing huge amounts of energy in the process. Following the first fusion experiments in the 1930s, fusion physics laboratories were established in nearly every industrialized nation. By the mid-1950s "fusion machines" were operating in the Soviet Union, the United Kingdom, the United States, France, Germany and Japan. Through these, scientists' understanding of the fusion process was gradually refined.

A major breakthrough occurred in 1968 in the Soviet Union. Researchers were able to achieve temperature levels and plasma confinement times - two of the main criteria to achieving fusion - that had never been attained before. The Soviet machine was a doughnut-shaped magnetic confinement device called Tokamak. From this time on, the tokamak was to become the dominant concept in fusion research, and tokamak devices multiplied across the globe. Producing fusion energy, it soon became clear, would require marshalling the creative forces, technological skills, and financial resources of the international community.

- The Joint European Torus (JET) [2] in Culham, U.K., in operation since 1983, was a significant step in this direction. JET is collectively used by the EURATOM (European Atomic Energy Community) Associations from more than 20 European countries. In 1991, the JET tokamak achieved the world's first controlled release of fusion power.
- The Tore Supra Tokamak [3] that is part of the Cadarache nuclear research centre holds the record for the longest plasma duration time of any tokamak: six minutes and 30 seconds.
- The Japanese JT-60 [4] achieved the highest value of fusion triple product - density, temperature, confinement time - of any device to date.

Achievements like these have led fusion science to an exciting threshold: the plasma energy breakeven point. Breakeven describes the moment when plasmas in a fusion device release at least as much energy as is required to produce them.

An important figure of merit toward fusion power plant is the so-called Q-value, defined as the ratio of fusion power output to the external power input to the plasma. The goal of a fusion power plant can be envisaged by a Q-value of around 30-50, steady state or very long-term operation. Unfortunately the present fusion community

has achieved Q-values around 1, in two of the world large Tokamaks (as previously mentioned).

The future devices are expected to highly improve the present performance, by achieving controlled ignition and extended burn of a deuterium and tritium plasma, with steady-state as an ultimate goal, thus demonstrating technologies essential to a commercial reactor in an integrated system, and performing an integrated test of the high heat flux and nuclear components required to utilize fusion power for practical purposes.

The next step foreseen to demonstrate the feasibility to obtain a Q value larger than 10 is the International Thermonuclear Experimental Reactor (ITER) project [5]. ITER is regarded as a suitable tokamak experimental reactor in the fusion research and development program in the world, which permits to deliver ten times the power it consumes. From 50 MW of input power, the ITER machine is designed to produce 500 MW of fusion power - the first of all fusion experiments to produce net energy.

But given the nature and magnitude of the challenge, national action alone was considered insufficient, and no nation could address this challenge on its own. Thus, twenty-three years ago, a group of industrial nations agreed on a project to develop a new, cleaner, sustainable source of energy. At the Geneva Superpower Summit in November 1985, following discussions with President Mitterand of France and Prime Minister Thatcher of the United Kingdom, General Secretary Gorbachev of the former Soviet Union proposed to President Reagan of the United States an international project aimed at developing fusion energy for peaceful purposes: the ITER project was born. The initial signatories were: the former Soviet Union, the USA, the European Union (via EURATOM) and Japan; then these countries were joined by the People's Republic of China and the Republic of Korea in 2003, and by India in 2005. Together, these seven nations represent over half of the world's population. In ITER, the world has now joined forces to establish one of the largest and most ambitious international science projects ever conducted. ITER, which means "the way" in Latin, will require unparalleled levels of international scientific collaboration. Key plant components, for example, will be provided to the ITER Organization through in-kind contributions from the seven Members. Each Member has set up a domestic agency, employing staff to manage procurements for its in-kind contributions. The ITER Members have agreed to share every aspect of the project: science, procurements, finance, staffing with the aim that in the long run each Member will have the know-how to produce its own fusion energy plant.

Selecting a location for ITER was a long process that was finally concluded in 2005. In Moscow, on June 28, high representatives of the ITER Members unanimously agreed on the site proposed by the European Union: ITER would be built at Cadarache, near Aix-en-Provence in Southern France.

The ITER Agreement was officially signed at the Elysée Palace in Paris on 21 November 2006 by Ministers from the seven ITER Members. In a ceremony hosted by French President Jacques Chirac and the President of the European Commission M. José Manuel Durao Barroso, this Agreement established a legal international entity to be responsible for construction, operation, and decommissioning of ITER.

On 24 October 2007, following the ratification by all Members, the ITER Agreement entered into force and officially established the ITER Organization.

The objectives of ITER are:

1. demonstration of high power amplification and extended burn of Deuterium and Tritium plasma;
2. demonstration of technologies essential to fusion power reactor, such as superconducting magnets, high-voltage heating systems, and high heat-flux components;
3. integrated testing of high heat-flux and nuclear components.

The main parameters of ITER are shown in Table 1.1.

The ITER Tokamak chamber, shown in Figure 1.1, will be twice as large as any previous tokamak, with a plasma volume of about 830 m^3.

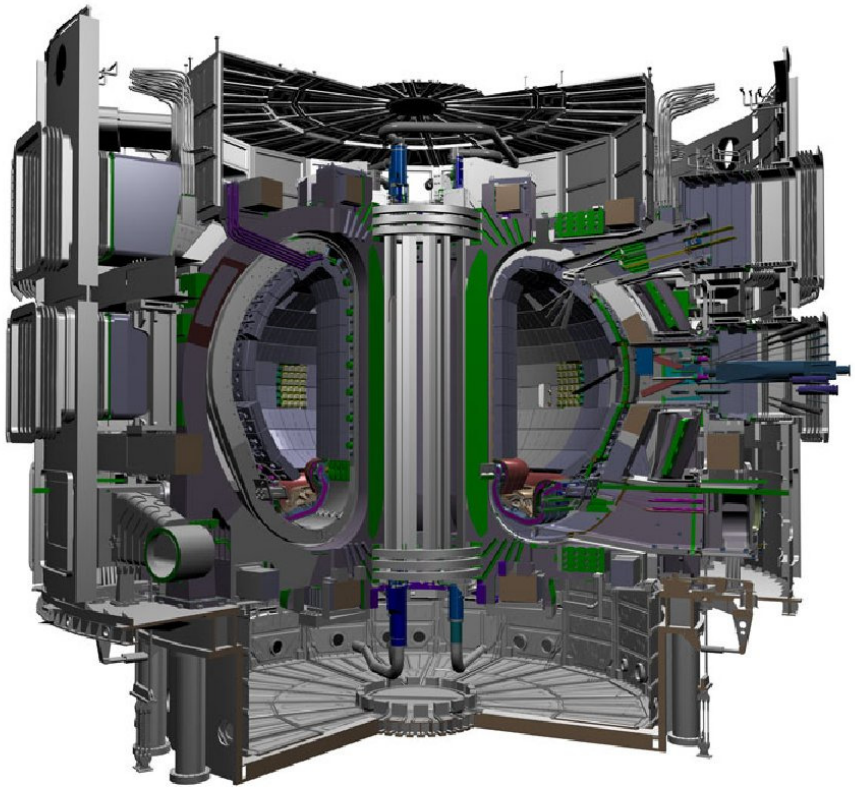

Figure 1.1 – *ITER cross section*

Table 1.1 – *ITER main parameters*

Total Fusion Power	500 MW
Power Amplification	10
Machine height	26 m
Machine diameter	29 m
Plasma Volume	837 m^3
Plasma major radius	6.2 m
Plasma minor radius	2 m
Plasma current	15 MA

1.3 DEMO

As the next step of ITER, it will be requested to have a concrete concept of the fusion power plant that can be constructed after the early results of ITER would be favorably obtained. The result of this conceptual study called as DEMO, although in a preliminary state, suggests that it is possible and useful to design development strategy of various technology issues in coherent and harmonized manner. The design will have to be evaluated and optimized for consistency, and to be continuously updated to reflect the new information from various fields of fusion technology. Also, depending on requirements for such power plant, there should be several variants for concept selection. For instance, construction year (early/late) or emphasis for fusion (economy/safety) will strongly affect the design and thus a point design may not be adequate.

Whereas ITER's main goal is to produce 500 MW of fusion power for at least 500 seconds, the goal of DEMO will be to produce at least four times that much fusion power on a continual basis. This level of power production (2 GW) is on the scale of a modern electric power plant.

At the same time, the DEMO reactor should also be so attractive and advanced that the future society and energy market would be interested in constructing a power plant based on its concept. Since the commercial plants are not experimental facilities, all technologies expected to be used in DEMO should be tested in advance.

Although to improve the economy will be a major objective, it does not mean that DEMO should achieve low Cost of Electricity (COE). It will be sufficient if it shows the positive evidence that low cost can be expected from the data that the DEMO will eventually provide [6].

A series of models of fusion power plants have been proposed and analyzed, in order to define the correct strategy and to assess the pertinence of the on-going activities. The European Power Plant Conceptual Study (PPCS) has been a study of conceptual designs for commercial fusion power plants [7]. It focused on five power

plant models, which are illustrative of a wider spectrum of possibilities [8] - [9], all based on the tokamak concept with approximately the same net electrical power output. These span a range from relatively near-term, based on limited technology and plasma physics extrapolations, to an advanced conception. All five PPCS plant models differ substantially from the models that formed the basis of earlier European studies; they also differ from one another, which lead to differences in economic performance and in the details of safety and environmental impacts. The main parameters of the five PPCS models are given in Table 1.2 from [7].

The PPCS study highlighted the need for specific design and R&D activities, in addition to those already underway within the European long term R&D programme, as well as the need to clarify the concept of DEMO. A detailed assessment of the PPCS models with limited extrapolations identified the physics issues that must be addressed to establish the DEMO physics basis.

But if there is a quasi-consensus today on a one-step fusion development strategy, there are discrepancies on the objectives of DEMO. It is often stated, without much justification, that DEMO should be very similar to a first Fusion Power Plant (FPP) and that it will differ mainly because of a lower availability. However, the first FPP will be funded, primarily, with private funds from a Utility and, to do so, the Utility will require enough evidence about the viability of the project. This means also that all components and processes to be implemented in the FPP have to be qualified. A component or process will be qualified after having operated in reactor relevant conditions for a duration comparable to its expected lifetime.

One of the main objectives of DEMO will be to qualify components and processes in reactor relevant conditions and at least 10 years of DEMO operations will be required to provide sufficient confidence to start construction of a FPP. Moreover, if the purpose of DEMO is to produce neutrons for testing, physics research will have only a secondary role: the DEMO physics basis must be worked out in ITER and any further plasma scenario optimization will have to be developed in parallel to DEMO (e.g. during ITER phase 2 operation or in satellite devices). A further major objective of DEMO will be to validate a reactor relevant maintenance scenario and the corresponding overall reactor architecture, which is today missing.

To qualify components and processed for the first FPP, DEMO will have to be flexible enough to allow the testing of different components, but the size of DEMO will be so large that the number of alternatives tested will have to be minimised. One

Table 1.2 – *Main PPCS plant model parameters*

Parameter	Model A	Model AB	Model B	Model C	Model D
Aspect ratio	3.0	3.0	3.0	3.0	3.0
Elongation (95% flux)	1.7	1.7	1.7	1.9	1.9
Triangularity (95% flux)	0.25	0.27	0.25	0.47	0.47
Major radius (m)	9.55	9.56	8.6	7.5	6.1
TF on axis (T)	7.0	6.7	6.9	6.0	5.6
Plasma current (MA)	30.5	30.0	28.0	20.1	14.1
β_N (total)	3.5	3.5	3.4	4.0	4.5
H_H (IPB98y2)	1.2	1.2	1.2	1.3	1.2
Bootstrap fraction	0.45	0.43	0.43	0.63	0.76
n/n_G	1.2	1.2	1.2	1.5	1.5
Q	20	16.5	13.5	30	35
Av. neutron wall load (MW m^{-2})	2.2	1.8	2.0	2.2	2.4
Av. heat load on FW (MW m^{-2})	0.6	0.5	0.5	0.45	0.5
Divertor peak load (MW m^{-2})	15	10	10	10	5
Z_{eff}	2.5	2.6	2.7	2.2	1.6

way to minimise this number is to perform tests, even if only partial in their scope, in separate, dedicated facilities.

Summing up all these concepts, it is not possible today to select a "preferred" DEMO concept since too many issues are still unresolved. At the technological level, the choice of a breeder blanket is still fully open. This choice depends on the performance of the various concepts being considered today, but not only. In particular, as it would be advantageous – if not necessary – to have a divertor cooled with the same fluid used to cool the blanket, the feasibility of a helium cooled divertor able to operate reliably is a major issue. At the engineering level, there is no satisfactory scheme for the replacement of the blanket. Finally, the design of all components and processes should integrate the requirement for high reliability in a more consistent way.

1.4 The Fast Track

During the Belgian presidency of the EU in the second half of 2001, Research Ministers requested an investigation into the feasibility of a "fast track" to fusion power generation. A group of independent experts, chaired by Professor David King, discussed this idea and reported their conclusions to the EU Council Presidency.

According to the experts, a fast track approach could demonstrate that electricity generation from fusion would be feasible within 20 to 30 years from the start of ITER construction. The "conventional" roadmap forecasts a timescale of about 50 years towards the commercial scale. The fast track would shorten this period by reducing from two to one the number of generations of experimental machines after ITER. Some of the technology tests planned for DEMO would be started in ITER, and the prototype power station step would include all the remaining technological developments as well as demonstrating electricity generation on a commercial scale. Initially this would require additional resources as more activities would progress in parallel, but the final goal could be substantially reduced.

The King Report [10] can be summarized as follows:

- ITER is the essential next step and should be constructed as soon as possible.
- Existing fusion devices should continue to contribute to the knowledge base as long as is feasible.
- Tests of breeding and high-grade energy extraction blanket modules for DEMO should be done in ITER.
- It is not necessary to foresee another experimental reactor after DEMO, but all experiments necessary to develop the commercial reactor technology should be performed in DEMO which should be a credible prototype for a power generating fusion reactor.
- A facility to test and verify materials exposed to fusion reactor irradiation conditions is required in parallel with ITER.

- Industry's role should be significantly enhanced during the realization of ITER.

1.5 The Broader Approach

According to the results of King Report, in Japan and Europe it has been recognized that not all the necessary information for the development of DEMO can be gathered by ITER alone and that other complementary facilities would accelerate the development of magnetic fusion.

In Tokyo, on 5 February 2007, the European Atomic Energy Community and the Government of Japan signed the "Broader Approach Agreement", a 10 year arrangement for cooperation in the field of controlled thermonuclear fusion.

The Broader Approach is aiming at the acceleration of the research and development towards the early realization of fusion power plant. In parallel with ITER collaboration Japan and Europe agreed to start the activity [11].

The Broader Approach Agreement includes the following three projects:

1. Engineering validation and engineering design activities for the International Fusion Materials Irradiation Facility (IFMIF/EVEDA);
2. International Fusion Energy Research Centre (IFERC);
3. Satellite Tokamak Programme (JT-60SA).

1.5.1 IFMIF/EVEDA

IFMIF is an intense 14 MeV neutron source to allow testing and qualification of materials in an environment similar to that of a future fusion plant, that is planned to be built in Rokkasho, Japan.

The IFMIF facility is characterized by its continuous operation at a high beam current. Each one of the two IFMIF accelerators has to produce 125 mA, 40 MeV Deuterium ion beam, steady state. This average beam current is more than two orders of magnitude higher than in the existing high energy accelerators, and requires well coordinated R&D to develop the accelerator technology and an efficient target technology.

The IFMIF/EVEDA project aims at producing a detailed, complete and fully integrated engineering design of IFMIF.

The project includes the following activities:

- the engineering design of the IFMIF facility, including safety assessment for a generic site and preparation of the technical specifications for the longest delivery components for the construction in future;
- the design and construction of the low energy section of one of the two IFMIF accelerators. Tests with full power beam will be conducted to demonstrate the feasibility and availability of the accelerator;

- the design, construction and tests of a scale 1:3 model of the Target Facility, including design and tests of its remote handling;
- the design, construction and tests of mock-ups of the Test Facility, including irradiation of the test set-up to relevant irradiation dose values to check performance under real operating conditions.

1.5.2 IFERC

In order to contribute to the ITER project and to promote a possible early realization of DEMO, the International Fusion Energy Research Centre (IFERC) is planned to perform the following three research and development tasks:

1. DEMO Design and R&D Coordination Centre;
2. Fusion Computer Simulation Centre;
3. Remote Experimentation Centre.

The DEMO Design and R&D Coordination Centre will play an important role in coordinating scientific and technological activities necessary to produce the DEMO power reactor design including design activities and technology R&D on key and long-term issues of common interest. The expected results will include the conceptual design of DEMO, in which the outcome from R&D activities is reflected.

The mission of the Fusion Computer Simulation Centre is to install and to operate a supercomputer for the simulation and modeling of ITER, of JT-60SA and other fusion experiments, and for the design of future fusion power plants as well as material research and research on possible improvement of power plant concepts, in particular for DEMO.

The Remote Experimentation Center (REC) will be developed as a remote facility for experimental campaigns preparation and data analysis for ITER. The REC could be able in future to monitor the ITER plant status, to prepare and transfer pulse parameter files to the ITER control system, presenting the main machine and plasma parameters in real time, and accessing promptly the experimental data for further analysis at REC. The REC will be tested on JT-60SA, and possibly on other tokamak prior to its application to ITER.

These three research and development tasks of IFERC are linked to each other. The Fusion Computational Simulation task, intimately linked to the ITER Remote Experimentation task, includes analysis and/or prediction of burning plasmas of ITER and of JT-60SA, and also supports design and tests of reactor technology systems.

1.5.3 JT-60SA

The JT-60U tokamak in Naka, Japan, will be upgraded to a superconducting tokamak JT-60SA [12], and will be exploited as a “satellite” facility to ITER.

The missions of the Satellite Tokamak are on large tokamak size plasmas:

- to support ITER by developing an improved understanding of physics issues, optimizing operation scenarios, testing possible future modifications and training scientists, engineers and technicians;
- to pursue an integrated exploration of steady-state, high beta DEMO relevant plasma scenarios with adequate power and particle control.

A picture of JT-60SA is shown in Figure 1.2.

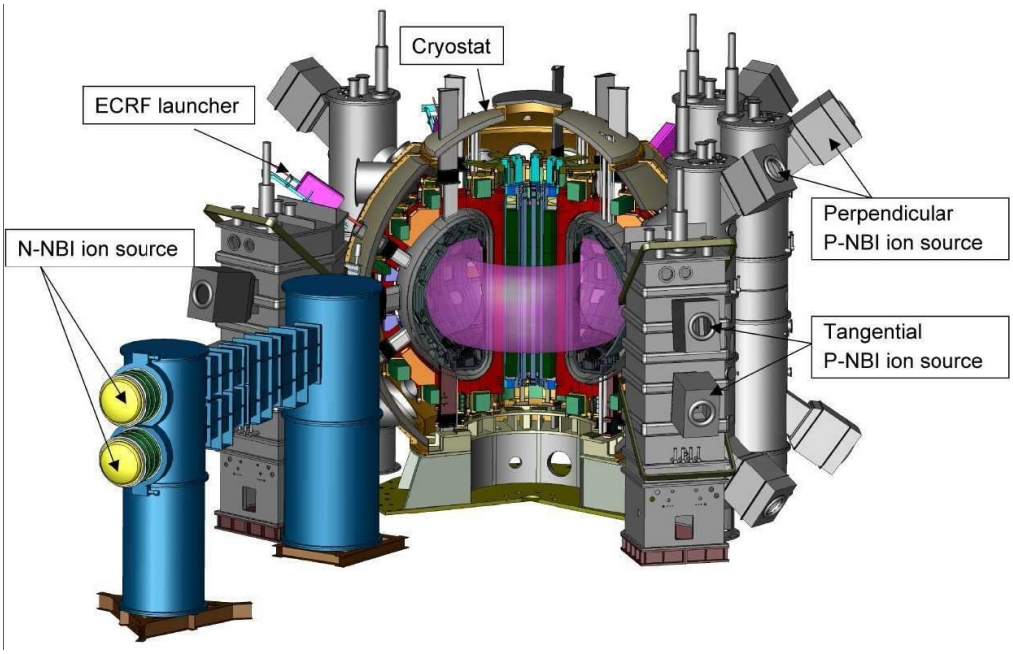

Figure 1.2 – *JT-60SA Tokamak*

Table 1.3 – *Basic parameters of JT-60SA*

Parameters	**Large Plasma (DN)**	**ITER Similar (SN)**
Plasma Current Ip (MA)	5.5	3.5
Toroidal Field Bt (T)	2.72	2.59
Major Radius (m)	3.01	3.16
Minor Radius (m)	1.14	1.02
Elongation, κ_{95}	1.83	1.7
Triangularity, δ_{95}	0.57	0.33
Aspect Ratio, A	2.64	3.10
Shape Parameter, S	6.7	4.0
Safety Factor, q_{95}	3.77	3.0
Flattop Duration	100 s	
Heating and CD power	41 MW × 100 s	
N-NBI power	34 MW	
ECRH power	7 MW	
PFC wall load	10 MW/m^2	
Neutron / year	4×10^{21}	

The typical parameters of JT-60SA are shown in Table 1.3. The maximum plasma current is foreseen to be 5.5 MA, with a relatively low aspect ratio plasma (R_p = 2.95m). Inductive operation with a flat top duration up to 100 s will be possible within the total available flux swing. The heating and current drive system will provide 34 MW of neutral beam injection and 7 MW of Electron Cyclotron Radio Frequency (ECRF). The divertor target is designed to be water-cooled in order to handle the expected heat fluxes for long time durations.

One of the JT-60SA main features is to be a superconducting tokamak, capable of confining break-even equivalent class high-temperature deuterium plasmas. The major tokamak components will be installed into the inner space of spherical cryostat with a diameter of about 14 m for the thermal shielding of superconducting magnets. In particular, all the superconducting magnets will be provided by protection circuits for avoiding major damages to the magnets in case of loss of the superconducting features.

The device flexibility will permit to explore the optimized configuration for ITER and DEMO, throughout operations in a wide range of plasma shapes (elongations and triangularities, shape factor $S=q_{95}Ip/(aBt)$) and aspect ratios (A=R/a down to 2.5), also including that of ITER. In particular, it is worth noting its capability to operate in both single and double null configurations.

A further JT-60SA target is the exploration of ITER relevant high density plasma regimes, which are above the H-mode power threshold with 40 MW high power heating. In particular, the study of power and particle handling at full power for 100 s with top and bottom water-cooled divertors compatible with maximum heat flux of 15 MW/m^2 will be performed.

Moreover, JT-60SA allows the exploration of full non-inductive steady-state operation with 10 MW / 500 keV tangential Neutral Beam Current Drive (NBCD) and 7 MW of Electron Cyclotron Current Drive (ECCD), as well as the exploitation of high beta regime with stabilizing shell covered with plates and internal Resistive Wall Mode (RWM) stabilizing coils and high power Heat & Current Drive system. JT-60SA is also designed to be eventually equipped with remote handling system to allow maintenance of in-vessel components.

The JT-60SA experimental time shall be 10 hours per day. Regeneration of cryo-panels for fuel pumping, wall conditioning by glow discharge cleaning, and cooling of cryo-panels shall be carried out overnight by an operation team for the cryogenic system operating on three shifts. The nominal repetition time is determined mainly by the duty cycle of 1/30 for NBI :100 s discharges with full NBI power shall be possible only every 3000 s due to the duty cycle capability of the injectors.

1.6 The Quench Protection Circuit of JT-60SA

The JT-60SA tokamak will be provided with 6 Equilibrium Field (EF), 4 Central Solenoid (CS) and 18 Toroidal Field (TF) superconducting coils.

NbTi superconducting conductor is planned to be used for the TF and EF coils, because their maximum field strength at the conductor surface are 6.4 T and 6.1 T respectively. For CS coils, instead, Nb_3Sn conductor is expected because the maximum field strength is in the range of 9-10 T to ensure the flux swing capability of about 40 Wb which is necessary to sustain the flat-top period of 100 s with the rated plasma current. [13].

In the case of superconducting coil quench or failure inside power supplies, fast extraction of the stored magnetic energy in the superconducting windings is necessary to avoid damage of machine and of power supplies components. For this purpose, a Quench Protection Circuit (QPC), object of this thesis, has to be provided for each superconducting coil. The core of the QPC is composed of a dc Circuit Breaker (CB) which remains closed in normal operation and, when activated, opens commutating the current into a discharge resistor. A back-up protection has to be provided in case of failure of the dc CB.

Under the framework of the Broader Approach Agreement, National Research Council (CNR) acting through Consorzio RFX will provide the QPCs of JT-60SA.

1.7 Thesis outline

This thesis focuses on the analyses performed to develop the conceptual design and to identify the key parameters of the QPC for JT-60SA.

Chapter 2 presents the analyses performed on the poloidal system of JT-60SA, in order to study the possible over-current in the poloidal magnet occurring in case of plasma disruption or QPC intervention.

After analyzing different technological solutions used for QPC in some other devices using superconductors, Chapter 3 describes the conceptual design worked out for the QPC of JT-60SA.

Chapter 4 describes the results obtained with the prototype of the hybrid mechanical-static circuit breaker included in the QPC conceptual design and developed at Consorzio RFX. Finally, the conclusions are reported in Chapter 5.

CHAPTER 2

2. Plasma Disruption and Quench in JT-60SA Poloidal Circuits

2.1 Introduction

The new satellite tokamak JT-60SA will be equipped with a number of magnets aimed at producing the magnetic fields for the generation and position control of the plasma current. Both superconducting and copper magnets will be installed. The toroidal circuit is composed of 18 superconducting magnets rated for 25.7 kA steady state current. The poloidal circuits are composed of 10 superconducting magnets, including 4 Central Solenoid (CS) and 6 Equilibrium Field (EF) coils, rated for 20 kA with a duty cycle of 100 s every 30 minutes and 2 copper Hybrid Control (HC) in-vessel coils rated for 5 kA. A sketch of the machine cross section is shown in Figure 2.1.

As shown in Figure 2.2, all the toroidal magnets are connected in series and are supplied by a single low voltage Power Supply (PS). Instead, the poloidal superconductors are inserted in ten separated circuits as shown in Figure 2.3 and Figure 2.4, each one independently fed by a dedicated power supply. Some of the poloidal circuits are also equipped with booster converter or switching network to aid plasma breakdown.

In case of loss of the coil superconducting status (quench) or in case of faults requiring a fast discharge of the magnets, the energy stored in the superconducting magnets has to be rapidly removed by means of Quench Protection Circuits (QPC). For this reason a QPC is connected in each circuit including a superconducting coil, and it is composed of a dc circuit breaker paralleled to a dump resistor, as showed in Figure 2.5. In normal operation the dc circuit breaker is closed and the coil current flows through it; in case of quench or in case of other severe circuit faults the dc circuit breaker is opened and the dump resistor is inserted in the coil circuit, permitting the rapid current discharge. An explosive activated fuse (pyrobreaker) is inserted in series to the circuit breaker and is operated as a backup protection in case of dc circuit breaker failure.

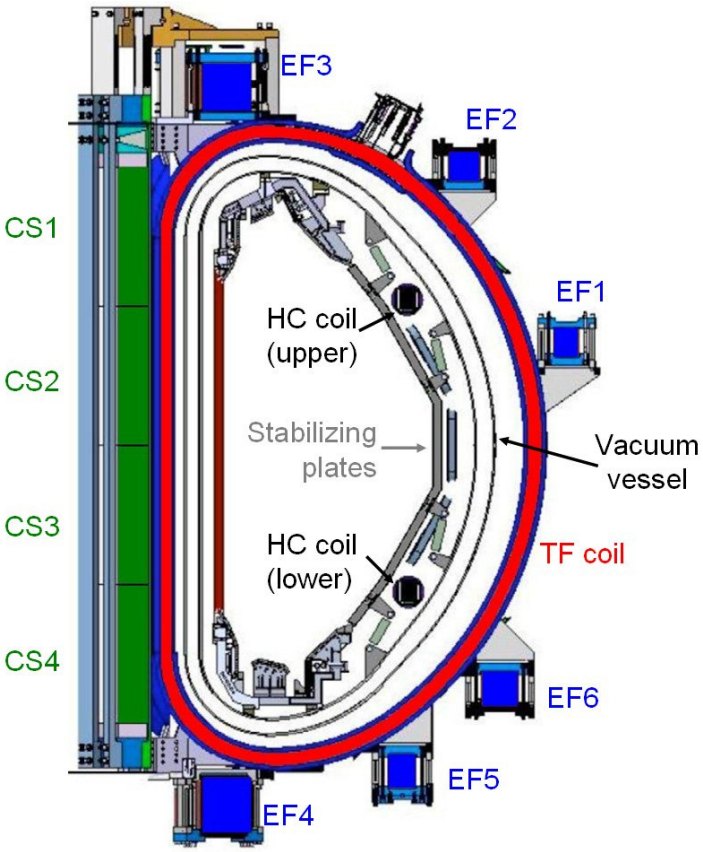

Figure 2.1 – *Poloidal cross section of JT-60SA*

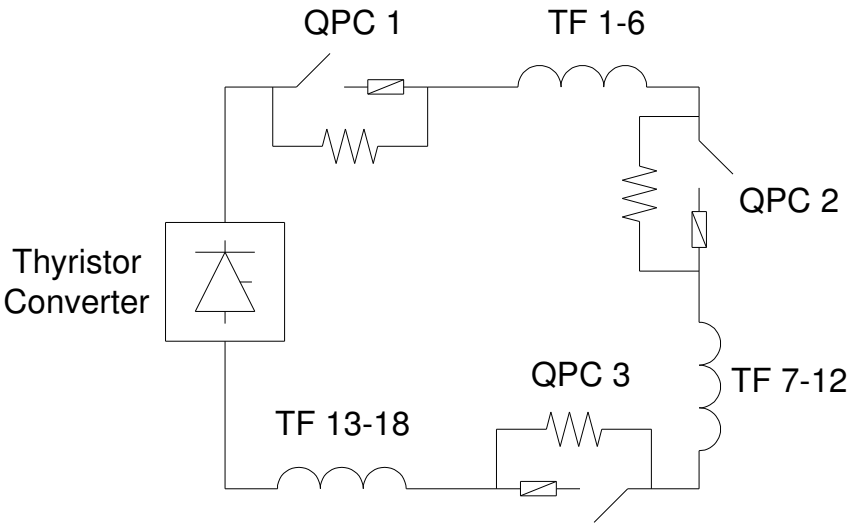

Figure 2.2 – *Toroidal Circuit*

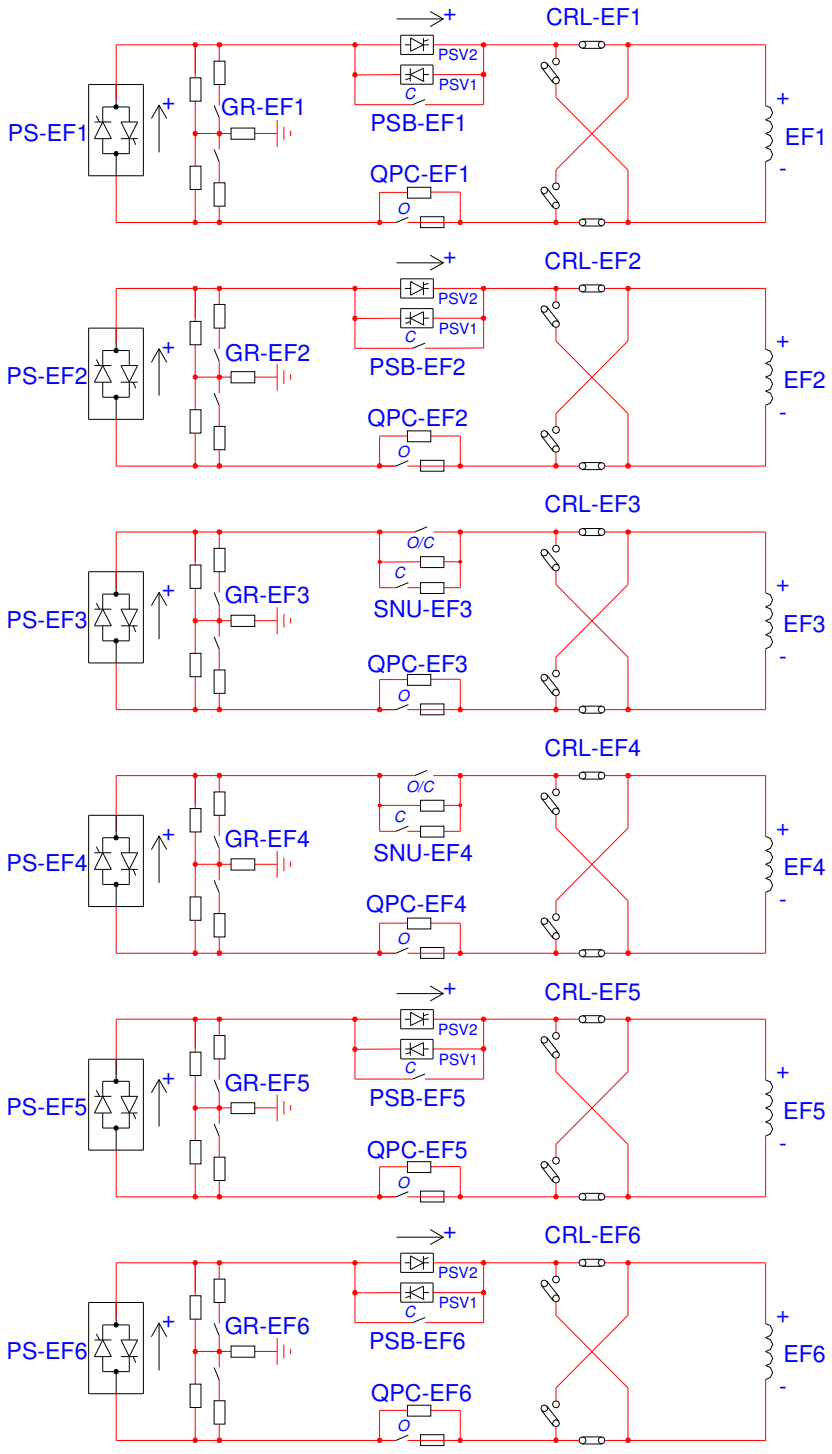

Figure 2.3 – *EF Circuits*

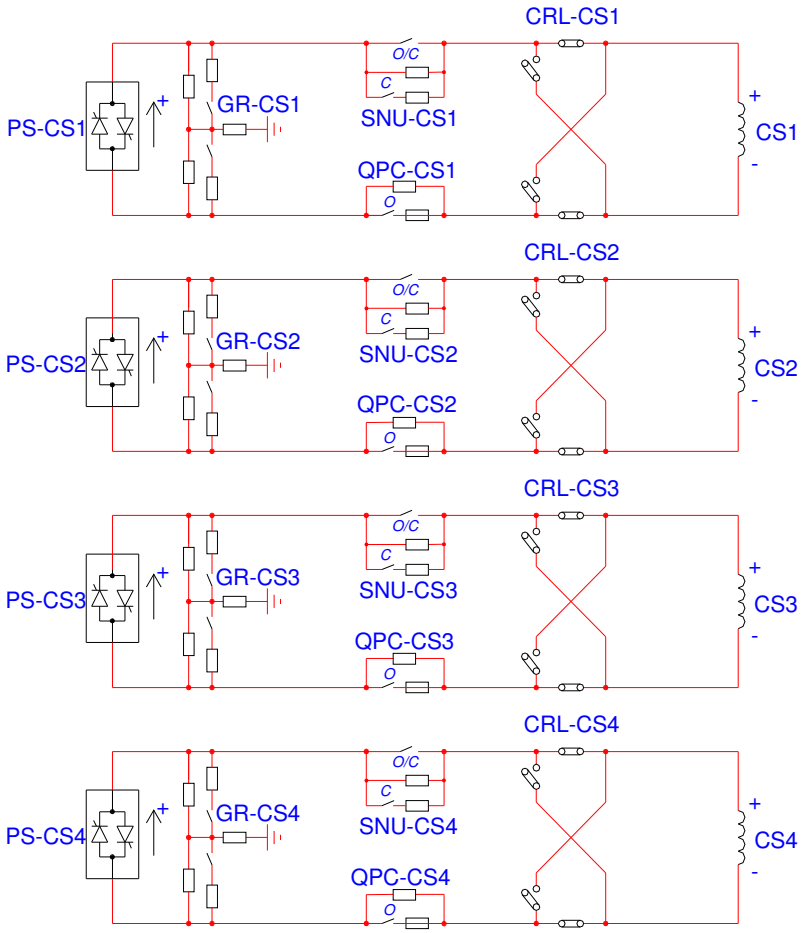

Figure 2.4 – *CS Circuits*

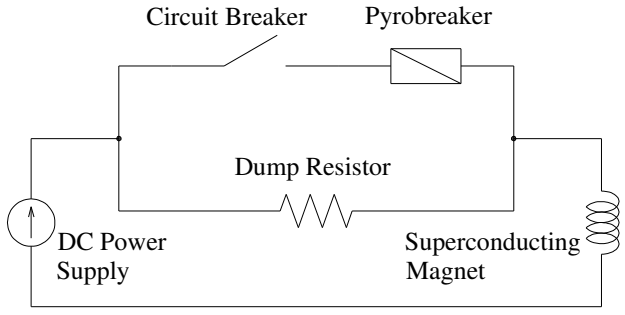

Figure 2.5 - *Conceptual scheme of the Quench Protection Circuit*

Table 2.1 – *QPC characteristics as resulting from superconductor requirements*

Characteristic	Toroidal QPC	Poloidal QPC
Unit number	3	10
Nominal voltage	2.8 [kV]	< 5 [kV]
Nominal current	25.7 [kA]	20 [kA]
Current polarity	Unidirectional	Bidirectional
Duty cycle	Steady state	100 s / 30 min
Maximum allowed I^2t	5.3 [GA^2s]	2 [GA^2s]
Maximum delay from command	1 [s]	1 [s]
Maximum delay for pyrobreaker operation	1 [s]	1 [s]
Maximum time to restart after intervention	60 [minutes]	30 [minutes]

The characteristics of the QPCs as resulting from the superconducting magnets requirements are shown in Table 2.1. However, the actual rating of the QPCs depends on the maximum current that under different situations can flow in the coils. In the toroidal circuit no significant over-current is expected, even in case of the faults analyzed in this work, because all toroidal coils are connected in series and they have no significant magnetic coupling with other conductors.

On the contrary the poloidal circuit is quite complex, due to the mutual coupling among the 10 poloidal superconducting magnets, the two Hybrid Control (HC) in-vessel coils, the vacuum vessel, the stabilizing plates and the plasma. In case of rapid variation of current in one of the circuits, overcurrent is induced in other mutual coupled circuits. Thus, the maximum current that the poloidal QPCs must interrupt could exceed the coil nominal current, and the assessment of such value requires a detailed analysis of the operation of the JT-60SA poloidal circuits with a complete model including all coupled elements.

The utility of working-out the poloidal circuit complete model is not only limited to the evaluation of the QPC maximum current, but it can be exploited for more general and global analyses. In fact the complexity of the poloidal circuits requires for taking into account all the mutual coupled elements to correctly reproduce their actual current waveforms both in normal and anomalous conditions. This means that the definition of the detailed specifications for the poloidal components and their optimization can be derived only by means of analyses performed using the complete model. Part of these studies have been published in Ref. [14].

2.2 JT-60SA Poloidal Circuit Model

A detailed axial-symmetric layout of all the poloidal conductors has been worked out as a first step, taking into account the dimensions of each element of the poloidal circuits at its operating temperature. The turn numbers, dimensions and positions of

Table 2.2 – *Coil geometrical characteristics*

Coil	Turn number	R (mm) @4K	Z (mm) @4K	ΔR (mm) @4K	ΔZ (mm) @4K
CS1	556	821.93	2386.5	327	1560.4
CS2	556	821.93	795.51	327	1560.4
CS3	556	821.93	-795.5	327	1560.4
CS4	556	821.93	-2387	327	1560.4
EF1	142	5801.3	1178.7	329.3	333.8
EF2	154	4607.1	3170.5	356.7	333.8
EF3	248	1913.1	4025	542.2	427.3
EF4	355	1913.1	-4117	542.2	610.8
EF5	152	3902.4	-3722	301.9	389.6
EF6	180	5039.2	-2774	356.7	389.6
HC in-vessel upper	16	4045	1665	148	204
HC in-vessel lower	16	4045	-1665	148	204

superconducting coils at the operating temperature of 4 K are shown in Table 2.2. In this table R and Z represent the horizontal and vertical coordinates, respectively, of the magnet central position in the axial symmetric coordinate system; ΔR and ΔZ are the horizontal and vertical sizes of the magnets.

As a second step each element has been discretized with a sufficient number of circular conductors, named filaments, to achieve a good approximation. For the CS and EF coils, the number of filaments, their position and their radius have been selected so as to precisely mimic the number and the geometrical characteristics of the conductors composing the coils. For the HC coils the number of filaments used for the mutual inductance matrix calculation is higher than the coil turn number; in order to have a more detailed discretization, a number of filaments six times the turn number has been used, and their radius has been calculated so as to completely cover the HC coil cross section area.

The JT-60SA vacuum vessel is torus-shaped and double-walled. The double-wall cavity is filled with borated water to enhance the neutron shielding capability of the vacuum vessel. Every 40 degree, the vessel is attached at the bottom to a gravity support with a pack of spring plates. In the model the vacuum vessel has been discretized with 154 conductors, placed in a central position in respect with the vessel inner and outer walls.

To improve plasma stabilization, stabilizing plates have been designed as a double-wall structure placed inside the vessel, and are covered with bolted carbon armour tiles on cooled heatsinks as a first wall. Similarly to the vessel, the stabilizing plates have been discretized with 36 conductors placed in a central position in respect with their inner and outer walls. The size, the position and the number of filaments discretizing vessel and stabilizing plates have been selected so that the diameter of each conductor is about the thickness of the vessel and stabilizing plates themselves and so that each filament results consecutive to the other. This thick discretization permits to reproduce

with a suitable approximation the different current distributions that could arise during the disruption, in particular in the passive elements close to plasma.

Three principal parameters contribute to the definition of equilibrium plasma current distribution: plasma self inductance l_P which characterizes the stiffness of plasma current profile, normalized plasma beta β_N which accounts for thermal energy content of plasma and the poloidal flux ψ_C linking the plasma geometric center which determines the Ohmic distribution of current in poloidal magnets.

Table 2.3 – *Position and current of plasma filaments*

Conductor number	R [mm]	Z [mm]	Current [MA]
1	3444.3	676.19	1.45
2	2720.4	1232.8	0.308
3	2493.5	676.19	0.605
4	2504.1	-395.68	0.574
5	2793.9	-910.95	0.502
6	3475.2	-395.68	2.040

As a first step the plasma has been discretized with six conductors, placed in a position and with a current distribution (see Table 2.3) so as to obtain a magnetic field similar to the one produced by a reference 5.5 MA plasma with $l_P = 4.60$ μH, $\beta_N = 1.2296$ and $\psi_C = 16.4$ Wb. Other more refined plasma discretizations will be

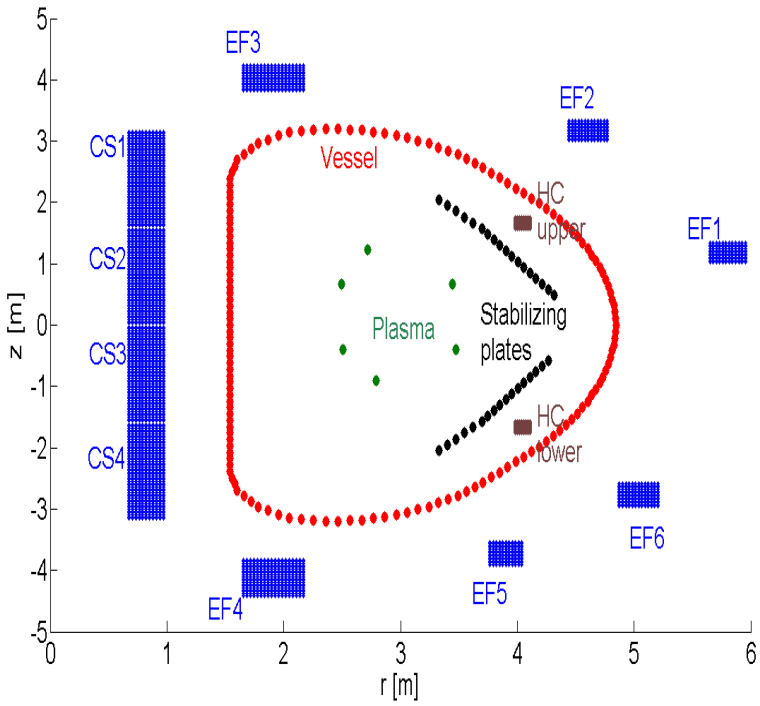

Figure 2.6 - *Geometrical model of the poloidal circuits of JT-60SA*

discussed in paragraph 2.3.3. A sketch of the obtained model is showed in Figure 2.6.

2.2.1 Mutual inductance matrix

For each filament conductor the self inductance value L_i has been calculated as:

$$L_i = 4\pi \cdot 10^{-7} \cdot r_i \cdot \left[\ln\left(\frac{8 \cdot r_i}{R} \right) - 1.75 \right] \tag{2.1}$$

where r_i is the filament major radius and R is the filament thickness.

The mutual inductance value $m_{i,j}$ of each couple of filaments used to model the coil and the passive elements of JT-60SA has been calculated according to Ref. [15]:

$$m_{i,j} = \frac{8\pi \cdot 10^{-7}}{k} \cdot \sqrt{r_i \cdot r_j} \cdot \left[\left(1 - \frac{k^2}{2} \right) \cdot J_1(k) - J_2(k) \right] \tag{2.2}$$

where:

$$J_1 = \sum_{p=0}^{4} A_p \cdot \left(1 - k^2\right)^p + \ln\left(\frac{1}{1-k^2} \right) \cdot \sum_{p=0}^{4} B_p \cdot \left(1 - k^2\right)^p ,$$

$$J_2 = \sum_{p=0}^{4} C_p \cdot \left(1 - k^2\right)^p + \ln\left(\frac{1}{1-k^2} \right) \cdot \sum_{p=0}^{4} D_p \cdot \left(1 - k^2\right)^p ,$$

$$\mathrm{A} = \begin{pmatrix} 1.38629436112 \\ 0.09666344259 \\ 0.03590092383 \\ 0.03742563713 \\ 0.01451196212 \end{pmatrix} \quad \mathrm{B} = \begin{pmatrix} 0.5 \\ 0.12498593597 \\ 0.06880248576 \\ 0.03328355346 \\ 0.00441787012 \end{pmatrix} \quad \mathrm{C} = \begin{pmatrix} 1 \\ 0.44325141463 \\ 0.06260601220 \\ 0.04757383546 \\ 0.01736506451 \end{pmatrix} \quad \mathrm{D} = \begin{pmatrix} 0 \\ 0.24998368310 \\ 0.09200180037 \\ 0.04069697526 \\ 0.00526449639 \end{pmatrix}$$

In order to find out a single value of self-inductance for each poloidal coil, the mutual inductance values of each single conductor composing each coil have been summed, since the current is the same in the series connected filaments. For vacuum vessel, stabilizing plates and plasma, the contributions of each single filament have been considered separately, in order to easily take into account the possible different current distributions. The resulting inductance matrix size is 207×207.

For vacuum vessel and stabilizing plates the equivalent resistance value of each filament has been calculated supposing that they are connected in parallel and subdividing the total resistance of the conductor proportionally to the length of the filament itself. For the coils it has been considered the total resistance value that is zero for CS and EF superconducting coils and 5.7 mΩ for HC coils.

The mutual inductance matrix and the resistance values have been inserted into a linear system representing the relation between current and voltage of each coil and filament:

$$\begin{cases} V_{Ci} = L_{Ci} \cdot \dfrac{di_{Ci}}{dt} + M_{CiVj} \cdot \dfrac{di_{Vj}}{dt} + M_{CiPk} \cdot \dfrac{di_{Pk}}{dt} \\ V_{Vj} = M_{CiVj} \cdot \dfrac{di_{Ci}}{dt} + L_{Vj} \cdot \dfrac{di_{Vj}}{dt} + M_{VjPk} \cdot \dfrac{di_{Pk}}{dt} + R_{Vj} \cdot i_{Vj} \end{cases} \tag{2.3}$$

where i_{Ci}, i_{Vj}, i_{Pk} are, respectively, the currents in the i-th coil, in the j-th conductor discretizing vessel or stabilizing plates and in the k-th element discretizing plasma; V_{Ci} are the voltages applied to the coils and V_{Vj} are the vessel/stabilizing plates voltages that have assumed as zero since they are short-circuited passive elements; L_{Ci} and L_{Vj} are the coil and vessel/stabilizing plates self-inductances; M_{CiVj}, M_{CiPk} and M_{VjPk} are the mutual inductances between coils, vessel and plasma, and R_{Vj} are the vessel resistances. Unknown terms are the currents in the coils and in the passive conductors, while the plasma current evolution is imposed. The coil voltage is applied externally, so as to have the possibility of simulating the converter applied voltage. In the model converters are considered as current controlled ideal voltage generators.

The solution of the described linear system permits to obtain the current waveforms in the poloidal circuits in different operating conditions. In particular the cases of plasma disruption and quench protection circuit operation have been widely analyzed. These results have been particularly useful for defining the maximum current in the coils, that is the maximum current value that the QPCs shall interrupt.

2.3 Plasma Disruption Simulation

Due to the strong mutual coupling, a plasma disruption could cause a significant current variation in the passive elements and in the poloidal coils. In such a situation, it is not easy to identify which are the parameters that have a real impact on the level of induced over-currents on the external coils, so a set of simulations has been performed using the developed model and changing the plasma disruption parameters such as plasma initial current value, plasma position, plasma current distribution and derivative.

During plasma disruption the converters feeding the CS and EF coils can contribute to limit the coil over-current, but it is possible that in some fault conditions they are by-passed. In order to take into account this realistic worst case in the performed simulations, the converters have been considered supplying zero voltage.

Since Eq. (2.3) represents a linear system, the maximum overcurrent in the coils occurs at the maximum plasma current; therefore the case of 5.5 MA was considered in the simulation.

2.3.1 Fixed position, 10ms plasma disruption

In the first case studied the six plasma filaments were kept fixed in the initial position during the disruption with the current in the filaments linearly decreasing from the initial value to zero in 10 ms.

Because of the analytical form of Eq. (2.3), the initial current value of the external superconducting coils at the time of plasma disruption has no effect on the induced coil over-current.

In fact the linear system described by Eq. (2.3) can be written in the following form:

$$\frac{\partial i(t)}{\partial t} = -M^{-1} \cdot R \cdot i(t) + M^{-1} \cdot v(t) \tag{2.4}$$

whose solution is

$$i(t) = e^{-M^{-1} \cdot R(t-t_0)} \cdot i_0 + \int_{t_0}^{t} e^{-M^{-1} \cdot R(t-t_0)} M^{-1} v(z) \partial z \tag{2.5}$$

It results that the initial current values i_0 are multiplied by the matrix function $e^{-M^{-1} \cdot R(t-t_0)}$. Since the resistance of superconductive coils is zero, the free evolution of the system with superconductive coils depends only on the initial current on passive conductors having a non zero resistance.

The current on the passive structures at the time of plasma disruption can be considered as zero, since they have very short resistive time constants (in the order of tens of milliseconds) if compared to the foreseen plasma current ramp-up and flat-top duration (in the order of seconds). For these reasons the initial current of coils and passive elements has been set to zero.

The obtained results in terms of over-current are shown in Figure 2.7 and Table 2.4. The maximum EF and CS coil over-current appears in coil CS2, exceeding 3 kA. A large over-current is present in HC in-vessel coils, up to about 35 kA for the upper coil and 27 kA for the lower one, that are rated for a nominal current of 5 kA.

Table 2.4 – *Coil over-currents in case of fixed position 6 filaments plasma disruption*

Coil	Over-current [kA]	Coil	Over-current [kA]
CS1	1.44	EF3	1.09
CS2	3.07	EF4	0.42
CS3	2.32	EF5	1.10
CS4	0.85	EF6	1.59
EF1	2.77	HC-upper	34.87
EF2	2.17	HC-lower	26.71

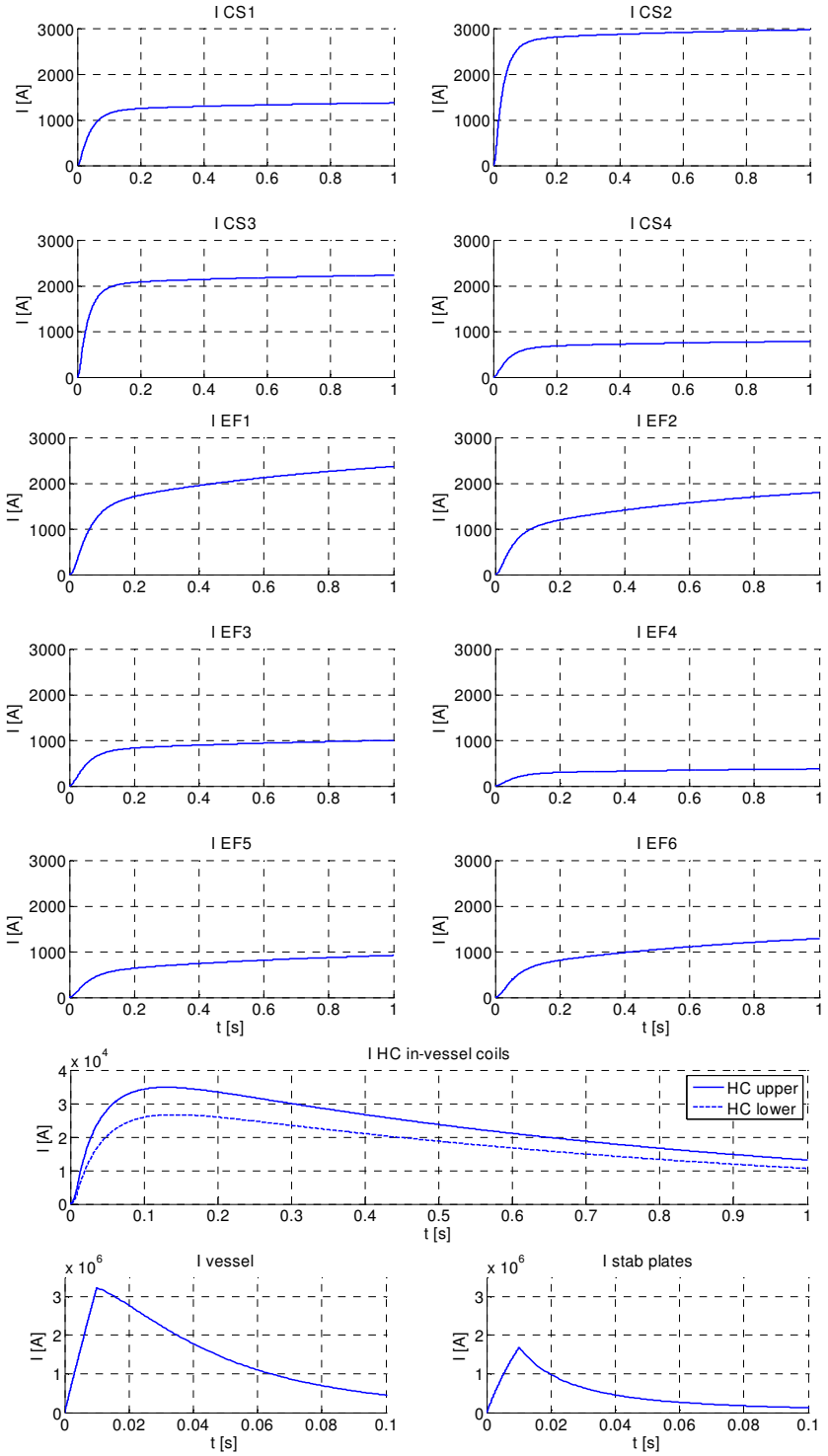

Figure 2.7 - *Overcurrents in case of plasma disruption obtained with the simplified linear model. Note the different time-scales of bottom panels*

2.3.2 Different plasma current derivative during disruption

As a second step, the plasma disruption has been simulated changing the plasma current derivative value, ranging from 5.5 MA / 1 ms to 5.5 MA / 100 ms. The obtained current waveforms in the external coils, two of which are shown as an example in the first two panels of Figure 2.8, are different only in the initial transient, but the regime over-current value is the same for each considered plasma derivative value, meaning that this disruption parameter has no influence on the level of induced over-current. It is possible to notice that, instead, the vessel induced current waveforms are heavily influenced by the plasma current derivative during disruption.

2.3.3 Plasma Current Distribution

The aforementioned analyses were made assuming a simple plasma model, composed of six filaments reproducing the magnetic field of reference plasma with a current of 5.5 MA. A more refined reference plasma model, composed of more than 3000 current filaments but with the same β_p and l_P reference values, has been used with the aim of evaluating the effect of the plasma discretization on the resulting external coil overcurrent. The results for the external superconducting magnets, shown in the third column of Table 2.5, do not wander more than 2% of the nominal current in respect to the ones obtained with the six filament model. It is therefore clear that the effect of realistic current profile is negligible for this study. On the contrary a significant difference is obtained in the HC coils, due to the fact that these are internal coils and are more affected by plasma current variation than external ones, since they are not shielded by the presence of low resistance vessel.

Table 2.5 – *Coil over-currents in case of plasma disruption with different plasma models*

Coil	**Coil overcurrent**			
	6 filaments	**Reference**	**Increased flux**	**Increased l_P**
CS1	1.44	1.15	1.16	1.12
CS2	3.07	2.70	2.69	2.71
CS3	2.32	2.57	2.56	2.59
CS4	0.85	1.02	1.03	1.00
EF1	2.77	3.07	3.11	3.20
EF2	2.17	2.07	2.09	2.11
EF3	1.09	0.92	0.94	0.92
EF4	0.42	0.50	0.51	0.50
EF5	1.10	1.32	1.34	1.34
EF6	1.59	1.91	1.93	1.96
HC-upper	34.87	34.21	34.37	34.89
HC-lower	26.71	32.96	33.0	33.54

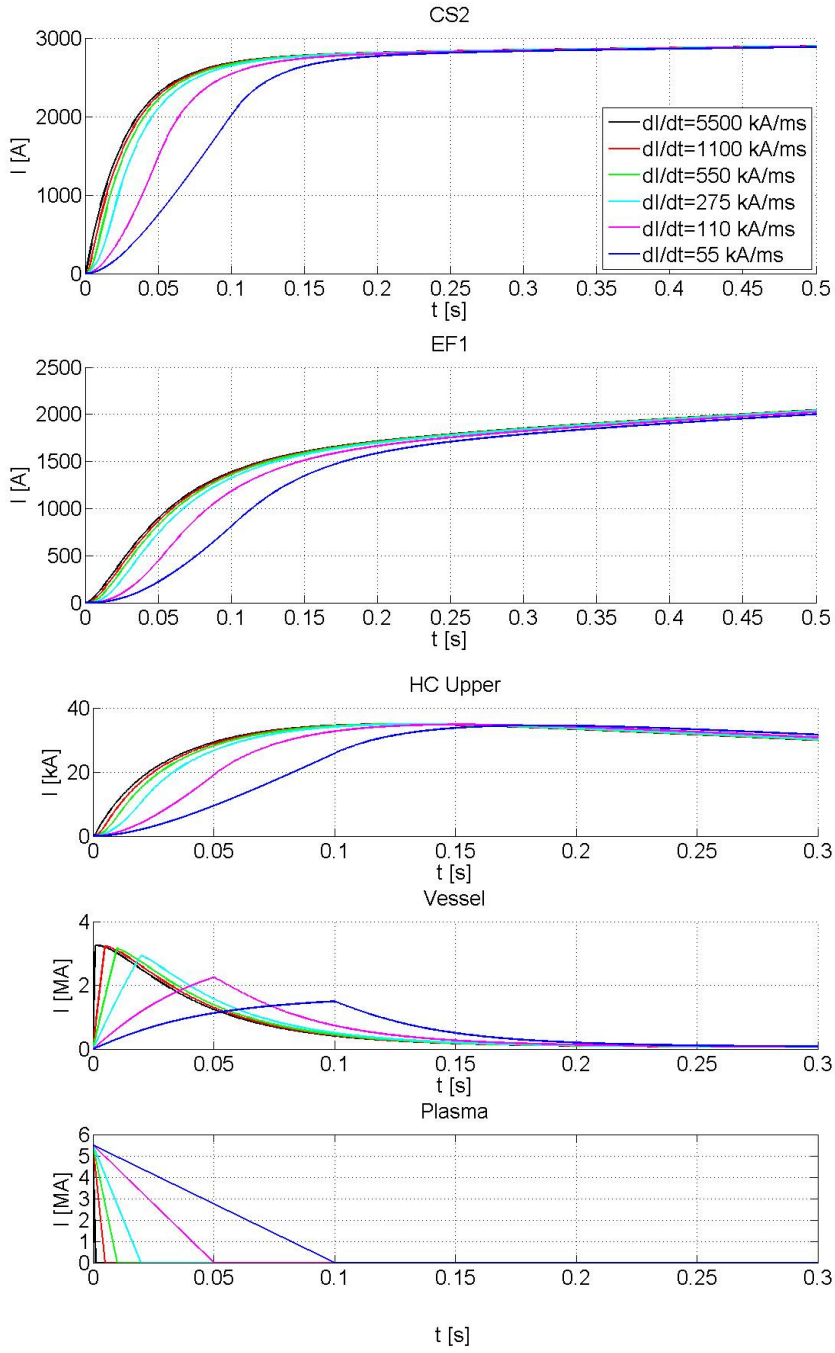

Figure 2.8 – *Overcurrents in coils CS2 and EF1, in Upper HC in-vessel coil and in Vessel in case of different plasma current derivative during plasma disruption*

A different initial magnetic field created by a different plasma current distribution at the time of disruption could lead to variations of the over-current values both in the HC in-vessel coils and in the superconducting coils, being changed the mutual coupling between coils and plasma. In order to investigate this possibility, a number of plasma scenarios has been considered among the possible plasma equilibrium conditions with 5.5 MA current.

Several equilibrium plasma current distributions have been simulated with the TOSCA code [16] considering different possible combinations of l_P, β_N and ψ_C, obtaining precise plasma current distributions with more than 3000 current filaments. The resulting detailed plasma models have been inserted in the zero-dimensional poloidal circuit model for simulating a disruption with plasma in a fixed position.

The results, reported in columns 4 and 5 of Table 2.5 for two plasma equilibria characterized respectively by an increase in flux consumption (l_P = 4.6 μH, β_N = 1.23 and ψ_C = 21.4 Wb) and an increase of l_P (l_P = 5.06 μH, β_N = 1.35 and ψ_C = 18.8 Wb) respect with the reference equilibrium, show that with the considered initial plasma current distributions only negligible variations are observed both in superconducting and in-vessel coil overcurrents, meaning that the variation of plasma parameters as flux consumption and l_P has negligible effect on coil overcurrent.

2.3.4 Plasma Vertical Displacement Event (VDE)

Finally, the effect of plasma movement during a disruption has been studied. In fact it is possible that the combined effect of current derivative and plasma movement could result in a higher overcurrent in the coils where the linked flux is diminishing.

The study of plasma VDE is a specific topic generally faced during the detailed mechanical design of passive structures such as vacuum vessel and stabilizing plates, since it represents one of the worst case conditions for such elements from the point of view of electro-mechanical stresses. The evaluation of the evolution of the plasma column position in case of a VDE is a complex task and it is generally worked out by means of specific plasma equilibrium codes. The VDE calculations performed by the JT-60SA work group for defining the mechanical stresses of in-vessel components with the DINA code [17] have been used as input for obtaining the time evolutions of some plasma current distributions in case of VDE.

The plasma column time evolution in terms of position and current has been fitted in a fixed grid covering all the in-vessel area, each point being a plasma filament. The current in each filament is changed in time so as to reproduce the plasma VDE. In this way it has been possible to reproduce the plasma VDE evolution using the plasma filament discretization inside the simplified linear model.

The results obtained in case of both upward and downward VDEs, as shown in Figure 2.9 for the two coils where the VDE effect is more remarkable, prove that the plasma movement in case of disruption determines the transient waveform of the current in the external coils, but has no influence on the coil over-current final value.

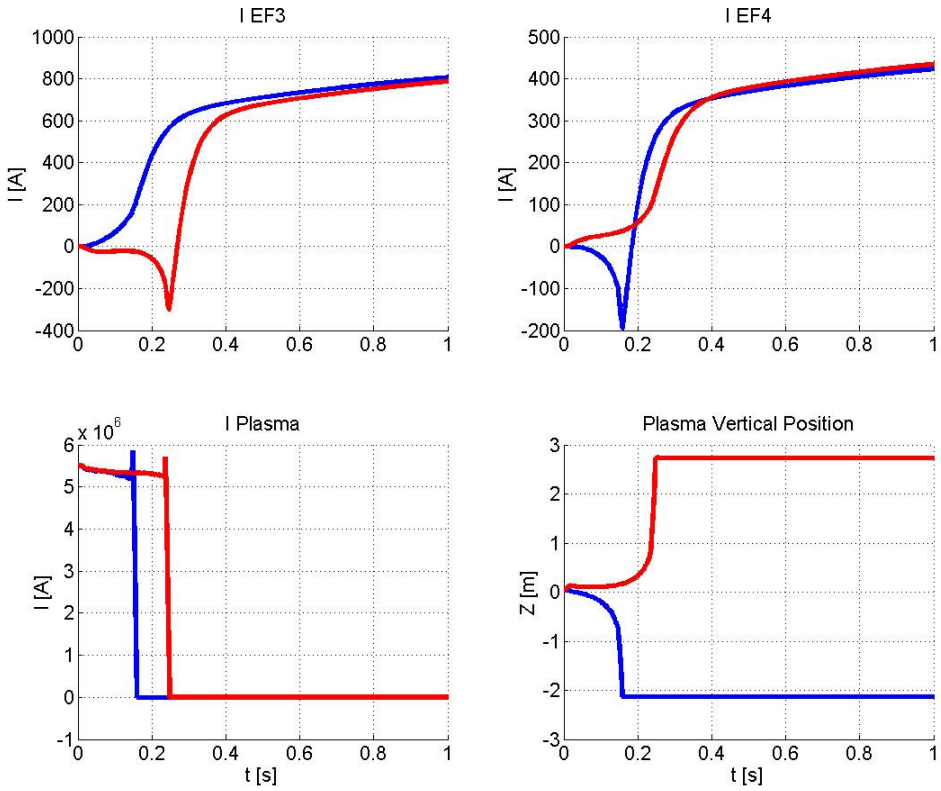

Figure 2.9 – *Overcurrents in coils EF3 and EF4 in case of Vertical Displacement Event (upward movement in red, downward movement in blue)*

It is interesting to notice that, as expected, the current in the coils where the plasma is approaching starts to become negative while it becomes positive in the coils where the plasma is departing from.

Moreover it is possible to assess that during the transient phase the coil over-current does not reach values higher than the final over-current. This assures that the VDE event is not cause of over-current higher than the ones obtained in a standard plasma disruption.

2.3.5 Maximum coil overcurrent in case of plasma disruption

Since the variation of plasma parameters as current derivative, current distribution and movement does not have a significant influence on the superconducting coil overcurrent, for finding out the maximum peak current value in one coil in case of plasma disruption, it is sufficient to take into consideration the maximum of the values shown in Table 2.5 for that coil, and to sum this value to the initial coil current value.

If the nominal coil current of 20 kA is considered as initial value, an unacceptable over-current value of more than 15% would be obtained for CS2 and EF1 coils, but this could lead to not realistic conditions: for example the current in CS coils reaches

the maximum rated value only before plasma breakdown, while when plasma current reaches 5.5 MA the current in CS coils has lower values. In order to take into consideration more actual initial coil current values, more than 300 realistic sets of coil current values, called snapshots, obtained from plasma equilibrium scan, have been considered.

Considering these snapshots, it results that in case of plasma disruption the higher coil current value is obtained in coil EF4, where the initial current at the time of plasma disruption is 19.95 kA and the final value is 20.46 kA. If other snapshots were proposed, with higher initial current in coils such as EF1 and EF2 where the plasma disruption causes higher over-currents, there would be the possibility of largely exceeding the coil nominal current value of 20 kA.

2.3.6 Model Validation with Comsol Multiphysics

A simplified axial-symmetric two-dimensional model of the poloidal circuits of JT-60SA has been developed using Comsol Multiphysics [18], a finite element analysis, solver and simulation software package. In the Comsol Multiphysics model the coils have been modeled as single turn massive conductors instead of being composed of a number of series connected conductors; the vessel and the stabilizing plates as continuous conductors and the plasma as 6 conductors as described in previous Section. Plasma disruption has been simulated using this Comsol Multiphysics model and the resulting coil current waveforms have been compared with the ones obtained with the linear system described in previous paragraphs, finding a good agreement as shown in Figure 2.10.

The comparison of the results obtained with the linear system and Comsol Multiphysics can be considered an effective way of validation, since the first is based on analytical calculation, while the latter is based on finite element model analyses involving magnetic field reconstruction.

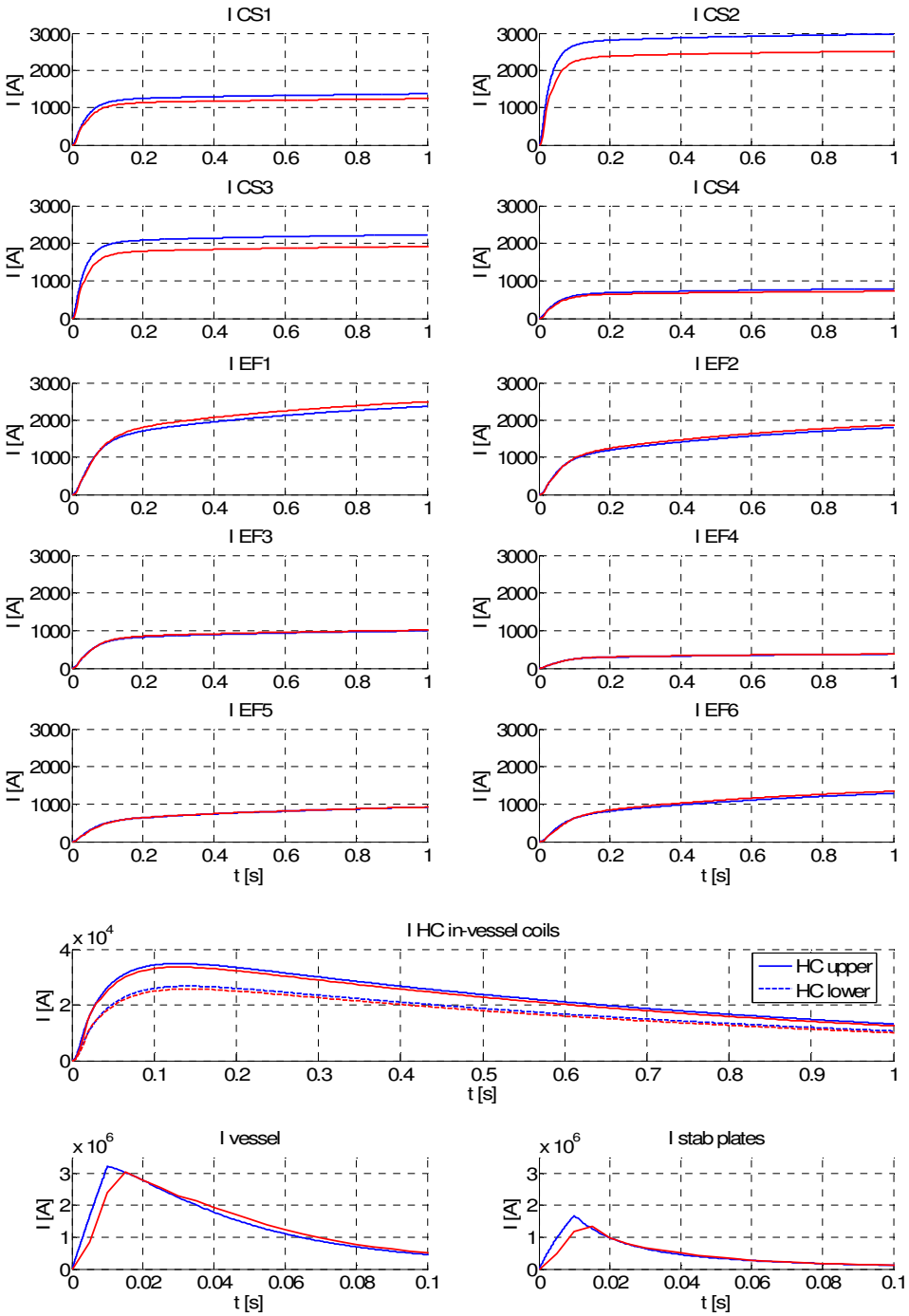

Figure 2.10 - *Overcurrents in case of plasma disruption obtained with the simplified linear model (in blue) and with Comsol model (in red). Note the different time-scales of the bottom two panels*

2.4 QPC Intervention Simulation

2.4.1 Intervention of a single QPC

In case of quench in one superconducting coil it is necessary to activate its QPC to rapidly zero the coil current. By means of the QPC activation, in fact, the dump resistor is inserted in the coil circuit and the current is zeroed with the time constant resulting not only from the R/L of the circuit but also from the mutual inductance with other poloidal circuits. For this reason, to analyze the operation of the QPC it is important to take into consideration the current variations in all coupled circuits and the developed model is a useful tool allowing to perform these studies.

The protection strategy presently adopted foresees that the QPCs are commanded not only in case of quench, but also in case of other faults in the circuits, to fast de-energize the coils; when the QPCs are commanded, all the converters are switched-off and bypassed by crow-bars.

All the QPC are operated in case of quench, while, in case of other faults, it could be acceptable in principle to command the intervention of the QPC in one circuit only. Due to the mutual coupling between coils, it is possible that the current variation in the coil where a single QPC is operated induces overcurrent in other coils.

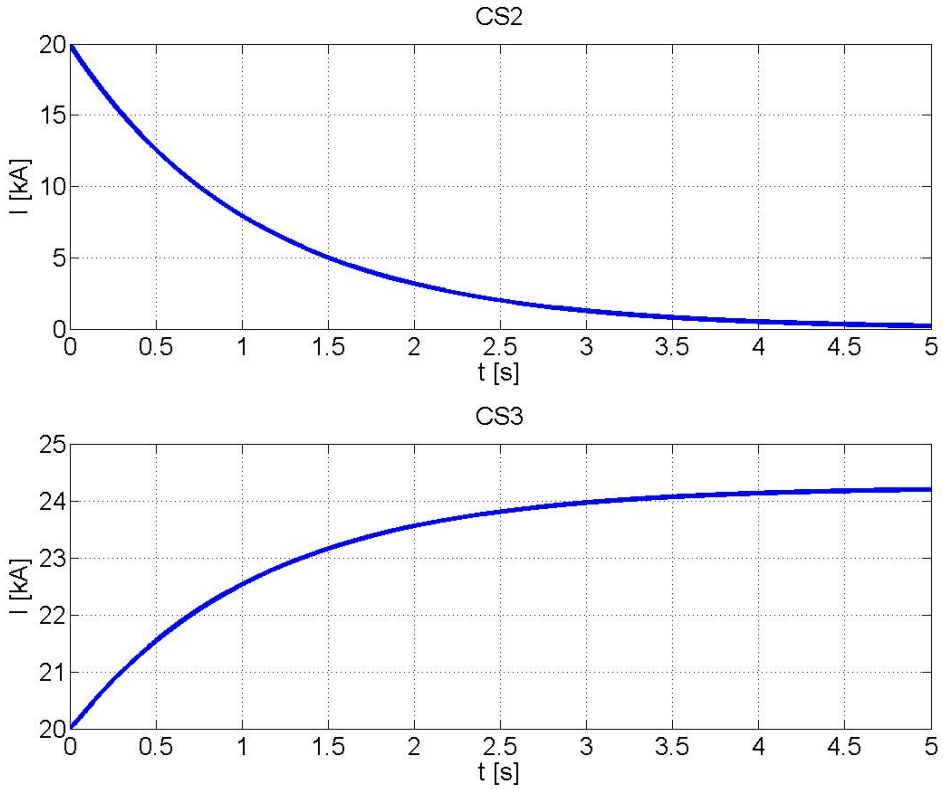

Figure 2.11 – *Overcurrent in CS3 coil in case of QPC intervention in coil CS2*

In order to study this case, the linear model has been used assuming that the QPC is operated in one coil circuit only, and all the converters are bypassed. In fact this condition represents the worst case in terms of maximum overcurrent, since the action of converters could help in limiting the coil overcurrent. With this kind of simulations it has been verified that the intervention of a single QPC could lead to excessive current variations in other coils, due to the mutual coupling among them.

A number of possible coil currents initial values have been considered, and the worst case has been found for CS coils: as shown in Figure 2.11, in case of operation of CS2 QPC, the current in CS3 coil can reach more than 24 kA, exceeding by far the coil nominal current. Such value would be too large to be tolerated by the coils; therefore it has been decided as protection strategy to activate always simultaneously all the poloidal QPCs.

2.4.2 QPC dc circuit breaker failure

In case of failure of the QPC dc circuit breaker, it is necessary to activate the backup pyrobreaker installed in series to the circuit breaker, so as to commutate the current into the discharge resistance. The maximum time between the QPC intervention request and the pyrobreaker activation is 2 s (see Table 2.1). In the time between the QPC activation request and the pyrobreaker activation, the current in the faulty circuit increases due to the mutual coupling with the other poloidal circuits where the current is decreasing. In this case it is necessary to evaluate the maximum current value reached in the faulty QPC.

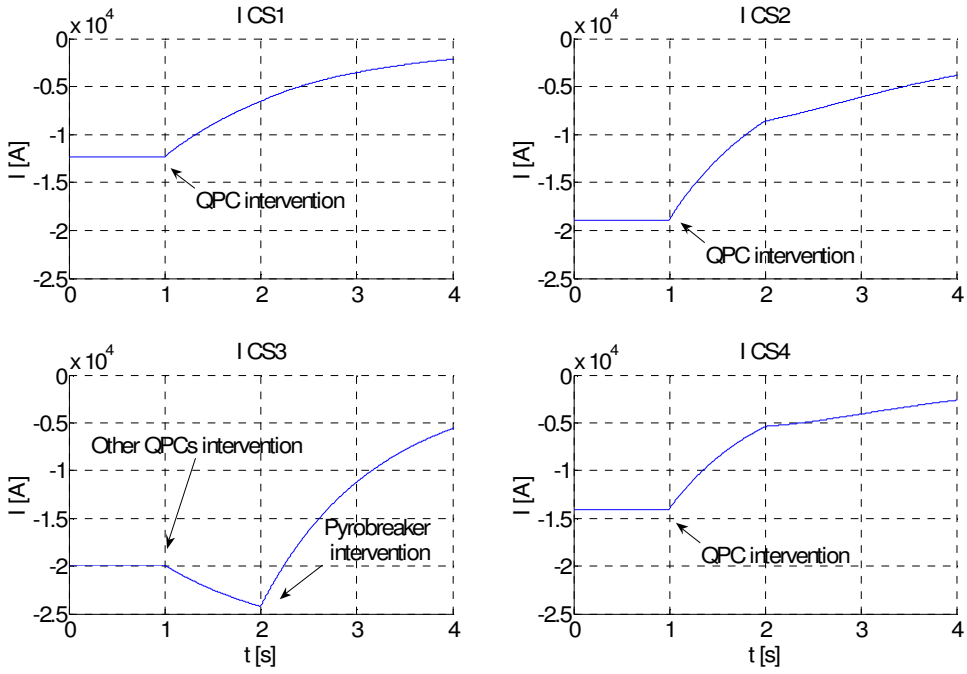

Figure 2.12 - *Overcurrent in CS3 coil in case of QPC dc circuit breaker failure*

Thus, for each QPC it has been simulated the case of dc circuit breaker failure starting with a number of possible initial coil current values. It results that the maximum current in case of pyrobreaker operation could exceed the coil rated value. The worst case is showed in Figure 2.12; it refers to the dc circuit breaker failure in the QPC of coil CS3 that leads to a maximum negative current of more than 24 kA before the pyrobreaker intervention. This too large current value could be decreased by reducing the time delay between QPC expected intervention and pyrobreaker activation. For example if this time is halved from 1 s to 0.5 s, the maximum current in coil CS2 would be limited to -22.5 kA.

2.5 Discussion of results

The studies of the plasma disruption and its effects on the coil overcurrents are quite complex and a large variety of phenomena has been taken into account. The analyses performed so far allowed to verify that the over-currents induced in the CS and EF coils are always positive, reach 3 kA (15% of the nominal coil current) and their amplitude does not significantly depend on plasma parameters such as current derivative, initial current distribution and plasma movement. In fact passive elements (stabilizing plates and vacuum vessel) act as flux conservers that, due to their very low time constants, rapidly move to a resistive current distribution. This means that they have a screen effect on external superconducting coils, whose overcurrent in case of plasma disruption depends only negligibly on plasma behaviour, and that the plasma parameter having a real impact on the coil overcurrent is just the initial current value.

The peak current in the coils has been found adding the calculated coil overcurrent values to the initial coil current values. More than 300 sets of initial current in the coils, obtained from a plasma equilibrium scan, have been considered. The results showed that the peak current in the coils always remained within 5% more than the nominal current. It has however to be pointed out that if other snapshots were proposed, with higher initial current in coils such as EF1 and EF2, where the plasma disruption causes higher over-currents, there would be the possibility of largely exceeding the nominal current value of 20 kA. Anyway it is possible to develop a real time application that, taking in consideration the plasma current and the coil current values in any instant, monitors if the device is running in a safe area or if, in case of plasma disruption, dangerous coil overcurrents could occur, therefore taking the opportune provisions.

The analyses of the QPC operation showed that the intervention of a single QPC can cause too high overcurrents, but this problem can be avoided commanding the QPC all together. On the contrary, in case of failure of the dc circuit breaker of one QPC a significant overcurrent can not be avoided; the worst case is obtained in coil CS3 where the maximum current could reach -24 kA. This value can be limited into an acceptable range by reducing the pyrobreaker activation time from 1 s, as required in the QPC specifications of Table 2.1, to 0.5 s.

It is therefore possible to obtain that the maximum current that poloidal QPCs have to interrupt both in case of plasma disruption and failure of a QPC dc Circuit Breaker is 22.5 kA, and this shall be the reference number for QPC design.

2.6 Dump resistor value optimization

The poloidal QPC dump resistors have to be designed so as to limit the maximum voltage across the coil under the maximum value of 5 kV and the coil I^2t during a quench event under the maximum tolerable limit of 2 GA^2s. The two requirements have to be suitably balanced, since the maximum I^2t is decreased increasing the resistance value, but this implies an higher voltage across the coil. Due to the mutual coupling between all poloidal coils it is not easy to optimize the QPC resistor value with the certainty that the maximum I^2t and voltage constraints are fulfilled under all possible operating conditions. For this kind of evaluation it is necessary to analyze the behavior of the poloidal circuits taking into account all the mutual coupled elements, and the developed model presented in the previous sections can be easily adapted for this study.

Starting from more than 300 sets of possible coil current initial values already used for the plasma disruption simulation, the poloidal QPC intervention has been simulated taking into account the 1s maximum time delay between the QPC intervention request and the actual intervention. A safe range of poloidal dump resistance values, from 0.25 Ω to 0.15 Ω, have been identified which allows not to exceed the limits, both in terms of voltage and I^2t.

The assumption of a reduced value for the dump resistors permits to design the QPC circuit breaker for a lower reapplied voltage, thus allowing to use a reduced number of series connected components. This would result in an increase of the QPC simplicity and reliability. For this reason it has been decided to select the value of 0.21 Ω for the poloidal dump resistors. This value is reduced in respect with the nominal value of 0.25 Ω showed in Table 2.1.

The simulation of QPC intervention has been performed using the selected dump resistor value under all conditions, including normal QPC operation and pyrobreaker intervention. In each simulated case, the resulting I^2t in the coils remains well under the maximum limit of $2GA^2s$.

It is therefore possible to obtain an optimized set of poloidal QPC specifications, as shown in Table 2.6.

Table 2.6 – *QPC optimized rating*

Characteristic	**Poloidal QPC**
Nominal voltage	4.2 [kV]
Nominal current	20 [kA]
Maximum interruptible current	22.5 [kA]
Maximum delay from command	1 [s]
Maximum delay for pyrobreaker operation	0.5 [s]
Dump Resistor	0.21 [Ω]

CHAPTER 3

3. QPC Conceptual Design

The specifications of the QPC for the superconducting magnets of JT-60SA are summarized in Table 3.1. Some of these characteristics derive from the superconductor requirements that are already described in Table 2.1; other specifications are the result of optimizations and analyses performed taking into account the interaction between the complete magnet system, as described in Chapter 2.

Table 3.1 – *QPC main specifications*

Characteristics	Toroidal QPC	Poloidal QPC
Unit number	3	10
Nominal voltage	2.8 kV	4.2 kV
Nominal current	25.7 kA	20 kA
Maximum interruptible current	25.7 kA	22.5 kA
Current polarity	Unidirectional	Bidirectional
Duty Cycle	Steady state	100 s / 30 minutes
Maximum allowed I^2t	5.3 GA^2s	2 GA^2s
Dump Resistor nominal value	$3 \times 0.11\ \Omega$	0.21 Ω
Maximum delay from command	1 s	1 s
Maximum delay for pyrobreaker operation	0.5 s	0.5 s
Maximum time between QPC intervention and restart of operation	60 minutes	30 minutes

As shown in Figure 3.1, a QPC is composed of three main components, namely a dc Circuit Breaker, a Pyrobreaker and a Dump Resistor, whose integrated working permits the correct operation of the QPC, assuring the protection of the superconducting magnets. In the following paragraphs the conceptual design of each

element of the QPCs for JT-60SA is illustrated, with particular emphasis on the design of the Hybrid dc Circuit breaker, which represents a very innovative solution to the problem of dc current interruption. Part of this study has been published in Ref. [19]

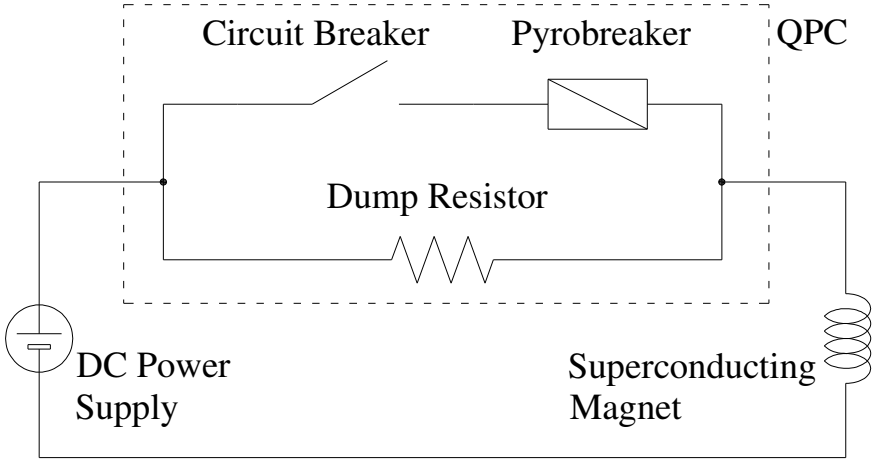

Figure 3.1 – *Scheme of the main elements composing a QPC*

3.1 Dc Circuit Breaker

Superconducting magnets rated for high values of continuous dc current, in the order of some tens of kA, are employed in a number of different applications where a high magnetic field is needed, such as superconducting magnetic energy storage, particle accelerators or plasma confinement devices. In case of quench it is necessary to rapidly remove the energy stored in superconducting magnets; this is generally obtained inserting in series to the superconductor a discharge resistor that in normal condition is short-circuited by a low impedance circuit breaker. When the circuit breaker is opened, it is necessary to interrupt the dc current flowing in the circuit breaker in order to commutate it into the dump resistor.

The arc formed at the opening of mechanical switches in ac applications is automatically extinguished at the current natural zero crossing, while dc applications present the intrinsic problem of extinguishing it. For this reason, the dc CB requires in general an external counter-pulse network to generate a current opposite to that of the CB so as to obtain a zero total current at the time of the contact opening, to blow out the arc.

Moreover, when the level of current to be sustained in steady state operation and then rapidly interrupted is very high, of the order of tens of kilo-amperes, it is difficult to find a single device satisfying the requirement. In the case of ITER, for example, the combination of a mechanical switch plus Vacuum Circuit Breaker (VCB) has been proposed by the EU Participant Team [20]. In normal operation, the continuous

current flows through the mechanical switch; after the quench detection, it is diverted to the VCB which then opens thus transferring the current to the discharge resistor.

In Weldenstein 7-X [21], a comparison among different alternatives still led to a solution based on industrial mechanical CB as the best compromise, in terms of availability, reliability and cost, for the design of the Quench Protection Units (QPU) rated 20 kA/8 kV. Also in this case, the rating requires however to provide bypass switches to sustain the continuous current.

In the Large Helical Device (LHD), QPUs were developed for the poloidal and helical superconducting coils, rated for 30 kA / 3 kV [22]; they are again based on Vacuum Circuit Breakers (VCB), but with power fuses in parallel so as to avoid the use of the external counter-pulse network. However, a significant drawback remains, consisting in the necessity of changing the fuse every time the system operates. A similar approach has been adopted in the QPU of the superconducting coils of the EAST Tokamak rated 15 kA / 3 kV [23]; DC CBs equipped with an air arcing elongation chamber are used. If the first fails, a second one with fuse in parallel acts as backup after 80 ms and then, in case of failure of both of them, a pyrobreaker opens after 200 ms.

Alternative design solutions based on static devices like Gate Turn Off thyristors (GTO), Insulated Gate Bipolar Transistors (IGBT) or IGCTs, controllable both at turn-on and turn-off, could be very attractive: interruption is arcless, very fast and it does not require a counter-pulse network; moreover static circuit breakers are almost maintenance-free. High power semiconductors have today high current breaking capabilities; however, the voltage drop in the on-state condition still remains quite high, thus causing high on-state losses. This is one of the main reasons they have not been widely used till now. In fact, if the dc circuit breaker is based on semiconductors only, too many elements in parallel and in series are necessary to sustain tens of kilo-amperes of dc current and some kilo-volts of reapplied voltage, with consequent high cost, low reliability and high level of losses in normal operation.

The combination of a mechanical switch to handle the continuous current with a static dc circuit breaker could be a very interesting solution because it combines the advantages of the mechanical switch and of the semiconductor; the combination can assure in fact, low on-state voltage and fast breaking, with a strong reduction of the problems related to the arcs. In this hybrid scheme, the semiconductor can be rated just for the current to be interrupted, thus allowing a full exploitation of the Safe Operating Area (SOA) capability of the large area devices.

This approach was already studied and implemented [20], [24], [25], but always considering thyristors, which require an external counter-pulse network to generate an artificial zero-crossing. However, this increases the system complexity and makes less effective the achievable cost reduction with respect to a solution implementing devices controllable both at turn-on and turn-off.

The current commutation from the BPS to the static CB is however a non negligible issue; in fact, the bypass switch has to sustain the arc during commutation and the static breaker has to turn-on with the arc voltage applied between anode and cathode, which is typically quite low. The capability of the BPS to operate in these conditions was verified during the test of the ITER switching prototype [20], while the

turn-on performance of static devices with low voltage applied is an open issue, faced up and analyzed in this thesis.

The static CB is composed of semiconductors connected in series and in parallel; the number of stages in series depends on the maximum voltage reapplied at the time of current interruption while the number of devices in parallel is affected by the total current to be interrupted, the conduction time, the current sharing quality and the maximum interruption capability of each device. In order to reduce the number of needed components, IGCTs were chosen among the available static devices controllable in turn-off, because they are rated for the largest value of interruptible current with a wide SOA. In particular the IGCT 5SHY35L4512 [26] and the IGCT 5SHY42L6500 [27], whose main characteristics are reported in Table 3.2, were selected due to their high nominal interruptible current of 4 kA, that could be further increased up to 6 kA [28] with a suitable snubber circuit.

However, when high current values have to be interrupted, special care has to be taken in ensuring well balanced connection of a significant number of IGCTs in parallel. The issue to be faced to confirm the feasibility of this design solution is related to the reliable turn-on of the IGCTs in parallel; in fact, they are commanded to turn-on with a low voltage applied, which is the BPS arc voltage and the applied voltage is further reduced in dependence of the number of IGCT stages in series. Moreover, the first turn-on of the fastest device inside each group of paralleled components could further lower the direct voltage across the others.

Experience gained with the IGCT dc circuit breaker of the toroidal power supply system of RFX-mod [29] assures that a reliable turn-on of paralleled IGCTs can be obtained with an applied voltage of some hundreds of volts, but for this hybrid dc CB there is not adequate confidence that the range of voltage applied by the BPS arc is sufficient.

Examples of similar applications with high number of devices in parallel were not found in literature; just one case was reported [30] but with only two IGCTs in parallel

Table 3.2 – *IGCT main characteristics*

Parameters	**Symbol**	**Value**	
		5SHY35L4512	5SHY42L6500
Repetitive Peak off-state voltage	V_{DRM}	4500 V	6500 V
Permanent dc voltage	V_{dclink}	2800 V	4000 V
Reverse voltage	V_{RRM}	17 V	17 V
Max. Controllable turn-off current (snubberless)	I_{TGQM}	4000 A	4200 A
Threshold voltage	V_{T0}	1.15 V	1.75 V
Slope resistance	r_T	0.21 mΩ	0.59 mΩ
Max. junction operating temperature	T_{vj}	125 °C	125 °C
Thermal resistance junction-to-case	$R_{th(jc)}$	8.5 K/kW	8.5 K/kW

to a mechanical switch; in addition, no specific provisions for the turn-on of both static components are there indicated.

In this chapter this issue is analyzed in detail and the reliable turn-on of IGCTs with low voltage applied has been proved by means of experimental tests. The design criteria of this hybrid CB are outlined and the comparison with a fully static solution is proposed to better highlight the advantages of the hybrid solution. Finally a reference design for the hybrid CB for the QPC of JT-60SA is defined.

3.1.1 Hybrid circuit breaker scheme and operation

The simplified scheme of the QPC with the proposed hybrid dc CB is shown in Figure 3.2. The CB is composed of a mechanical By-Pass Switch (BPS) paralleled to a static breaker made up of the necessary stages in series to sustain the reapplied voltage; each stage is composed of a number of paralleled IGCTs that permits to safely interrupt the QPC maximum current. In the study described below, just one stage in series was assumed because this is sufficient for the scope of the analysis. A series connected pyrobreaker, able to interrupt the current in case of circuit breaker opening failure, is installed for safety reason as a backup protection.

The sequence of actions needed to open the CB is reported in Figure 3.3. The BPS very low resistance and its capability to sustain high dc currents permit the continuous flow of high current in normal conditions with limited conduction losses. When a QPC intervention is needed, an opening command for the BPS and a turn-on command for the static breaker are generated (time *t1* in Figure 3.3). After a delay due to mechanical inertia, the BPS contacts open (time *t2*) and an arc is formed, whose voltage forces the nominal current *In* to commutate from the BPS to the static CB. In order to limit the arcing time in BPS and the associated contact erosion the impedance of the circuit involved in the current commutation must be kept very low, so that the current commutation, terminating at time *t3*, does not last more than some ms (interval

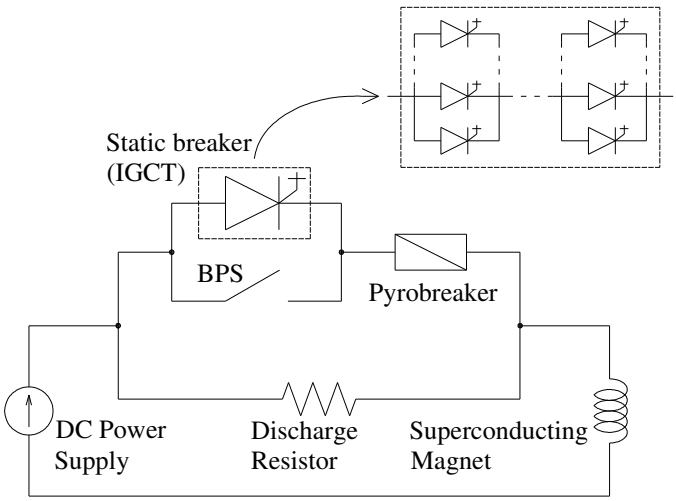

Figure 3.2 – *Scheme of QPC composed of hybrid dc circuit breaker*

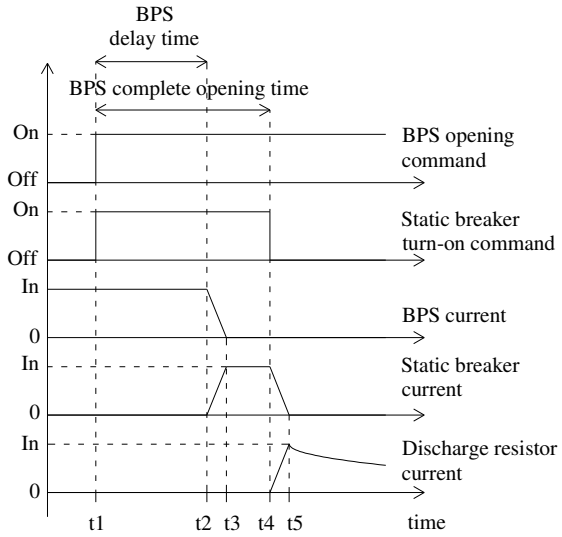

Figure 3.3 – *Sequence of operations needed to open the hybrid circuit breaker*

t2 – t3).

Then, to avoid current commutation failure it is necessary that the static CB is maintained in the on-state until the BPS contacts are fully open (time *t4*). In this way, the full voltage that appears when the static CB is turned-off and the current is transferred to the discharge resistor (time *t5*) is reapplied to BPS only after *t4*, thus minimizing the risk of arc re-strike.

The time interval *t1 - t4*, between the BPS opening command and the contact fully-open position, depends on the switch technology and can range from tens to hundred of milliseconds. On the contrary, the IGCT turn-off time (interval *t4 - t5*) is very short, of the order of microseconds.

3.1.2 Turn-on of IGCTs in parallel

As mentioned before, an issue of the design of this hybrid CB is the reliable turn-on of IGCTs in parallel with low voltage applied. This point implies two aspects: one, more general, is related to the operation and turn-on of IGCTs connected in parallel and the second, more specific for this application, is addressed to verify if the BPS arc voltage, applied between anode and cathode, is sufficient to assure a reliable turn-on of the IGCTs.

3.1.2.1. Turn-on of IGCTs connected in parallel

A general concern about the reliable turn-on of static devices and IGCTs connected in parallel, even with high voltage applied, is that when the first component starts to conduct it reduces the voltage applied to the others to the value of its conduction voltage drop limited to few volts that could result smaller than the minimum value

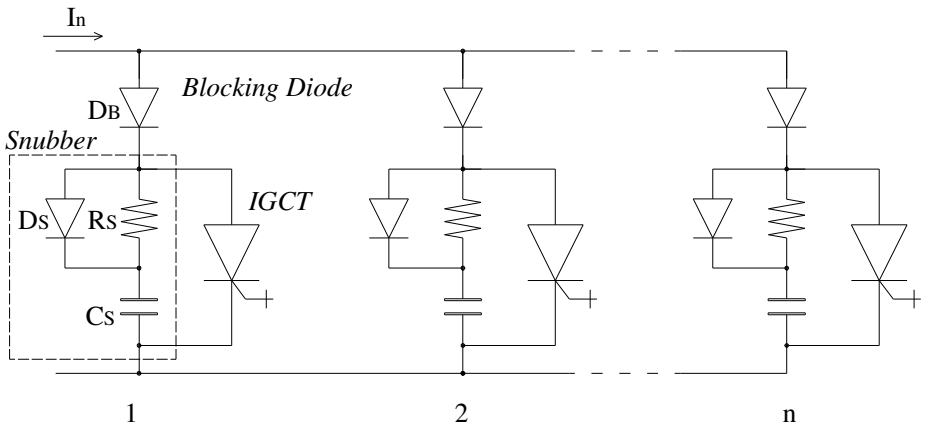

Figure 3.4 – *Circuit assuring turn-on reliability of n parallel IGCTs*

necessary for the turn-on of the remaining ones. In this application, the risk is that the whole BPS current is not shared between all paralleled IGCTs and the conducting IGCT could work outside from its SOA, with high probability of interruption failure.

In order to avoid this problem it is necessary that sufficient voltage remains applied to each paralleled IGCT until it is turned-on. This can be guaranteed if the IGCTs are provided with a diode in series and a suitable snubber circuit for voltage clamp during turn-off. Figure 3.4 shows the proposed scheme for the static CB, composed of "n" parallel branches, each made of an IGCT with a turn-off snubber and a reverse voltage blocking diode DB connected in series.

The circuit of Figure 3.4 is connected in parallel to the mechanical BPS (see Figure 3.2): when the BPS opens and the arc is formed, the capacitor C_S is rapidly charged through the diode D_S by the applied arc voltage. When the first IGCT starts conducting, its snubber capacitor is discharged via its resistor R_S which limits the peak current in the IGCT, while the other capacitors remain charged thanks to the presence of the diodes DB. In this way, the BPS arc voltage remains applied to each IGCT, even in presence of a possible jitter between the actual turn-on of different IGCTs.

An interesting aspect of this scheme is that reliable turn-on of paralleled IGCTs does not require additional component besides those anyway necessary or useful in this IGCT implementation. In fact, the turn-off snubber should be provided to limit the voltage derivative during IGCT turn-off, thus permitting to increase the maximum value of IGCT interruptible current. As for the series diode D_B, being the IGCT an asymmetric turn-off device not able to withstand reverse voltage higher than ten volts, it allows making the IGCT a "Reverse Blocking" device [31]. A conservative design approach would suggest providing this feature even if reverse voltage is not expected across the IGCTs in normal operation.

3.1.2.2. Turn-on of IGCTs with low voltage applied

The need for a reliable turn-on of IGCTs with a low voltage applied is a peculiar characteristic of the considered hybrid dc circuit breaker.

At present, no precise information about the minimum voltage value to turn-on the IGCTs are available, therefore specific tests have been made to verify if the BPS arc voltage is sufficient to assure the reliable turn-on of the IGCTs connected in parallel.

3.1.3 Test to verify the reliable IGCT turn-on with low voltage applied

3.1.3.1. Test circuit

The test circuit shown in Figure 3.5 has been set-up; a converter connected to a variable resistance permits to apply different values of voltage to the devices under test. These are two IGCTs 5SHY 35L4512 connected in parallel, equipped with a turn-off snubber circuit (C_S = 6 μF, R_S = 4.5 Ω) like the one described above, and a series connected blocking diode. Two additional inductances ($L_{1,2}$ = 2 μH) protect IGCTs against possible excessive current derivative. The current is measured in the two branches in parallel by means of shunt resistors ($R_{1,2}$ = 3 mΩ) that have also the aim of improving current sharing between the IGCTs.

At a desired time the converter is turned-off, entering in freewheeling mode; afterwards, the two IGCTs are turned-on and the current flowing in the variable resistance is commutated into them.

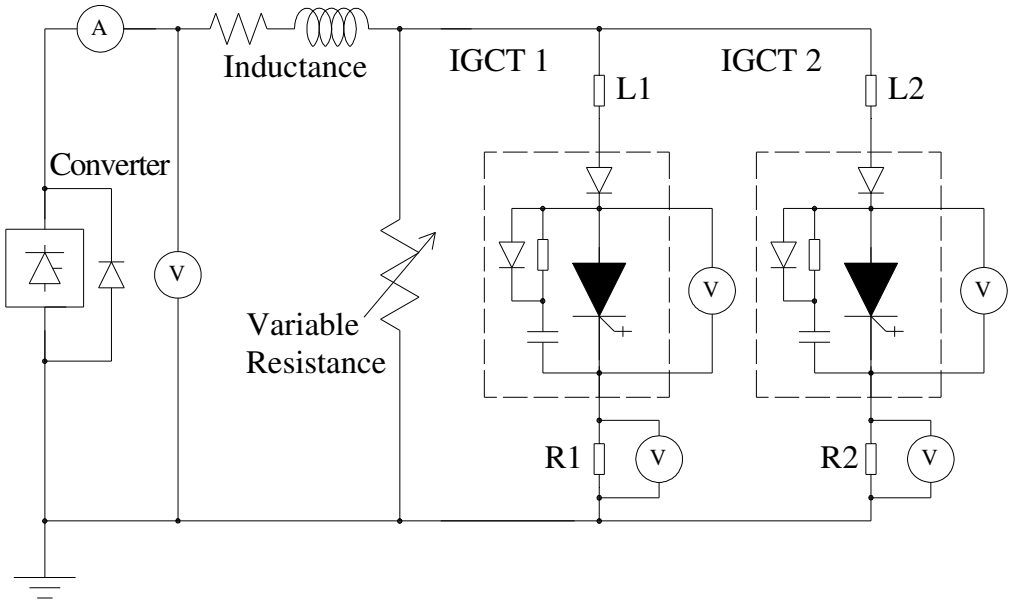

Figure 3.5 – *Circuit used to test the turn-on reliability of paralleled IGCTs*

3.1.3.2. Test results

More than one hundred pulses have been performed in order to explore the IGCT turning-on performance with different combinations of initial current and voltage values. The maximum converter current was 4 kA and the different resistance values set down to 2.5 mΩ allowed exploring the full range of voltage values interesting for this case, from several tens to few volts.

The typical waveforms of current and voltage during IGCT turn-on are reported in Figure 3.6; at the turn-on command, the voltage measured across the IGCT drops rapidly. The current and voltage shapes were very repeatable in the different pulses and no strange fluctuations were observed, proving the IGCT turn-on reliability.

With an applied voltage higher than about 2 V, the turn-on of both the IGCTs was always observed. On the contrary, in some pulses with an applied voltage lower than 2 V, there was a turn-on failure of both IGCTs and the current continued circulating through the resistor. It can therefore be stated that for the employed IGCTs an applied voltage larger than 2 volts assures a reliable turn-on of the devices.

The current commutation appears very slow (Figure 3.6); this is due to the low value of the voltage applied and to the inductance of the commutation path between the resistance and the IGCTs in this test circuit. This does not represent a problem for the IGCT, since at the time of IGCT turn-on the voltage drop across the IGCT rapidly

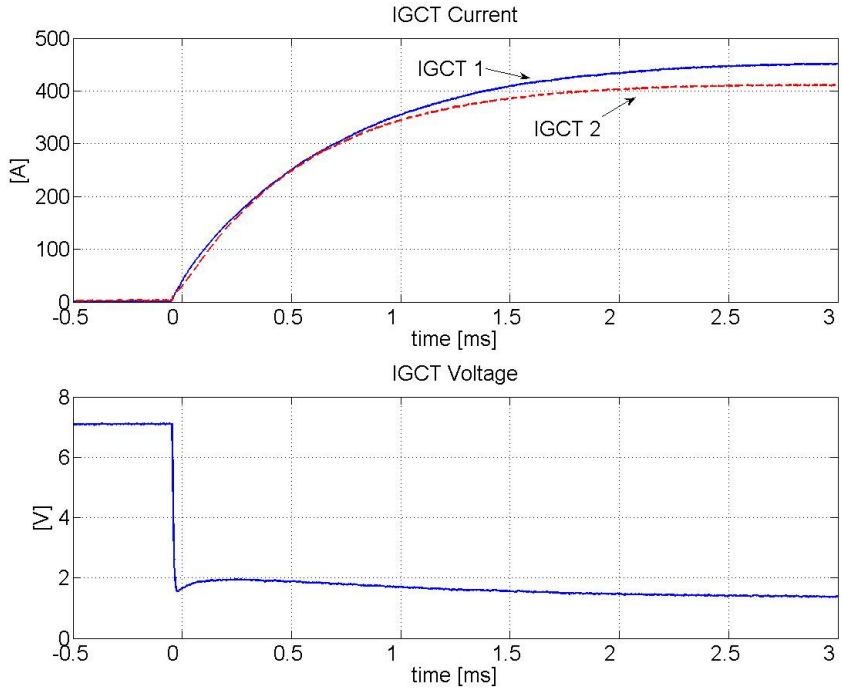

Figure 3.6 – *Typical IGCT current and voltage waveforms during turning-on*

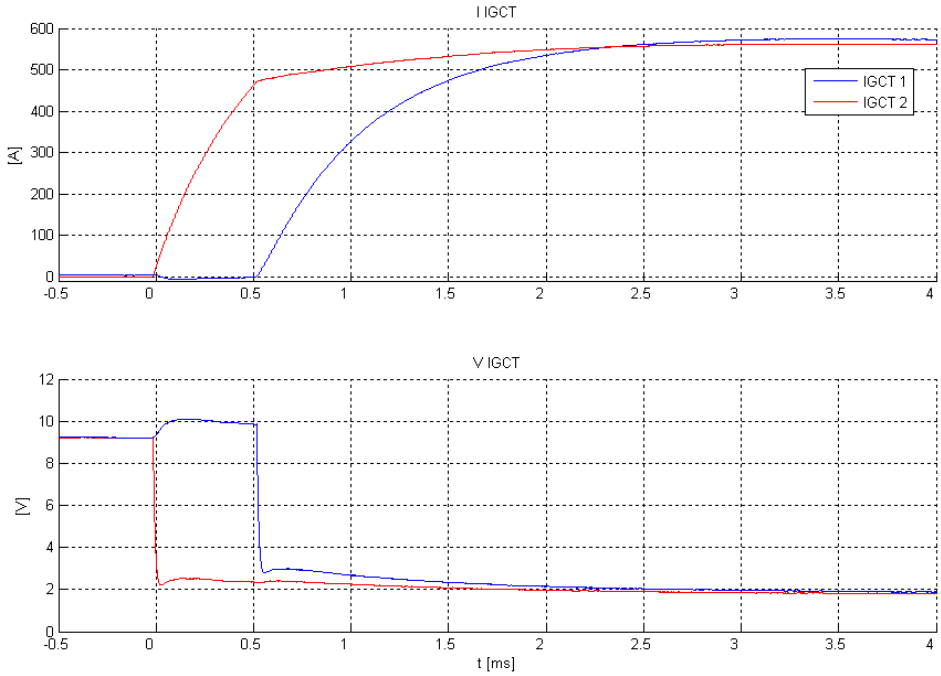

Figure 3.7 – *IGCT current and voltage waveforms in case of 500 μs delay between the turning-on commands*

decreases to the normal conduction values and therefore the power dissipation in the static components, obtained as product of the voltage and the current values, remains inside the normal conduction range. The duration of the current commutation is a parameter that influence the duration of the arc current across the mechanical BPS in the hybrid CB. Therefore particular care shall be taken in the design of the hybrid CB to minimize the inductance of the connections between the BPS and the IGCTs so as to reduce the duration of the current commutation and, consequently, of the BPS arc current as much as possible, but it is expected not to be much slower than some ms.

Some doubts could arise about the quality of the turn-on in terms of distribution of the current across the component area due to the low voltage applied, but the expected current commutation in the IGCTs of the hybrid CB should be sufficiently slow (some ms) to permit the redistribution of potential un-homogeneities during the current increase.

Finally, in order to prove the effectiveness of the combination of the snubber circuit with the blocking diode in making the two paralleled IGCTs independent of each other during turn-on, a delay (up to 500 μs) was introduced between the two turning-on commands of the IGCTs. A reliable IGCT turn-on was observed even in these cases, as shown in Figure 3.7, thus proving the robustness of the provision in assuring the component turn-on even in case of jitters, which could be caused both by differences among the semiconductor characteristics and by delays in the command generation.

3.1.3.3. Discussion

The carried out tests demonstrate that an applied voltage of few volts between cathode and anode is sufficient to assure a proper turn-on of IGCTs in parallel, thus proving the feasibility of a high-current hybrid CB based on IGCTs. Another important information provided by the results of these tests is that the BPS arc voltage, which should be of the order of some tens of volts, is sufficient to assure the turn-on even of several IGCTs stages in series, thus proving that this scheme can be implemented in applications with several kV of reapplied voltages.

The results suggest a comment also on the blocking diode provided in series for maintaining the voltage applied to each IGCT until it is turned-on: if few volts are enough, this level of voltage could be assured even by the small resistance inserted in series to each IGCT to improve current sharing among components and used for current measurement. In fact, even if a single IGCT starts to conduct before the others, its own voltage drop summed to the voltage drop of this additional resistance should provide a sufficiently high voltage to permit the safe turn-on also of the remaining IGCTs in parallel.

It is important however to point out that in the hybrid CB, the provision of the diode in series, of the additional resistances, even if in the order of some mΩ, as well as the insertion of inductances for current derivative limitation, can be neglected from the point of view of energy dissipation, since their conduction is limited to the short time interval of IGCT conduction.

3.1.4 IGCT Circuit Breaker Design Criteria

3.1.4.1. IGCT 5SHY 35L4512

A tentative design of the component number to be used for the static CB is performed considering the characteristics of the two types of selected IGCTs. In this section the sizing with IGCT 5SHY 35L4512 is considered, while the sizing with IGCT 5SHY 42L6500 is analyzed in the following section. With IGCT 5SHY 35L4512, the number of stages to be connected in series can be chosen assuming that the maximum reapplied voltage after current interruption on the static CB remains sufficiently below the repetitive peak off-state voltage; a safety factor of 70%, leading to a maximum reapplied voltage of 3 kV could be considered reasonable. This means that for toroidal QPCs, rated for a nominal voltage of 2.8 kV each paralleled IGCT branch can be composed of a single IGCT, while for poloidal QPCs, rated for a nominal voltage of 4.2 kV, it is necessary to connect in series two IGCTs for each paralleled branch.

The study of the number of paralleled components is generally worked-out considering the maximum interruptible current and the maximum i^2t value allowed by the selected component. The i^2t values reported in the IGCT datasheet are referred to half sinusoidal current waveforms; these data are not sufficient to evaluate the performance of the device with longer pulses at lower currents, typical of the considered application.

Therefore, a thermal model of the device has been set up and the junction temperature variation has been analyzed. It has been assumed that the IGCT maximum operating junction temperature T_{MAX} is 125 °C and the maximum interruptible current is equal to 6 kA. In order to minimize the number of paralleled static components it is convenient to optimize the quality of the current sharing and to exploit their maximum interruptible current; this can be achieved if the junction temperature increase is limited by shortening the IGCT conduction time.

3.1.4.1.1. Thermal Analysis

Generally the heat conduction processes can be modelled by an equivalent circuit consisting of R/C elements, as illustrated in Figure 3.8, where the heat is equivalent to the current, the thermal resistance and the heat capacity of each layer of the device correspond to the electrical resistance and capacitance, respectively, and the temperature increase of each layer is equivalent to the voltage across the corresponding capacitor.

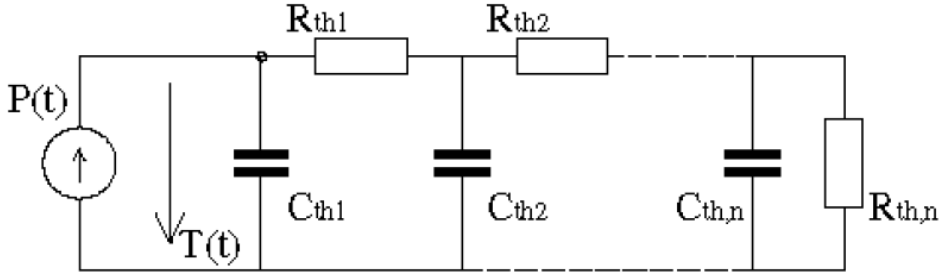

Figure 3.8 – *Equivalent electrical circuit modeling heat conduction*

When the component internal temperature distribution is not under investigation and only the junction temperature increase is of interest, the thermal impedance can be calculated with a simplified model using the partial fractional representation [32]

$$Z_{th}(t) = \sum_i R_i \left(1 - e^{-t/\tau_i}\right) , \tag{3.1}$$

where R_i and τ_i represent the thermal resistances and time constants, generally provided on the device data sheet. For both type of considered IGCTs these values for the junction-case (JC) layers are reported in Table 3.3. The values for the case-heatsink (CH) and heatsink-water (HW) layers depend on the selected heatsink: the ones reported in Table 3.3 have to be considered values resulting from the Consorzio RFX experience and are assumed for the following calculations. In any case the heatsink influence on junction temperature increase is relevant only for the temperature evaluation in a time period exceeding some seconds.

Table 3.3 – *Thermal resistances and time constants for IGCT 5SHY 35L4512 and IGCT 5SHY 42L6500 equipped with reference heatsink*

Layer	JC1	JC2	JC3	JC4	CH	HW
R_i [°C/kW]	5.562	1.527	0.868	0.545	3	5
τ_i [s]	0.5119	0.0896	0.0091	0.0024	4	8

This simple model seems adequate to estimate the evolution of the IGCT junction temperature in this application; in fact for conduction time of the order of 1 s, the approximation introduced considering constant the external temperature of the component is acceptable.

The thermal model for the IGCT 5SHY 35L4512 has been worked out using the thermal resistance and time constant values reported in Table 3.3. The time evolution of the IGCT junction temperature has been studied applying current steps to the IGCT thermal model, simulating the current commutation from the BPS, up to the IGCT maximum interruptible current of 6 kA. The obtained junction temperature evolutions for 1 s, starting from a room temperature T_{Room} = 25 °C, are reported in Figure 3.9. The upper curve shows that the maximum exploitation of the current interruption capability (6 kA) can be obtained only if the IGCT conduction time remains under 500 ms; in fact this assures not to exceed the maximum junction temperature T_{MAX} = 125 °C (red dashed line).

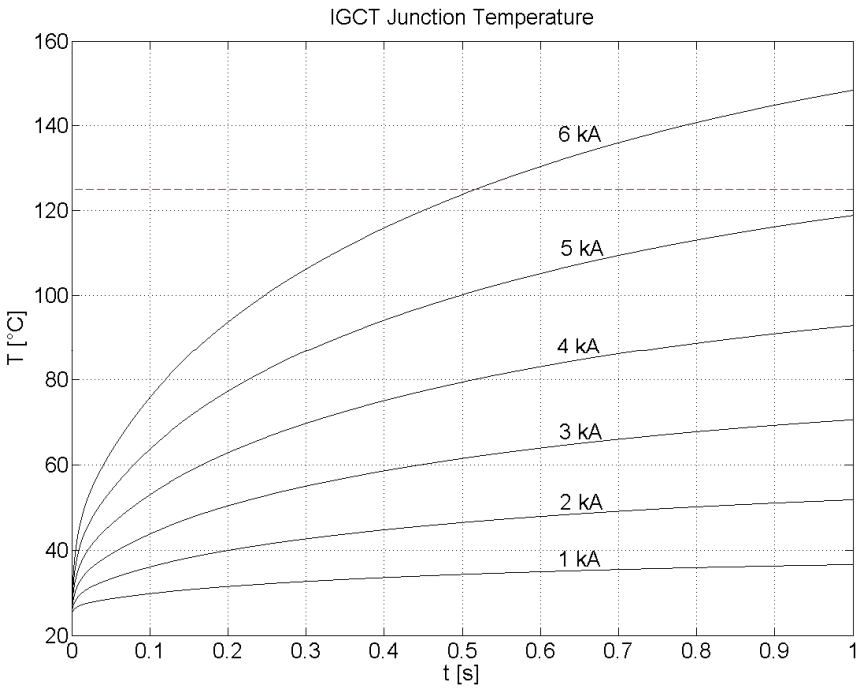

Figure 3.9 – *Time evolution of 5SHY35L4512 IGCT junction temperature with current steps up to 6kA*

The IGCT conduction time is determined by the BPS opening time (interval t_2 - t_4 in Figure 3.6); just to take a significant example, the BPS used in [20], tested for a current of 70 kA and a voltage of 24 kV, guarantees an opening time of about 450 ms at 70 kA, which is under the maximum IGCT conduction time that permits not to exceed T_{MAX}.

If a CB failure prevents the current from interrupting it is necessary to activate the pyrobreaker. The IGCT junction temperature keeps on increasing up to the pyrobreaker intervention, since the current is still flowing in the static components. It is therefore necessary to estimate the pyrobreaker intervention time to calculate the value of the maximum junction temperature reached. The opening time of a prototype pyrobreaker for ITER [33] allows very fast current interruption of the order of fractions of milliseconds; this pyrobreaker however is a prototype, therefore there is little experience on repeatability of its performances.

It is worthwhile to note that in case of pyrobreaker intervention the current interruption does not have to be performed by the IGCTs, therefore the components are not subjected to reapplied voltage and it is possible to accept that in such condition their junction temperature increases more than T_{MAX}. The junction temperature evolution corresponding to an IGCT current of 6 kA (upper curve in Figure 3.9) shows small derivatives for values exceeding T_{MAX}, therefore also if the sum of the times for the detection of the static CB failure and for pyrobreaker intervention led to a IGCT conduction time of 1 s, the junction temperature would remain under 150°C.

The precise definition of the temperature limits and of the necessary design margins are however matters to be defined by the manufacturers in phase of detailed design.

3.1.4.1.2. Sizing of IGCT CB

Assuming that the maximum operating junction temperature T_{MAX} = 125 °C must not be exceeded, the resulting number of IGCT 5SHY35L4512 to be connected in parallel, for each series stage, as a function of the current to be interrupted and of the IGCT conduction time, is reported in Figure 3.10.

3.1.4.2. IGCT 5SHY 42L6500

Analyses similar to the ones described in foregoing section have been repeated considering IGCT 5SHY 42L6500. With this component, assuming a safety factor of 70% on the repetitive peak off-state voltage, it results that a maximum reapplied voltage of 4.5 kV can be tolerated by a single component. Since the nominal voltages of toroidal and poloidal QPCs are 2.8 kV and 4.2 kV respectively, just one IGCT can be used for each paralleled branch.

In order to study the number of components to be connected in parallel, a thermal model for IGCT 5SHY 42L6500 has been developed, using the thermal parameters reported in Table 3.3.

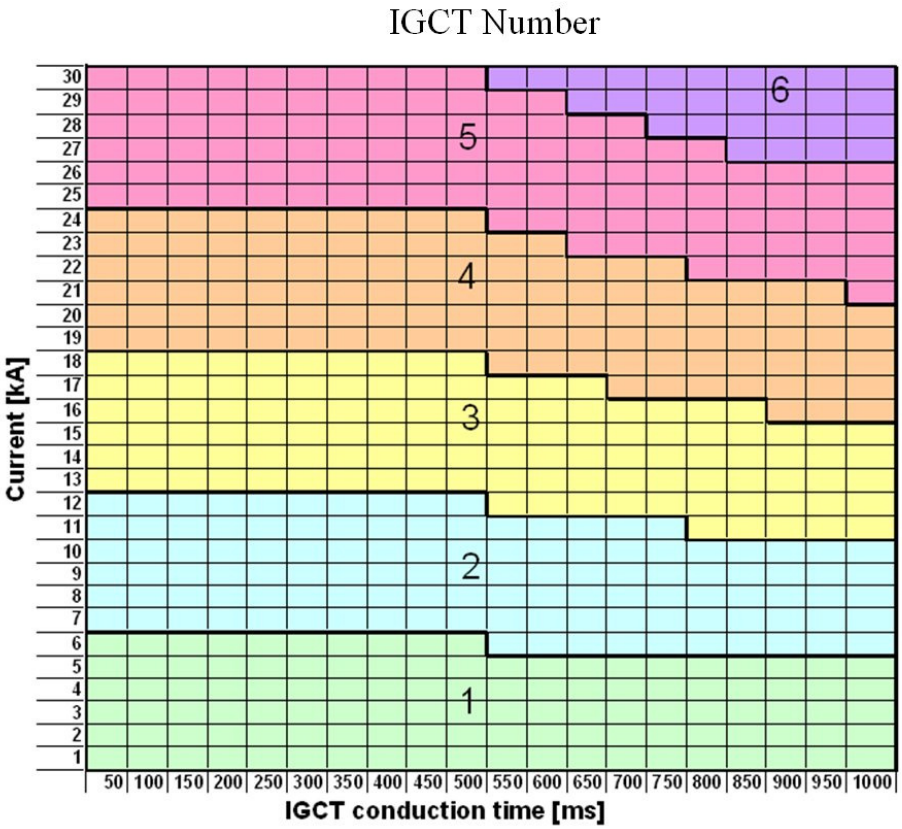

Figure 3.10 – *Number of 5SHY35L4512 IGCT to be connected in parallel depending on the current to be interrupted and on the IGCT conduction time*

The time evolutions of the IGCT 5SHY 42L6500 junction temperature, as resulting applying current steps to the IGCT thermal model, simulating the current commutation from the BPS, up to the IGCT maximum interruptible current of 6 kA, are reported in Figure 3.11.

It is clear that with IGCT 5SHY 42L6500 it is not possible to fully exploit the maximum interruptible current of 6 kA, unless the IGCT conduction time is reduced less than 70 ms. Unfortunately, this is not a viable solution with the considered mechanical switch technology. Therefore, considering an IGCT conduction time of 0.5 s it is necessary to limit the current in each IGCT under 3.7 kA to remain under the safety limit of 125 °C for the junction temperature.

Assuming that the maximum operating junction temperature T_{MAX} = 125 °C must not be exceeded, the resulting number of IGCT 5SHY42L6500 to be connected in parallel, for each series stage, as a function of the current to be interrupted and of the IGCT conduction time, is reported in Figure 3.12.

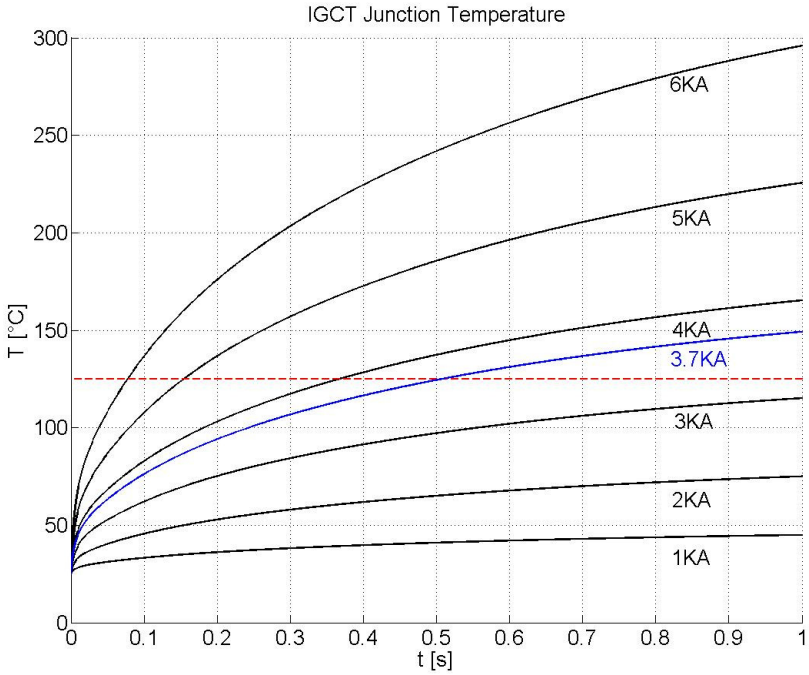

Figure 3.11 – *Time evolution of 5SHY42L6500 IGCT junction temperature with current steps up to 6kA*

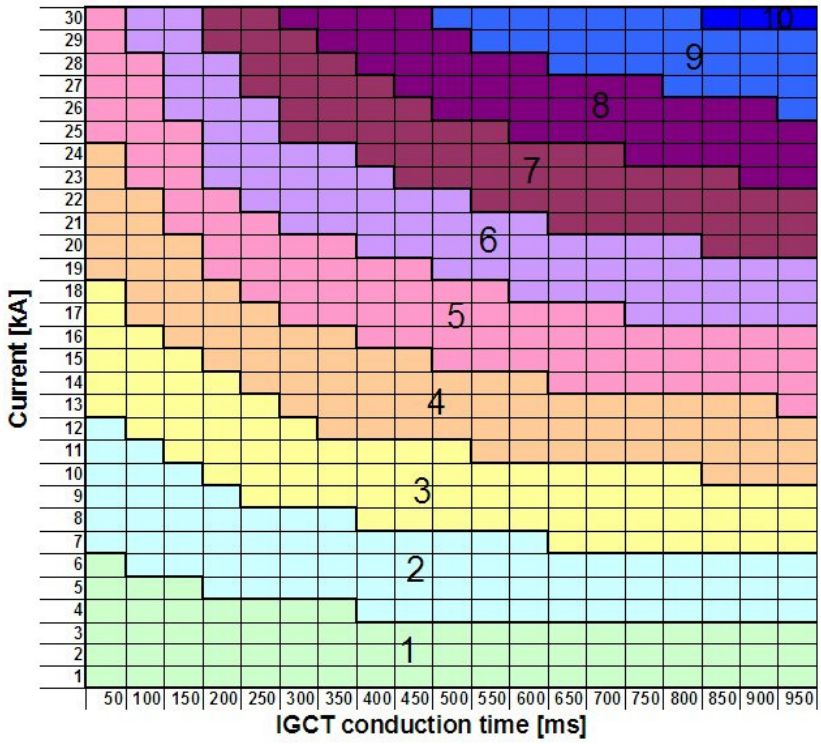

Figure 3.12 – *Number of 5SHY42L6500 IGCT to be connected in parallel depending on the current to be interrupted and on the IGCT conduction time*

3.1.5 Comparison between IGCT 5SHY 35L4512 and 5SHY 42L6500

The junction temperature increase of the IGCT 5SHY 42L6500 presented in Figure 3.11 is higher than the increase of IGCT 5SHY 35L4512 shown in Figure 3.9, with the same current applied. This does not depend on the thermal characteristics that are the same for the two IGCTs, as shown in Table 3.3, but on the threshold voltage and slope resistance characteristics that, as shown in Table 3.2, are higher for IGCT 5SHY 42L6500, resulting in an higher power dissipation during conduction.

In fact IGCT 5SHY 35L4512 belongs to the 35L4500 IGCT family, that is commercially available since some years. In particular IGCT 35L4512 is a component that, by means of special manufacturing techniques, has been optimized for reducing the conduction power dissipation, at the cost of having higher power dissipation at turn-on and turn-off if compared to the other devices of 35L4500 series. On the contrary IGCT 5SHY 42L6500 is a recently available component that has not been optimized in terms of conduction power dissipation. At present the manufacturer is studying the possibility of obtaining IGCTs with the same characteristics of the 42L6500 type, but with reduced threshold voltage and slope resistance.

3.1.6 Comparison Between Only Static and Hybrid CB

The major advantage of the hybrid CB in respect with a fully static design consists in the much lower on-state power losses. In fact the current conduction in the static components is limited to short time intervals, reducing their energy dissipation. The same reason allows also the insertion in the hybrid solution of additional devices, such as inductances for limiting current derivative or series connected resistances for improving current sharing, which would represent an undesirable source of power dissipation in the fully static CB.

An additional benefit introduced by the hybrid solution, at least the one using IGCT 5SHY35L4512, is that it allows taking maximum advantage of the potentialities of high turn-off current values of large area semiconductors, minimizing the number of paralleled components.

In fact in [34] it was proved that the power losses in steady state operation are the major constraint in sizing a fully static circuit breaker. This means that the number of paralleled components is not a function of the maximum current to be interrupted during circuit breaker opening, but it has to be selected on the basis of the steady state current value following thermal constraints, in order to keep the device junction temperature under a reasonable safety value in normal operation. In the case of fully static circuit breaker it is not possible to exploit the SOA of the static devices: for the IGCT 5SHY 35L4512 a steady state current value of 3.3 kA is sufficient to reach the maximum junction temperature of 125 °C. As a consequence it is not possible to exploit the IGCT maximum interruptible current value of 6 kA obtainable with a suitable snubber circuit.

A comparison between the static and the hybrid CB was made, in order to quantify the saving in terms of number of components allowed by the latter configuration. Given a certain dc current value and assuming a value of reapplied voltage compatible

Table 3.4 – *Number of 5SHY35L4512 IGCTs to be connected in parallel for each stage connected in series*

	Rated Current [kA]					
	5	**10**	**15**	**20**	**25**	**30**
Static	2	4	5	7	8	10
Hybrid	1	2	3	4	5	5

with a single series component, a BPS opening time smaller than 500 ms and an ambient temperature of 25°C, the number of IGCTs to be connected in parallel for the "static" and "hybrid" design has been summarized in Table 3.4.

As concern the power losses in normal operation, in the hybrid design they are only due to the BPS resistance that, for mechanical switches, can be assumed smaller than few micro Ohm. Assuming for instance a BPS resistance of 5 μΩ and a steady state current of 30 kA, the hybrid implementation during normal operation would dissipate only 4.5 kW while the constant power dissipation of the fully static implementation would result in 53 kW for every stage of paralleled IGCTs, excluding the contribution of the diodes and resistors in series. If the voltage rated value requires the series connection of more IGCT stages, the resulting power loss in normal operation becomes a multiple of the aforementioned value for the fully static CB, while it presents no variations for the hybrid solution.

3.1.7 Design of the Hybrid CB for the JT-60SA QPC

3.1.7.1. The Poloidal QPC

The poloidal QPC shall be rated for a nominal current of 20 kA, with a maximum interruptible current of 21 kA. The nominal value of the dump resistor 0.21 Ω determines a nominal reapplied voltage of 4.2 kV. It means that it is necessary to use two stages of IGCT 5SHY 35L4512 connected in series, while one single stage of paralleled 5SHY 42L6500 IGCTs can be considered as safely sufficient for holding the reapplied voltage (safety factor of 1.5%).

As analyzed in previous sections the number of paralleled IGCTs depends on the BPS opening time. Assuming an opening time of 300 ms for the BPS, from Figure 3.10 and Figure 3.12 it results that the number of paralleled IGCTs not to exceed the maximum junction temperature of 125°C is 4 for the IGCT 5SHY35L4512, and 5 for the IGCT 5SHY 42L6500.

In summary it results that for the poloidal QPC the minimum number of IGCTs to be connected in series and in parallel is 8 using IGCT 5SHY35L4512 and 5 using IGCT 5SHY 42L6500.

Since poloidal QPC shall be able to interrupt bidirectional current, two possibilities should be considered, as shown in Figure 3.13: the use of a diode rectifier bridge, allowing the use of a unidirectional static circuit breaker (right panel) or the use of a bidirectional static circuit breaker (left panel). This latter option would imply to

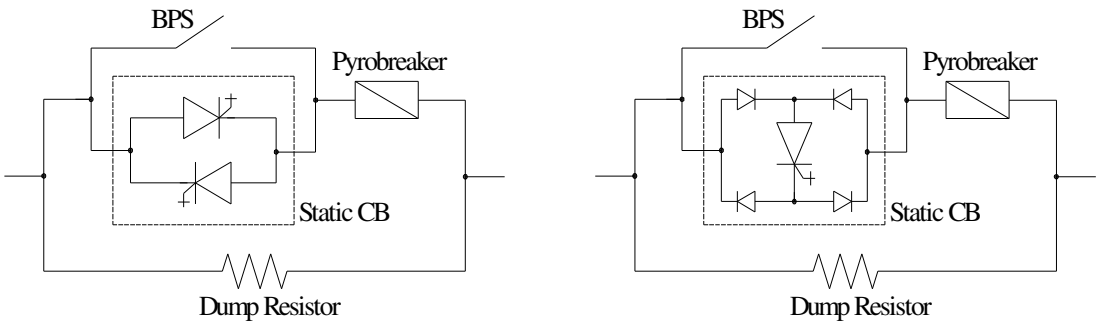

Figure 3.13 – *Simplified hybrid reference scheme of the QPCs for the poloidal circuits with bi-directional Static CB (left) or with unidirectional Static CB with diode bridge (right)*

double the total number of employed IGCTs, since it is necessary to connect in anti-parallel a sufficient number of IGCTs for interrupting negative current.

3.1.7.2. The Toroidal QPC

The toroidal QPC shall be rated for a nominal current of 25.7 kA. Three QPC units are inserted in the toroidal circuit of JT-60SA, so as to reduce the voltage applied across the coils. The value of 0.11 Ohm for the dump resistors determines a reapplied voltage of 2.8kV. This voltage permits to use just one stage of paralleled IGCTs, both considering IGCT 5SHY35L4512 and IGCT 5SHY 42L6500: in the first case the safety factor would be 1.6 and in the latter case it would be 2.3.

Assuming also for the toroidal QPC BPS an opening time of 300 ms, from Figure 3.10 and Figure 3.12 it results that the number of paralleled IGCT not to exceed the maximum junction temperature of 125 °C is 5 using IGCT 5SHY35L4512 and 7 using IGCT 5SHY 42L6500.

3.2 Pyrobreaker

The Pyrobreaker is a back-up protection which shall be operated in case of failure of the Hybrid CB. The Pyrobreaker consists in an explosively actuated CB, with characteristics of high reliability, since it represents a backup element of a protective device.

The main characteristics of the pyrobreaker for the QPCs of JT-60SA are shown in Table 3.5.

At present, two technical solutions are available for the construction of a pyrobreaker rated for the values of Table 3.5: the first is a commercial product, named “Is-limiter” [35], generally used for the protection of short-circuits in medium voltage distribution systems, the second one is a prototype [33] built by the Efremov Institute (St. Petersburg) for ITER experiment. Both solutions have pros and cons, including economical aspect, therefore the decision of which one will be employed for the QPCs

shall be taken by the manufacturer during the phase of detailed design. In the following paragraphs the main characteristics of both solutions are described.

Table 3.5 – *Main characteristics of QPC pyrobreaker*

Characteristics	Toroidal QPC Pyrobreaker	Poloidal QPC Pyrobreaker
Nominal current	25.7 kA	20 kA
Maximum interruptible current	25.7 kA	22.5 kA
Maximum reapplied voltage	2.8 kV	5 kV
Maximum intervention time	0.5 s	0.5 s

3.2.1 The Is-limiter Pyrobreaker

The Is-limiter pyrobreaker consists in principle of an extremely fast switch, able to carry a high rated current but having a low switching capacity, and a high rupturing capacity fuse arranged in parallel. In order to achieve the desired short opening time, a small explosive charge is used for opening the switch main conductor. When the main conductor is opened, the current continues to flow through the paralleled fuse, where it is limited within fraction of milliseconds and then finally interrupted. The normal current path and the path of current after opening the main conductor are shown in Figure 3.14.

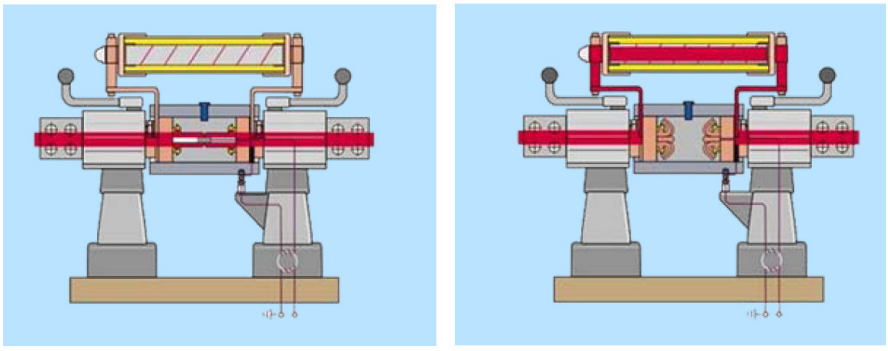

Figure 3.14 – *Main phases of Is-limiter pyrobreaker intervention: before intervention (left) and after explosion (right)*

There are available Is-limiters rated for a nominal current of 4kA and a rated voltage of 12kV. Since the current to be interrupted for the QPC of JT-60SA is higher than the nominal current, it is necessary to connect in parallel a number of Is-limiters sufficient to not exceed the rating of the device. This is possible and has already done in other applications [36], but could lead to a reduction of the pyrobreaker reliability, due to the fact that each parallel connected Is-limiter has to work without failure in order to perform a complete current interruption.

Another issue associated to the use of Is-limiter is the fact that current interruption is performed by the fuse connected in parallel to the main conductor, that operates according to its time-current characteristic curve. This means that with low value current there is the possibility that the fuse requires a long time to melt, with the extreme case that it never operates in presence of very low current. This aspect shall be taken into account for the selection of the fuse to be integrated inside the Is-limiter, since its nominal current, i.e. the current under which no fuse melting is expected, shall be compatible with the requirements of protection of the coils.

Nonetheless, the fact that the Is-limiter is a commercial product with many examples of industrial applications represents a good point in its favour.

3.2.2 The Efremov Laboratory Pyrobreaker Prototype

In the design of components for ITER, the development of a pyrobreaker rated for a nominal current of 60 kA, reapplied voltage of 17.5 kV and opening time of 0.2 ms was based on the large experience existing at the Efremov Institute (St Petersburg) in this field.

The pyrobreaker developed [33] is a very reliable, single action (with replaceable parts) component triggered by a pyrocharge. It consists of two parts, operated with separate explosive charges, that are triggered together (by one signal). The first part is a multigap pyrobreaker able to interrupt the current under high (up to 20 kV) voltage; the second is a disconnector able to withstand this voltage for long time. The current interruption is based on multi-cuts of a thin copper cylinder cooled by water which helps also to extinguish the arc which appeares when the cylinder is being destroyed by the charge explosion.

All planned tests have been performed: minor modifications have been made in steps to further improve the performance. In the final test, 30 pulses with current commutation at 66 kA were performed successfully.

The same technology could be used for the realization of the JT-60SA QPC pyrobreakers, that are rated for values well under the ones required by ITER. The advantage of this solution is that only one device would be used, without the need for connecting more devices in parallel. Anyway this is a prototype pyrobreaker which reliability should be further assessed.

3.3 Dump Resistor

Table 3.6 – *Main characteristics of Dump Resistors*

Characteristics	Toroidal QPC Pyrobreaker	Poloidal QPC Pyrobreaker
Nominal value	0.11 Ω	0.21 Ω
Maximum current	25.7 kA	22.5 kA
Maximum voltage	2.8 kV	5 kV

The dump resistors shall be able to dissipate the magnetic energy stored in the magnets.

The main characteristics of resistors for JT-60SA QPC are shown in Table 3.6.

3.3.1 The Toroidal Dump Resistors

For the toroidal QPC the nominal energy is well defined, since the dump resistance of toroidal circuit is composed of 3 resistors with a nominal value of 0.11 Ω connected in series. Therefore the maximum energy to be dissipated in each resistor is approximately 350 MJ, that is one third of the magnetic energy stored in the toroidal coils.

The toroidal dump resistors will be located in a semi-outdoor environment, therefore no particular constraints related to heat dissipation are applicable: the mass of conductor composing resistors shall be selected so that no excessive overtemperature is reached with the nominal energy. Assuming to use AISI 310 as material for the resistors, and to limit the maximum over-temperature under 200 °C, considering as adiabatic the resistor heating, the resulting mass of each resistor is m_{AISI} = 3500 kg.

3.3.2 The Poloidal Dump Resistors

For the poloidal QPC the nominal energy that has to be dissipated in each resistor depends on the inductance of the coil considered and on the maximum current of 20 kA, as shown in Table 3.7. Poloidal coils are mutually coupled, therefore it is necessary to take into account also the magnetic energy associated to mutual inductances. In the worst case (not realistic) with 20 kA in all coils simultaneously, the stored energy could reach very high values. A more realistic estimate of the stored energy value can be obtained considering different sets of coil current values obtained from plasma equilibrium scenarios (snapshots), as already discussed in Chapter 2.

Moreover it has to be taken into account that in case of mis-operation of the QPC Circuit Breaker the pyrobreaker is activated. This implies that in the faulty circuit the dump resistor is inserted with a delay that can reach up to 0.5 s; due to the mutual coupling with the other coils where the current is decreasing, the current flowing in the faulty circuit increases, raising the energy to be dissipated by the dump resistor.

The maximum values of stored energy obtained considering more than 300 realistic snapshots and taking in consideration the possibility of pyrobreaker intervention is shown in Table 3.7.

The values of dump resistor nominal energy showed in Table 3.7 have been selected in order to group them into three classes for practical purposes (namely type A 70 MJ, type B 100 MJ and type C 200 MJ), taking a good margin in respect with the energy value obtained considering the mutual inductance, the pyrobreaker intervention and the probable coil current values from the snapshots.

Table 3.7 – *Poloidal Dump Resistor energy values*

Coil	Energy without mutual inductance and 20kA [MJ]	Energy with mutual inductance, snapshots [MJ]	Energy with mutual inductance, 20kA in all poloidal coils [MJ]	Dump Resistor Nominal Energy [MJ]
CS1	59.7	39.1	99.9	70
CS2	59.7	85.1	111.8	100
CS3	59.7	92.5	112.1	100
CS4	59.7	49.0	100.7	70
EF1	110.2	135.2	212.6	200
EF2	95.5	105.0	178.3	200
EF3	67.1	28.4	104.3	70
EF4	127.3	92.1	209.5	200
EF5	75.0	47.2	160.9	100
EF6	143.2	137.8	292.2	200

Assuming to use AISI 3010 as material and considering as adiabatic the heating of the resistors during the dissipation of the energy, in order to limit the over-temperature under $\Delta T = 200°C$ the mass for the three types of resistors has to be selected according to Table 3.8.

Table 3.8–*Poloidal Dump Resistor mass values*

Coil	Resistor Type	Nominal Energy [MJ]	Mass [kg]
CS1	A	70	700
CS2	B	100	1000
CS3	B	100	1000
CS4	A	70	700
EF1	C	200	2000
EF2	C	200	2000
EF3	A	70	700
EF4	C	200	2000
EF5	B	100	1000
EF6	C	200	2000

3.3.2.1. The Poloidal Resistor Cooling

The dump resistors of poloidal QPCs of JT-60SA will be located in different power supply rooms, as shown in Table 3.9, which include other power supply equipments. It is necessary to evaluate if the increase of room temperature due to the energy dissipation of dump resistors exceeds the maximum allowed indoor temperature.

The characteristics of the ventilation system of the rooms are shown in Table 3.10.

Table 3.9 – *Poloidal QPC location*

QPC	Room
CS1, CS4, EF1, EF2, EF3, EF4, EF5, EF6	Rectifier Room
CS2, CS3	VCB Room

Table 3.10 – *Air ventilation system characteristics*

Rooms/Areas	Room volume	Ventilation	Max indoor temperature
Rectifier room	22608 m^3	414000 m^3/h	40 °C
VCB room	10689 m^3	69140 m^3/h	40 °C

In order to evaluate the variation of the room air temperature, a simplified thermal model of the dump resistor has been developed, as shown in Figure 3.15, where C_R is the thermal capacity of the resistor, R_{CONV} is the thermal resistance of the heat flow between the dump resistor and the room air, C_{AIR} is the thermal capacity of the air inside the room, R_{AIR_OUT} is the thermal resistance of the heat flow between the room air and the external air and T_{AIR_OUT} is the temperature of the external air. The simplified thermal model has been obtained under the assumption that the resistors are built as "open frame" structures able to dissipate the heat directly into the room air, without being enclosed inside cubicles limiting heat dissipation.

The resistor thermal capacity has been calculated as the resistor mass multiplied by the specific heat of stainless steel. The thermal resistance R_{CONV} has been calculated as:

$$R_{CONV} = \frac{1}{\alpha_{air} \cdot A_{\mathrm{Re}\,sistor}}, \tag{3.2}$$

where α_{air} is the convection coefficient assumed as 15 W/m^2K and $A_{Resistor}$ is the resistor surface.

In order to have an indicative estimation of the resistor heat exchange surface a tentative geometrical design of the resistors has been worked out, considering that they are composed of a number of rectangular cross section bars connected in series. For each resistor the bar length and cross section have been calculated so that the resistor has the nominal value of 0.21 Ω and the total mass has the nominal value of Table 3.8.

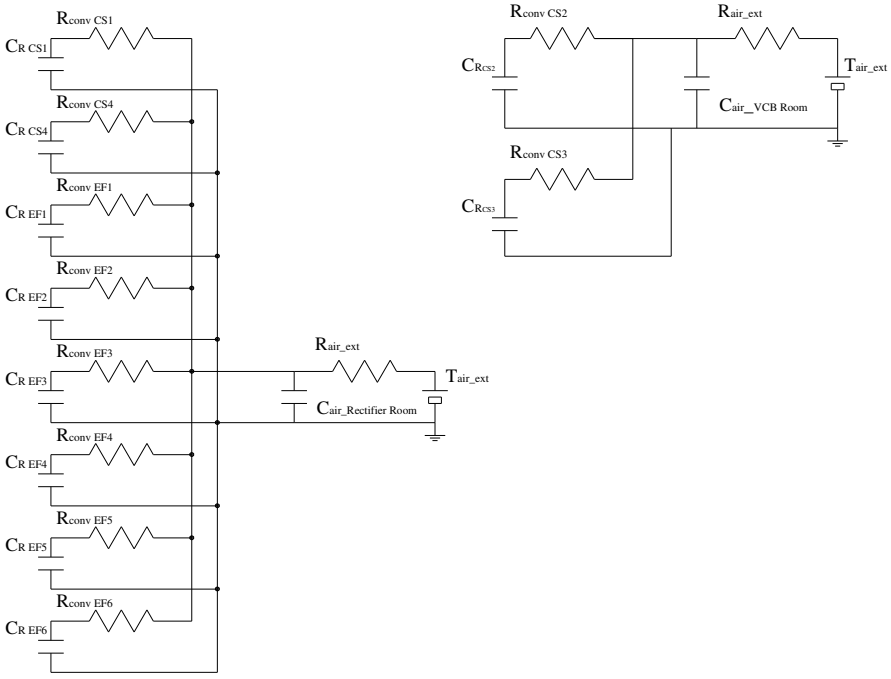

Figure 3.15 – *Simplified thermal model of dump resistors*

The air room heat capacitance and the heat flow resistance between the air room and the external room depend on the considered room. The calculation can be made using the following formulas:

$$C_{air} = m_{air\_room} \cdot cs_{air}$$
$$R_{air\_out} = \frac{1}{\frac{\partial m_{air}}{\partial t} \cdot cs_{air}} \tag{3.3}$$

The values shown in Table 3.11 have been used for the calculation.

Table 3.11 – *Thermal capacity and resistance values*

	Type A	Type B	Type C
C_R [MJ/K]	0.35	0.5	1
R_{CONV} [K/W]	1.826×10^{-3}	1.289×10^{-3}	0.649×10^{-3}
$C_{Air\ Rectifier\ Room}$ [MJ/K]	27.37		
$R_{Air\ Rectifier\ Room}$ [K/W]	7.18×10^{-6}		
$C_{Air\ VCB\ Room}$ [MJ/K]	12.94		
$R_{Air\ VCB\ Room}$ [K/W]	43.0×10^{-6}		

Assuming that the values of the room air initial temperature and of the external air temperature are 25 °C, the time evolution of the temperatures of the resistors and of the air inside the room can be calculated with the simplified model, considering that each dump resistor has an initial temperature that depends on the energy it dissipates.

Considering that each dump resistor dissipates its nominal energy, the resulting resistor temperature and room temperature waveforms are shown in Figure 3.16 and Figure 3.17.

In the most probable case that each resistor dissipates the energy values corresponding to column 2 of Table 3.7, the resulting resistor temperature and room temperature waveforms are shown in Figure 3.18 and Figure 3.19.

Finally the not realistic case of all coils with 20 kA, corresponding to the energy values of column 3 of Table 3.7 has been analyzed. The resulting resistor temperature and room temperature waveforms are shown in Figure 3.20 and Figure 3.21.

The results obtained in the three analyzed cases are summarized in Table 3.12.

3.3.2.2. Discussion of results

The obtained results demonstrate that the air room over-temperature never exceeds 9°C, nor in the unrealistic case of a 20 kA current in all poloidal coils. Moreover the time to restart with another pulse after QPC intervention, evaluated as the time to cool down the dump resistor temperature below 50 °C, never exceeds 1700 s, fulfilling the QPC operational requirements.

It is worthwhile to stress that the results have been obtained considering that the initial room temperature and the external air temperature are 25 °C. It is clear that in case of higher initial room temperature the maximum air temperature reached in the rooms will be higher and that in case of higher external air temperature the resulting time to restart with another pulse after QPC intervention will be longer.

Table 3.12 – *Results obtained in the three analyzed cases*

	Rectifier Room		**VCB Room**	
	Max air temperature [°C]	Time to cool the resistors under 50°C [s]	Max air temperature [°C]	Time to cool the resistors under 50°C [s]
Case 1: Nominal energy	32	1500	30	1500
Case 2: Energy from snapshots	29	1200	29.5	1400
Case 3: 20kA in all the coils	34	1700	31	1500

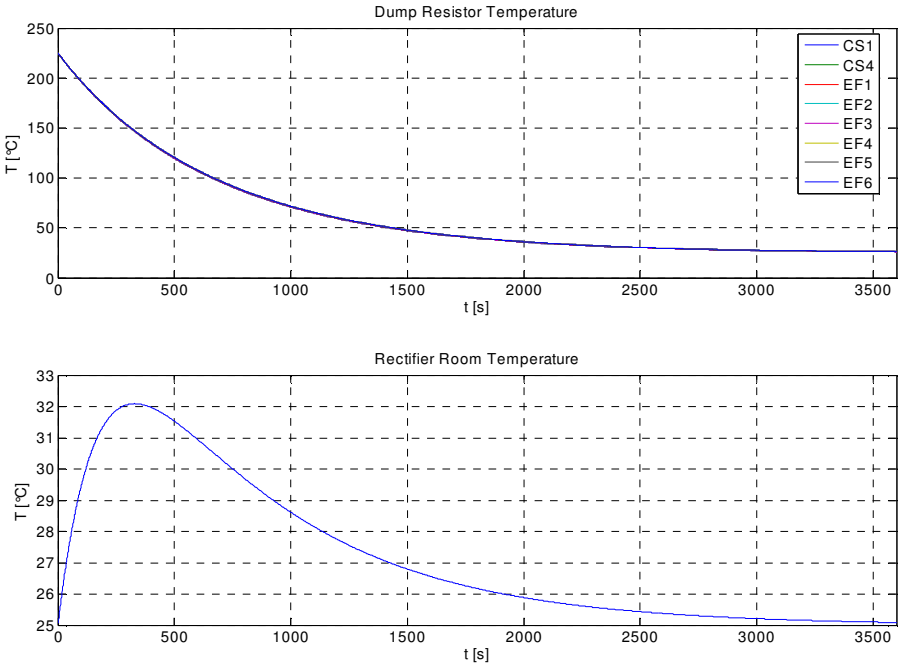

Figure 3.16 - *Temperature of the resistors and of the air in Rectifier Room with dump resistor nominal energy*

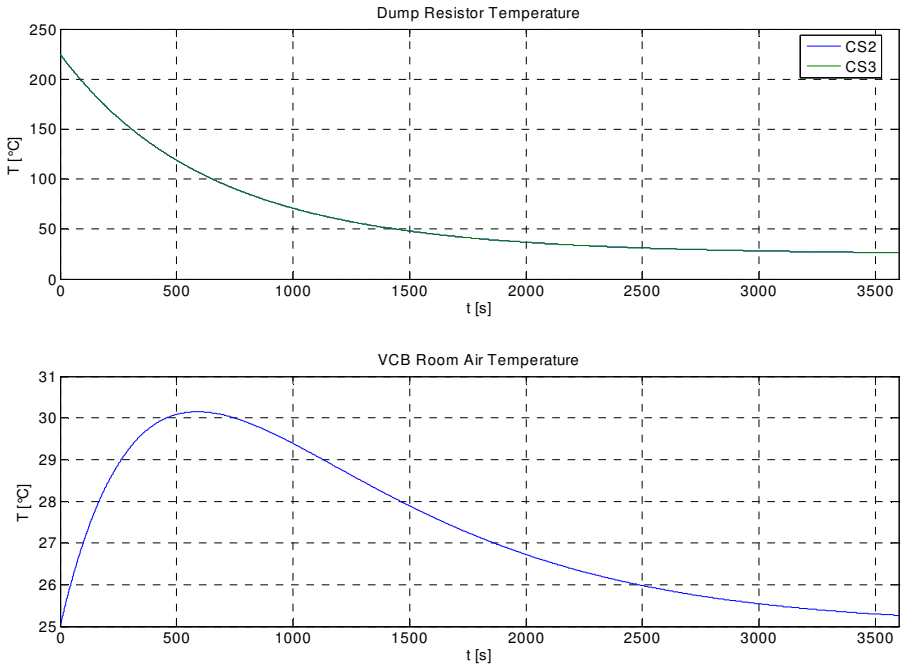

Figure 3.17 - *Temperature of the resistors and of the air in VCB Room with dump resistor nominal energy*

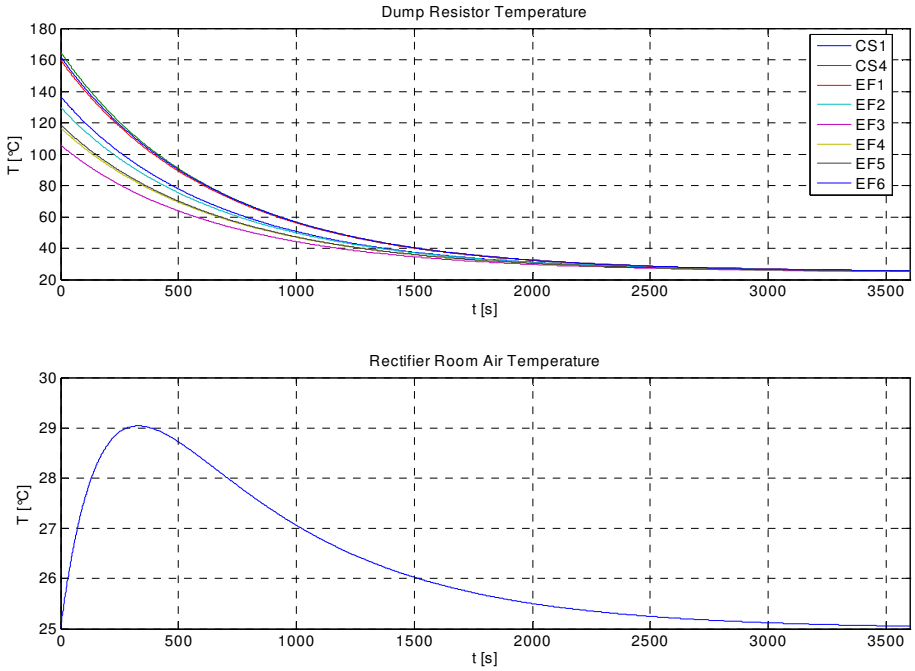

Figure 3.18 - *Temperature of the resistors and of the air in Rectifier Room with dump resistor energy obtained from snapshots*

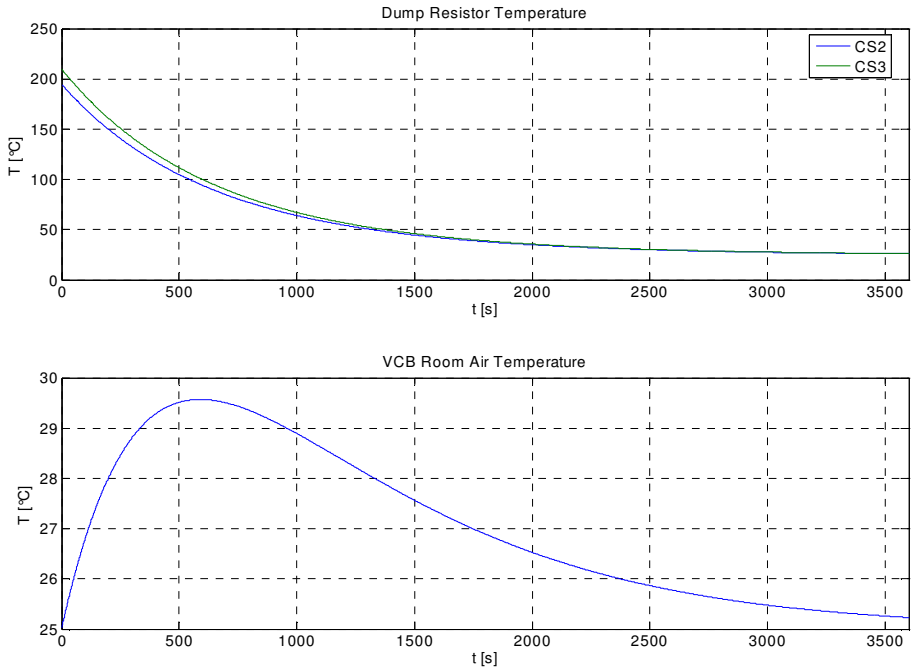

Figure 3.19 - *Temperature of the resistors and of the air in VCB Room with dump resistor energy obtained from snapshots*

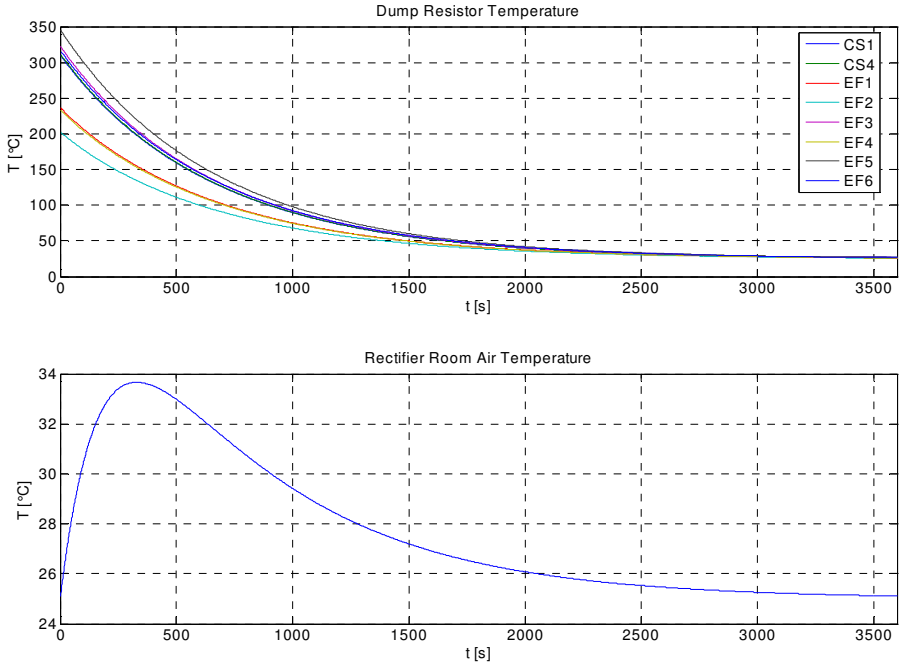

Figure 3.20 - *Temperature of the resistors and of the air in Rectifier Room in case of 20kA current in all coils*

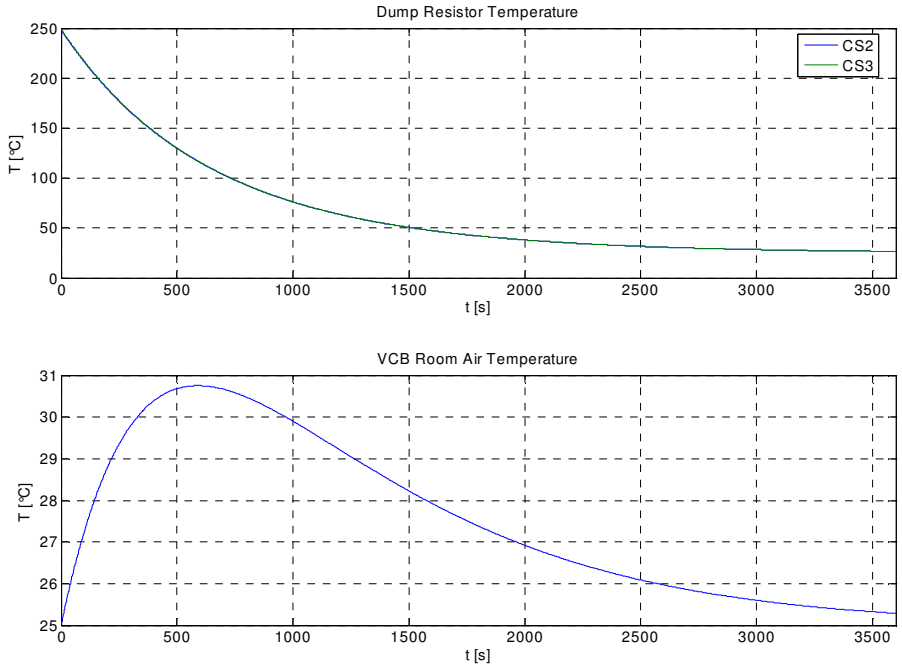

Figure 3.21 - *Temperature of the resistors and of the air in Rectifier Room in case of 20kA current in all coils*

CHAPTER 4

4. QPC Hybrid Mechanical-Static Circuit Breaker Prototype

4.1 Reasons for developing a Prototype

The most innovative part of the QPC is represented by the Hybrid Mechanical-Static Circuit Breaker. In fact the combination of a mechanical By-Pass Switch (BPS) with a IGCT static Circuit Breaker (CB) has never been used for conducting and interrupting high current values up to the values needed for the QPC of JT-60SA.

An open issue resulting from the integration of the mechanical BPS and the static CB technologies refers to the reliability of current commutation between the two elements.

The correct operation of the Hybrid CB requires that the voltage of the arc current appearing at the BPS terminals when it starts opening is able not only to turn-on the IGCTs connected in parallel, but also to drive the complete current commutation from the BPS to the static devices. In fact, as the current is increasing in the Static CB, also the voltage drop across it will increase and there is not enough confidence that the arc voltage is sufficient to complete the current commutation process.

No experience is available on this field: as presented in Chapter 3, some experimental tests have been successfully performed using two IGCTs connected in parallel to a resistor, but they were mainly aimed at evaluating the possibility of having a safe turn-on of more paralleled IGCTs with low voltage applied, so as to assess the feasibility of the hybrid CB concept based on IGCT technology.

Therefore, the study of the behaviour of the arc voltage and of the current commutation represents a key point for the assessment of the reliability of the hybrid CB operation, that can be suitably investigated only by means of experimental tests.

For these reasons it has been decided to develop a prototype of the QPC Hybrid CB, whose operation will permit to gain experience on the current commutation from the mechanical BPS to the Static CB and to test the reliability of such technical solution, possibly learning how to improve it.

4.2 The Prototype

A prototype of the QPC Hybrid CB has been set up at Consorzio RFX connecting in parallel a mechanical BPS and a static CB based on IGCT technology.

4.2.1 The Mechanical BPS

The Mechanical BPS used for the prototype is shown in Figure 4.1. This is the mechanical BPS used for ITER tests [20]. It is rated for a nominal current of 60 kA dc continuous and a nominal voltage of 17.5 kV. It is provided with 12 contacts, 6 of them located in the upper part and the remaining 6 in the lower part. Each contact consists in a main contact in parallel to a sacrificial contact. The main contacts have a lower contact impedance, therefore when the BPS is closed the majority of the current passes through them. When the BPS is commanded to open, the opening of sacrificial contacts requires a time longer than the opening of the main contacts. This means that when the BPS is opening the current commutates from the main contacts to the sacrificial contacts and the arc is formed across the latter ones. This permits to operate

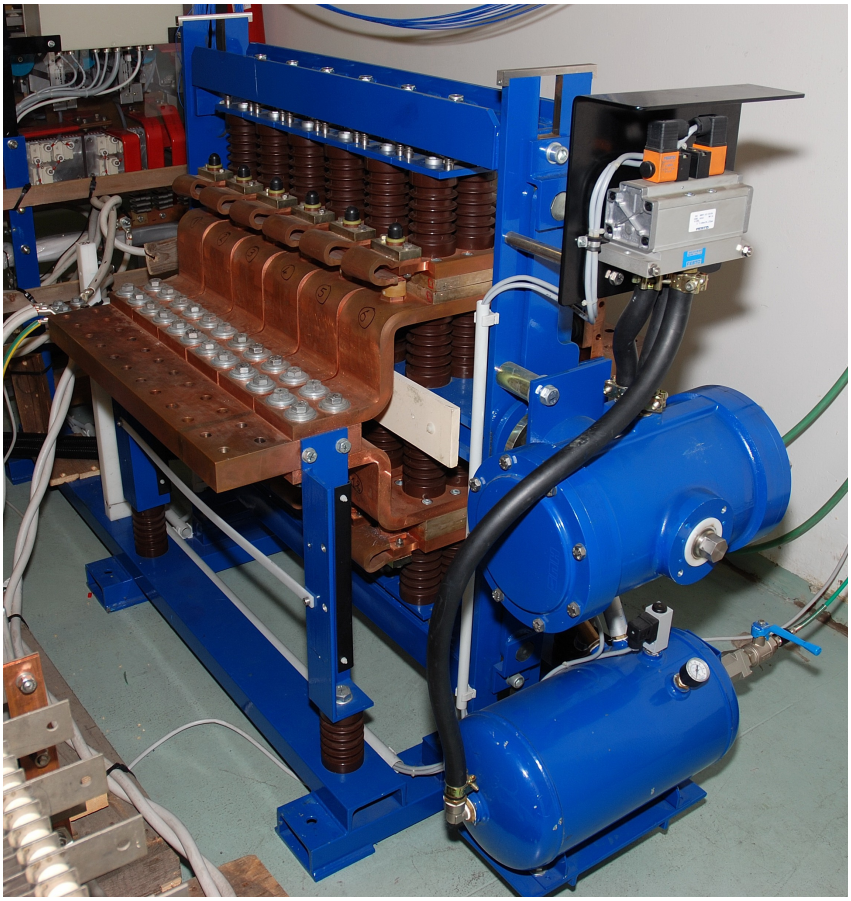

Figure 4.1 – *Picture of the BPS used for the Hybrid CB prototype*

the BPS preserving the main contacts and the routine maintenance can be performed only on the sacrificial contacts, with a save of money and time.

The whole resistance of BPS in closed status is less than 1 μΩ.

The BPS is opened by a pneumatic actuator, operating at a pressure of 6 bar. The delay between the opening command and the beginning of the opening is about 230 ms. This delay is due to the pneumatic actuator and to the mechanical inertia of the BPS (the total weigth of the BPS is about 2000 kg). When the distance between contacts is about 20 mm a micro-switch commutates its position, signaling the BPS open status. This happens about 350 ms after the opening command. Finally, about 450 ms after the opening command, the BPS is completely opened with a contact distance of about 50 mm.

4.2.2 The Static CB

The Static CB used for the prototype, showed in Figure 4.2, is a static current interruption module supplied by Ansaldo for the toroidal circuit of RFX [29].

It is composed of 3 paralleled IGCT 5SHY32L4512, provided with snubbers for current derivative limitation during turn-on and voltage clamp during turn-off. A diode for blocking inverse voltage is connected in series to each IGCT.

The Static CB is able to interrupt unidirectional dc current up to 10kA, with a

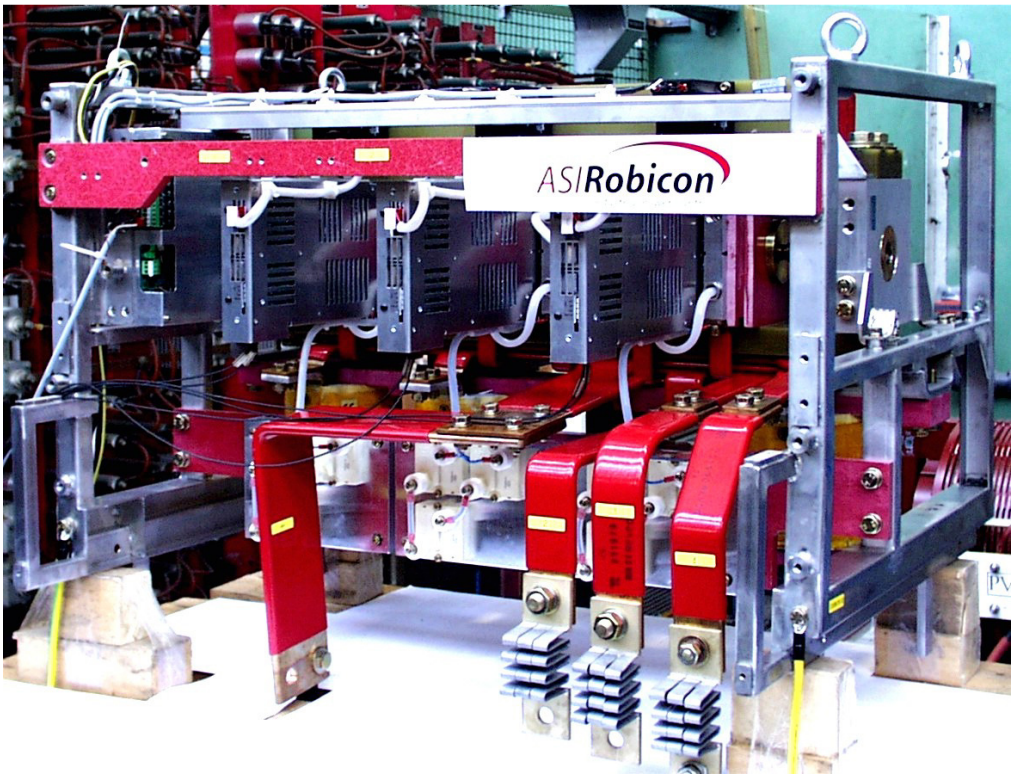

Figure 4.2 – *Picture of the static circuit breaker used for the Hybrid CB prototype*

maximum voltage of 4 kV (maximum no load voltage without commutation). It is designed for a duty cycle of 0.5 s every 10 minutes.

The current in each IGCT can be measured by means of shunt resistors that have also the aim of assuring a good current sharing between the three devices.

4.3 The Test Circuit

A test circuit for operating the Hybrid CB prototype has been set up at the Consorzio RFX laboratory. A simplified scheme is shown in Figure 4.3, a picture of the test circuit is shown in Figure 4.4.

A current up to 10 kA is supplied by a thyristor converter rated for 16 kA and 1.5 kV, normally used for supplying the toroidal circuit of RFX, into the series connection of a resistor (R = 0.1 Ω), an inductance (L = 1.5 mH) and the Hybrid CB prototype. A discharge resistor of 75 mΩ, simulating the QPC dump resistor, provides the commutation path for the current after the Hybrid CB opening.

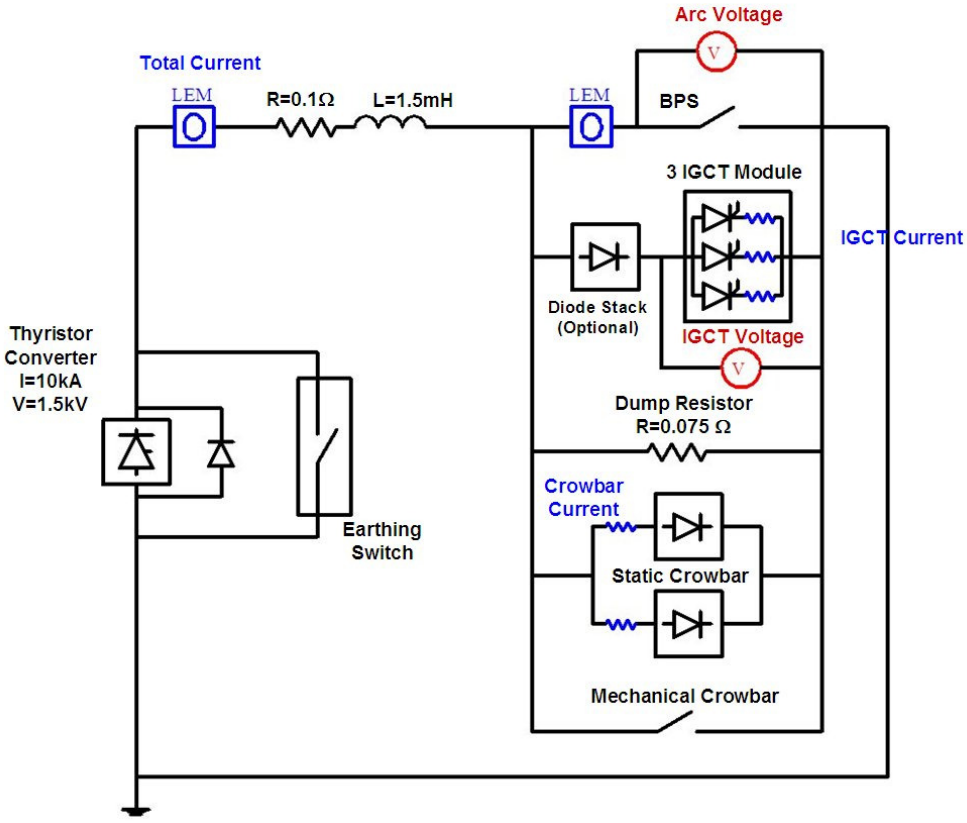

Figure 4.3 – *Electrical scheme of the test circuit set up at Consorzio RFX*

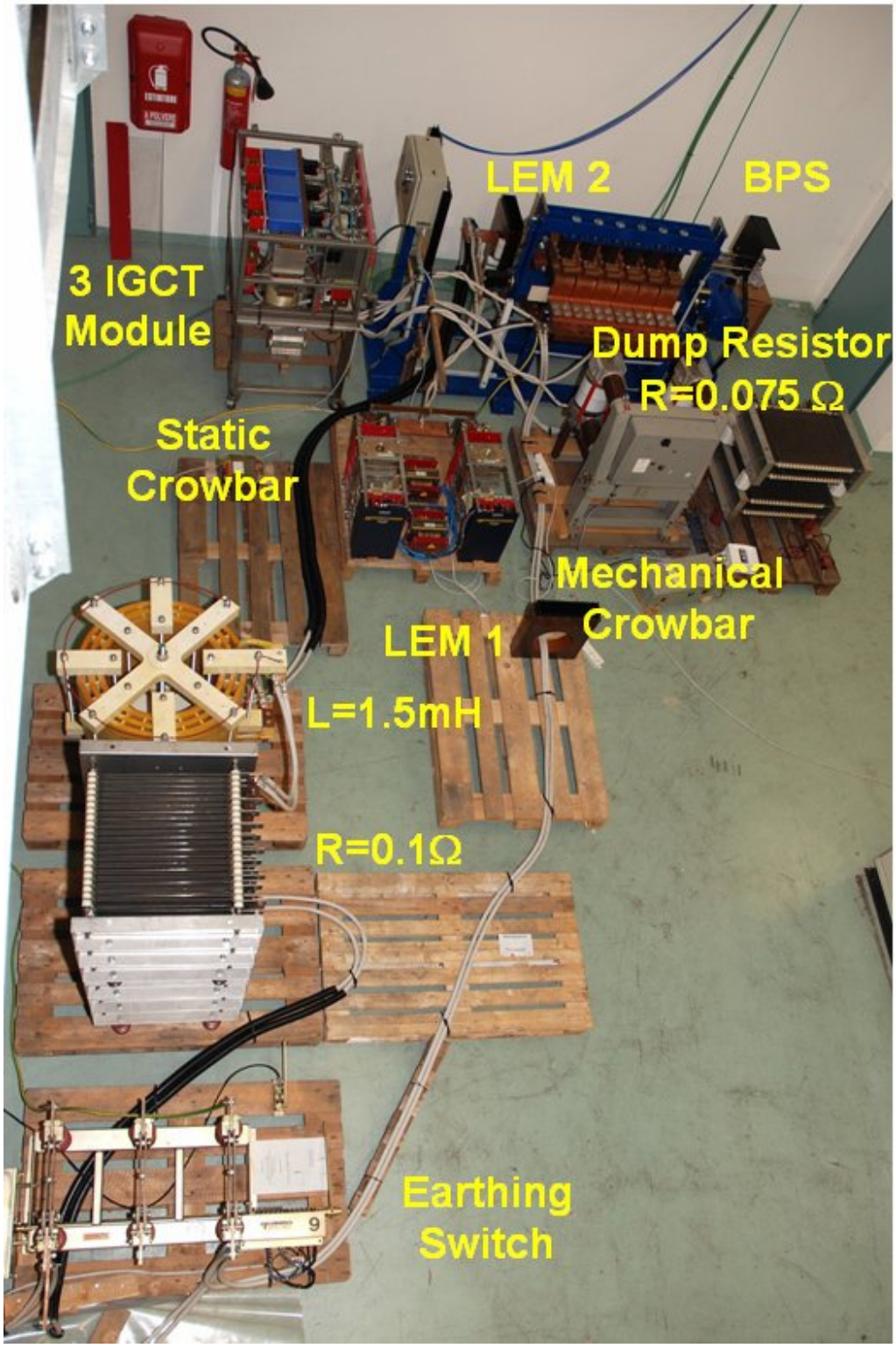

Figure 4.4 – *Picture of the test circuit set up at Consorzio RFX*

A making switch is connected in parallel to the Hybrid CB, in order to provide a low impedance path for the current in case of mis-operation of the Hybrid CB. This making switch is composed of a static crowbar connected in parallel to a mechanical switch. The static crowbar, consisting in two paralleled Gate Turn Off Thyristors (GTO) 211QS26923B, allows for a very rapid intervention of the making switch (in the order of micro seconds) but with limited I^2t capacity, while the mechanical switch has slow intervention time (in the order of 30 ms) but higher I^2t capacity.

4.4 The Control

The operation of all the test circuit devices is coordinated by a very fast control system that performs also fault detection and protection intervention.

This system has been implemented using a Field Programmable Gate Array (FPGA) control board that has been programmed so that it receives as inputs the status of the circuit power components and the current and voltage measurements acquired from the field and it generates in real-time the commands for performing the desired operation sequence.

The current and voltage measurements shown in Figure 4.1 and listed in Table 4.1 are at first normalized into 0-10 V signals, then converted in optical signals by means of opto-electronic interfaces that permit to insulate the control from the power part and finally sent to the control system where they are re-converted into 0-10 V signals that are monitored in real time during the pulse by the control system.

Table 4.1 – *Acquired Measurements*

Measure	Name	Range	Transducer
Total current	I TOT	0 - 10 kA	LEM
BPS current	I BPS	0 - 10 kA	LEM
IGCT current	I IGCT 1,2,3	0 - 4 kA	Resistive shunts
GTO current	I GTO 1,2	0 – 8 kA	Resistive shunts
Total Voltage	V TOT	0 – 1 kV	Voltage divider
BPS arc voltage	V BPS	0 – 50 V	Voltage divider with clamp
IGCT voltage	V IGCT 1,2,3	0 – 1 kV	Voltage divider
Converter current	I CONV	0 – 16 kA	Resistive shunt
Converter Voltage	V CON	0 – 1.5 kV	Voltage divider

In order to guarantee the safe operation of the test circuit it is necessary to monitor in real time that all the safety limits in terms of current, voltage and I^2t are not exceeded and that the status of the components is correct according to the operation sequence. Since the FPGA system used for performing control is very fast (the time

cycle is less than 20 ns) and it permits to monitor in real-time the components' status and the current and voltage measurements, it has used also for performing fault detection and protection intervention.

The list of the main detected faults is shown in Table 4.2. In case of fault the control system automatically performs a protective sequence consisting in turning-off the thyristor converter and closing the crowbar. This permits to by-pass the hybrid CB prototype so as to create a low impedance path for the current that avoid the onset of dangerous situations for the mechanical switch and the static module. Moreover the turn-off of the converter assures that the current flowing in the test circuit rapidly decreases to zero with the time constant of 15ms imposed by the series connected resistor and inductance.

Table 4.2 – *Main Alarms*

Alarm	Description
BPS status not ok	The BPS remains closed after opening command
IGCT status not ok	The IGCT status does not match the IGCT turn-on and turn-off commands
BPS current restrike	Some time after BPS opening command the current in BPS is not zero
Current commutation failure	Some time after IGCT turn-on the current is not completely commutated in IGCTs
Current for too long time in IGCTs	Some time after IGCT turn-off the current in IGCT is not zero
Max I^2t in IGCT	The I^2t in one IGCT is exceeding a set limit
Maximum current in IGCT	Current in one IGCT is exceeding a set limit
Maximum current	Total current is exceeding a set limit
Maximum voltage	Total voltage is exceeding a set limit

4.5 Operation sequence

Before the starting of the pulse sequence, the converter is off, the BPS is closed, the IGCTs are turned-off and the crowbar is open.

At the beginning the converter is turned-on and it starts to supply the predefined current. When the current reaches the desired value the BPS opening command and the IGCT turn-on command are generated. When the BPS is completely open and the current is transferred into the IGCTs the converter is turned off, the IGCT are turned off and the current starts to commutate in the paralleled resistor.

A simplified scheme of the operation sequence is shown in Figure 4.5. The sequence is managed on the basis of pre-settable times, so that it is possible to change the operation sequence before performing the pulse.

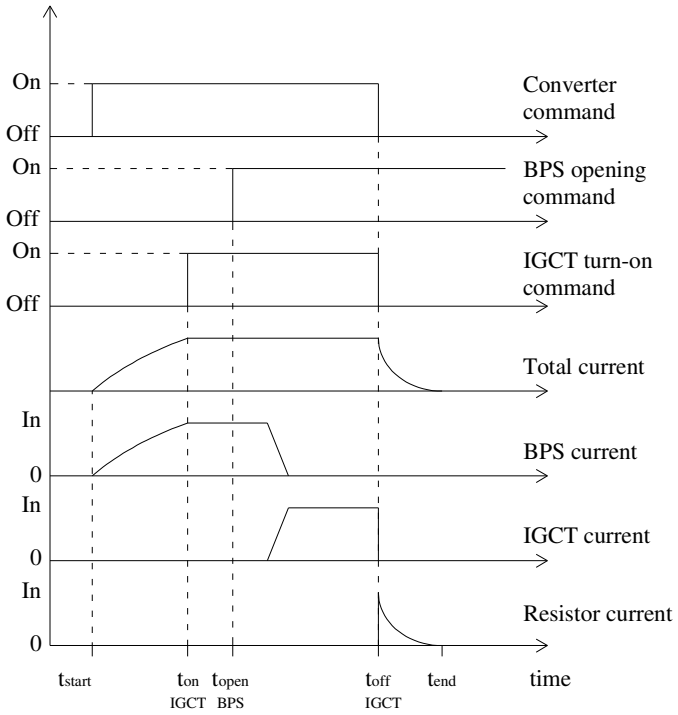

Times

t_{start}: Converter turn-on;

$t_{on\ IGCT}$: IGCT turn-on;

$t_{open\ BPS}$: BPS opening command;

$t_{off\ IGCT}$: IGCT turn-off and converter turn-off;

t_{end}: end of pulse

Figure 4.5 – *Normal operation sequence*

4.6 High current interruption tests

The prototype was used with a maximum current of 7 kA. The results obtained in case of commutation and interruption of a current of 7 kA are shown in Figure 4.6 and Figure 4.7.

The BPS and the IGCTs are commanded to open and to turn-on, respectively, at the same time t=50 ms. The contacts of BPS start to separate at t=280 ms and an arc is formed, whose voltage drives the current commutation from the BPS to the IGCTs.

The current commutation has a duration of 4 ms, a time that permits the arc voltage to reach the maximum value of 24 V. At time t=284 ms all the current is commutated into the IGCTs and the arc is extinguished: the voltage at the BPS terminals is the voltage drop across the IGCT module that is about 20 V. The IGCTs turn-on simultaneously without problems and the current sharing between them is very good, with a current unbalance lower than 3% of the total current. There is a difference of about 250 A between the IGCT current and the total current. This difference is the current flowing in the 75 mΩ resistor connected in parallel to the IGCTs, due to the IGCT module voltage drop.

When the BPS is completely open at t=400 ms the IGCTs are commanded to turn-off and the current is commutated into the discharge resistor with a reapplied voltage of 500 V. The dielectric insulation of the BPS contacts is guaranteed by the sufficient distance of 50 mm and no current re-strike appears across them.

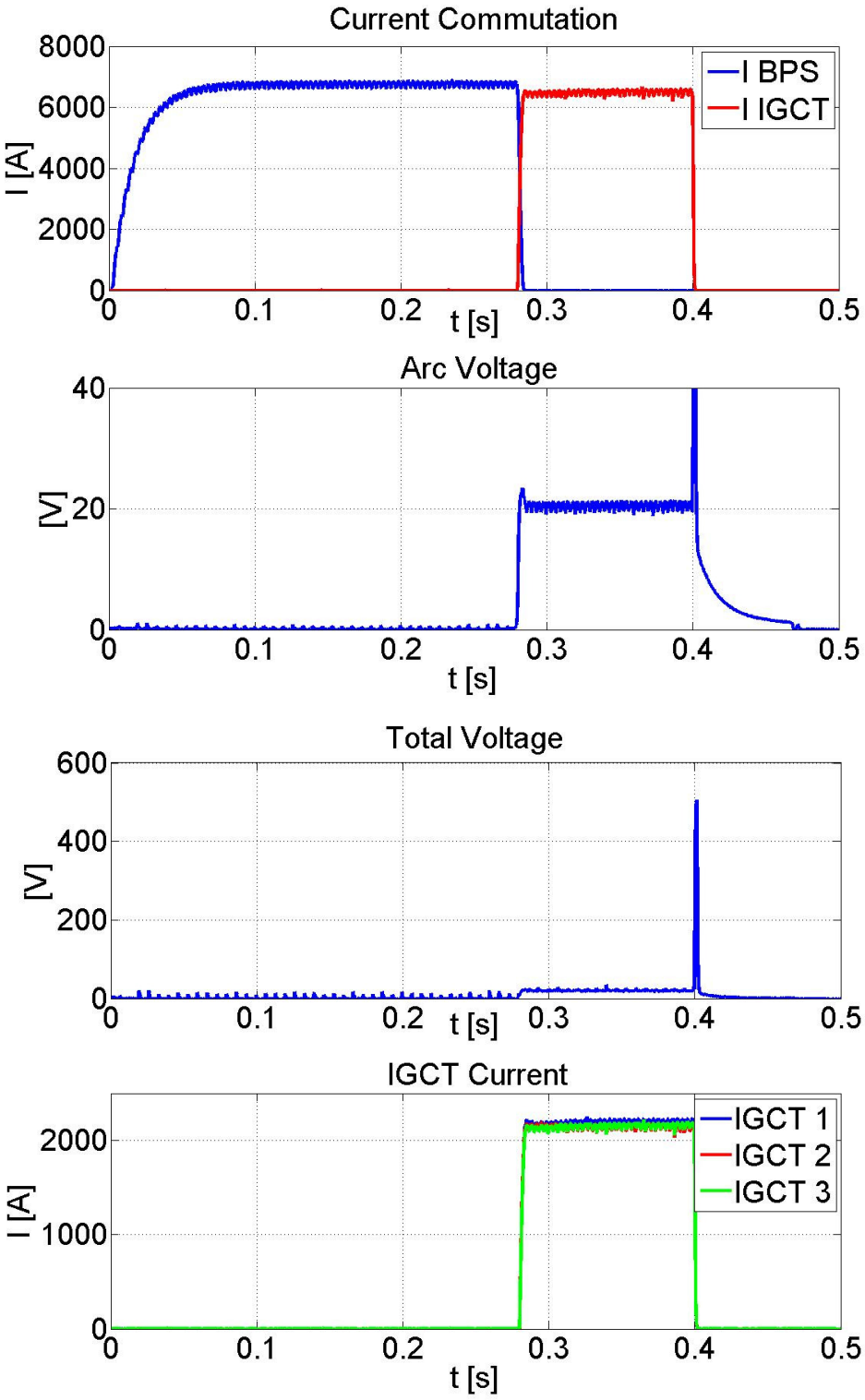

Figure 4.6 – *Results of commutation and interruption of 7 kA current*

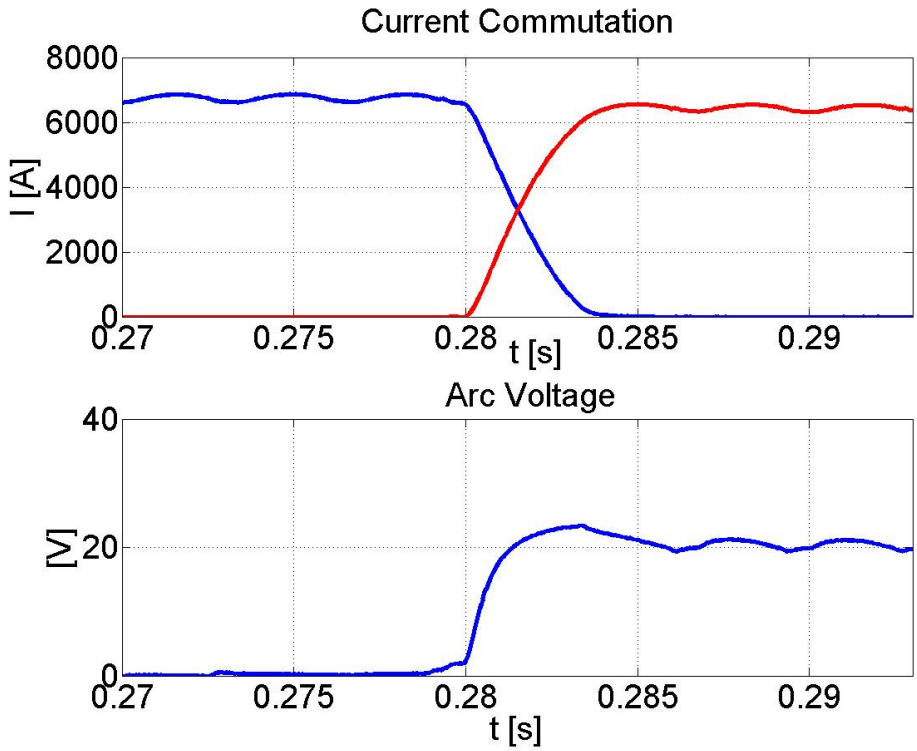

Figure 4.7 – *Zoom of 7 kA current commutation*

4.7 Arc voltage test

The voltage drop across the IGCT module is due to the IGCT impedance, the blocking diode impedance and the shunt resistor for current measurement. With a current in each branch of 2.3 kA the resulting voltage drop is about 20 V. With a higher current the voltage drop across each branch of the static module would be higher and there is the possibility that the arc voltage is not sufficient to completely commutate the current from the BPS to the IGCTs, causing a persistence of the arc. In this case it is not possible to interrupt the current, in fact when the IGCTs are turned off the current would be re-commutated in the BPS, preventing the current interruption. In order to investigate the arc voltage behavior during BPS opening without current commutation some pulses have been performed introducing an intentional delay in the IGCT turn-on command. In the pulse whose waveforms are shown in Figure 4.8, the BPS is commanded to open at t=50 ms, its contacts start moving at t=279 ms but the IGCTs are commanded to turn on only 16 ms after arc current creation at the BPS terminals, at t=295 ms.

During the first milliseconds, the arc voltage appearing when the BPS contacts start separating has the same waveform observed in the pulses where the IGCT are already turned-on at BPS opening and the current commutation is occurring, but in this case

the current commutation is not possible and the arc voltage keeps on increasing since the distance between BPS terminals is increasing. When the IGCT are finally turned on, the arc voltage has reached a value of about 35 V.

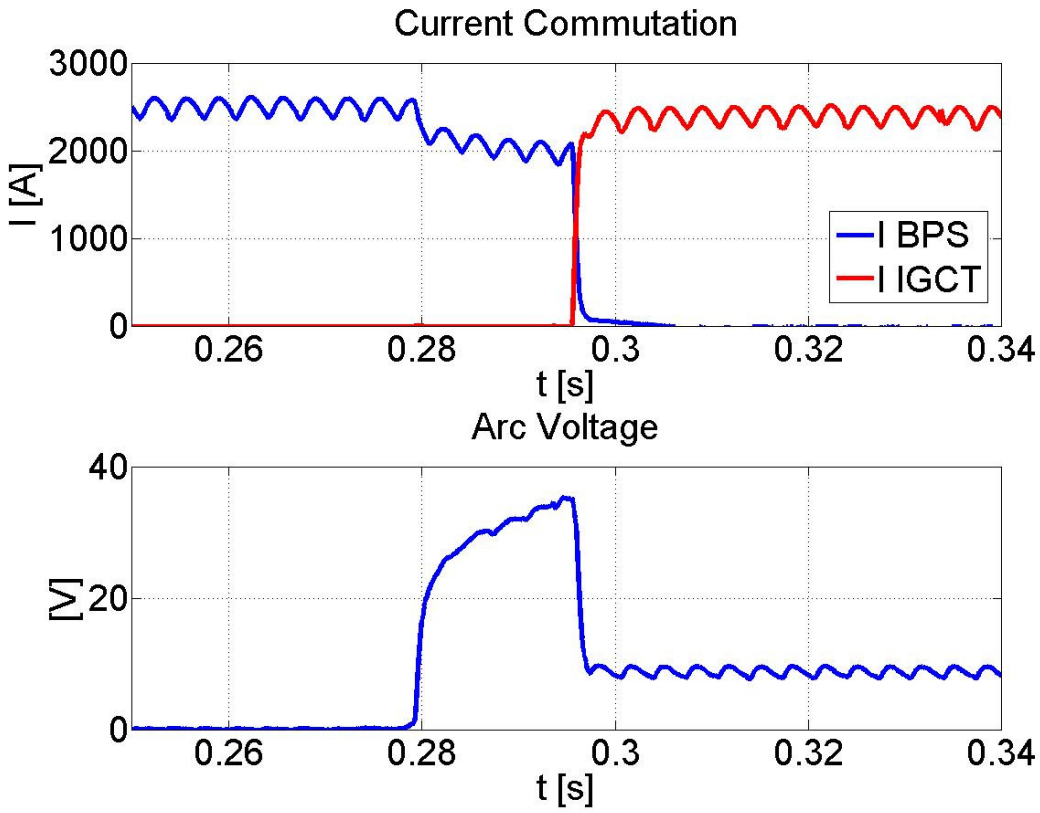

Figure 4.8 – *Results of current commutation with a 16 ms delayed IGCT turn-on*

The observed increase of arc voltage permits to assess the reliability of current commutation from the mechanical BPS to the static CB, that represented one of the most important aspect to be studied in deep detail.

In fact, as the current in the Static CB is increasing, also the voltage drop across it will increase and it is possible that the initial arc voltage is not sufficient to drive the complete current commutation. Fortunately, as the BPS contacts are separating, also the arc voltage increases, helping the current commutation process.

Of course it is not possible to have too high voltage drop across the static CB, otherwise the current commutation will last a long time, speeding up the BPS contact wearing, with the extreme case of failure of current commutation. For this reason not only the impedance of the Static CB, but also the stray inductances related to the connection with the BPS should be minimized.

4.8 Discussion of results

More than one hundred pulses have been performed with the Hybrid dc CB prototype, with current values up to 7 kA.

In all performed pulses a rapid and complete current commutation from the BPS to the static CB has been observed, followed by current interruption performed by static CB without BPS arc restrike. This result represents an experimental assessment about the reliability of the Hybrid CB proposed as solution for the CB of JT-60SA QPC.

In both pulses where the IGCT turn-on command was issued before BPS opening and after it, all the three IGCTs start conducting with a good current sharing also in dynamic condition. Therefore, from the point of view of optimizing the IGCT turn-on sequence, it is not possible to identify a preferable solution between issuing the IGCT turn-on command before or after BPS opening time. Conversely, from the point of view of minimizing the arc current duration across the BPS contacts and consequently reducing the contact wearing, it is better to turn-on the IGCTs before the arc formation. Since no current is observed in IGCTs before the effective BPS opening, it is possible to simplify as much as possible the operation sequence, issuing simultaneously the BPS opening command and the IGCT turn-on command.

4.9 Future work

The results obtained with the Hybrid CB prototype can be further enriched by new tests and studies that are going to be done in the next future.

The next planned current interruption tests will be performed with higher current values, up to the prototype nominal current of 10 kA.

Moreover, the insertion of an additional impedance between the BPS and the static CB will allow to more deeply study the arc voltage behaviour and the current commutation reliability, and the use of a fast camera will allow to correlate the arc voltage with the BPS contact moving.

Finally, experience with the use of the recently released IGCT 5SHY 42L6500 will be easily gained simply by replacing the IGCTs 5SHY 35L4512 presently installed in the static CB module with the new ones.

CHAPTER 5

5. Summary and Conclusions

5.1 JT-60SA

In the direction of the development of a magnetic confinement fusion reactor, it has been recognized that the ITER experiment is not enough to obtain all the needed information. For this reason the Broader Approach Agreement between Europe and Japan has been signed, including the building of the JT-60SA experiment, a ITER Satellite Tokamak.

JT-60SA is designed for performing long lasting plasma pulses, with a flat-top duration of 100 seconds. For limiting the power dissipation, JT-60SA will be equipped with toroidal and poloidal superconductors. In order to avoid damaging the magnets in case of loss of superconducting characteristics (quench), a protection system able to rapidly remove the magnetic energy stored in the coils is inserted in the circuit of each superconductor, named Quench Protection Circuit (QPC).

The magnet protection in case of quench is obtained inserting a dump resistor in the magnet circuit, able to dissipate the magnetic energy reducing to zero the magnet current.

The Italian National Research Council (CNR), acting through Consorzio RFX, is in charge of providing the QPCs for all the superconducting magnets of JT-60SA.

5.2 Analyses

In order to define the design specifications of the QPC, it has been necessary to take into consideration not only the nominal current value of each coil, but also to identify the maximum current value that can flow in the magnets in different conditions.

In fact, there is the possibility that in case of fault or anomalous condition an overcurrent could appear in the superconducting magnets. It is therefore necessary to

design the QPC so that they are able not only to carry that current exceeding the nominal values, but also to interrupt it and to commutate it in the dump resistor. In particular the anomalous conditions considered are the plasma disruption and the QPC intervention.

For the toroidal magnets no particular overcurrent is expected in such conditions, since they are all connected in series and they have no significative coupling with other circuits.

Different is the condition of poloidal magnets. In fact they are connected in separate circuits and they have a significative mutual coupling between them and with other poloidal conducting elements such as HC in-vessel coils, stabilizing plates, vacuum vessel and plasma itself.

For identifying the maximum coil current values I developed an axial-symmetric model of all poloidal coupled elements that permitted to simulate in detail the event of plasma disruption and QPC intervention.

5.2.1 Plasma disruption

In particular I analyzed the effect of different aspects of the plasma disruption phenomenology like plasma position and movement, current distribution and derivative, finding out that the shielding effect of stabilizing plates and vacuum vessel plays an important role and so these plasma figures determine only the coil current waveform but they do not have influence on the final poloidal coil overcurrent, that depends only on the initial plasma current value.

In all the plasma disruption cases I analyzed, the current waveform during transient phase does not reach values higher than the final value, assuring that the sizing of QPC can be evaluated considering only the final overcurrent value.

Summing the possible initial coil current values to the maximum overcurrent value for each superconducting coil in case of plasma disruption, I obtained the maximum current that can flow in the poloidal QPCs. In particular it results that in case of plasma disruption the maximum current value in poloidal magnets exceeds only of 500 A the nominal current of 20 kA.

5.2.2 QPC operation

In case of operation of a single poloidal QPC, it is possible that induced overcurrents appear in other poloidal circuits. I simulated this condition with the developed model and it results that a current of -23.9 kA could appear on Central Solenoid (CS) coils, largely exceeding the nominal value of 20 kA. For this reason it has been modified the QPC intervention strategy, requiring the simultaneous intervention of all poloidal QPCs.

A similar event can occur in case of failure of one QPC, requiring the intervention of the pyrobreaker backup protection: in the time between the failure detection and the backup protection intervention, the current in the circuit of the faulty QPC can significantly increase due to the mutual coupling with other circuits where the current

is decreasing. I simulated also this case with the developed model, finding out that a maximum current of 24 kA could appear in CS coils. For reducing such values under the tolerable value of 22.5 kA it has been decided to tighten the QPC specifications, reducing the maximum delay between failure detection and backup protection intervention from 1 s to 0.5 s.

5.3 QPC Conceptual Design

Having defined the detailed specifications of the QPC, it has been possible to develop its conceptual design, with particular attention to the design of the dc Circuit Breaker.

After having considered a number of possible solutions, some of those already implemented for quench protection in other superconductive devices, a hybrid mechanical-static solution has been considered for the dc circuit breaker of JT-60SA QPC. This is an innovative design, based on the parallel connection of a mechanical by-pass switch (BPS) and a static circuit breaker (CB) based on Integrated Gate Commutated Thyristor (IGCT) devices.

This solution brings together the advantages of both integrated technologies: the low power dissipation of mechanical BPS and the fast arc-less current interruption of static CB, resulting in a simple and reliable circuit breaker, requiring a reduced maintenance level and low operation cost.

I performed a detailed sizing of the number of required static components taking into consideration two types of IGCTs.

The conceptual design has been performed also for the other QPC components:

- For the pyrobreaker I analyzed two possible solutions: one based on the parallel connection of some devices commercially available and one based on a prototype device realized for the QPC of ITER.
- For the dump resistors I performed a tentative sizing, taking into consideration the nominal energy value for the toroidal QPCs, while for poloidal QPCs, due to the mutual coupling among poloidal circuits, I considered an intermediate energy value between the nominal and the maximum ones.

5.4 Hybrid dc CB prototype

The mechanical - static hybrid solution proposed for the dc circuit is innovative since it was never employed for high current value circuit breakers. In order to gain experience on the current commutation from the mechanical BPS to the Static CB and to test the reliability of such technical solution, possibly learning how to improve it, I developed and tested at Consorzio RFX a prototype of the hybrid mechanical-static dc circuit breaker.

I performed more than one hundred pulses with the Hybrid dc CB prototype, with current values up to 7kA.

In all performed pulses a rapid and complete current commutation from the BPS to the static CB has been observed, followed by current interruption performed by static CB without BPS arc restrike. In order to study the phenomenology of the arc voltage appearing at BPS opening, in some pulses I intentionally delayed the static CB turn-on, and it has been observed that the arc voltage value increases as the distance between BPS contacts increases.

These results represent an experimental assessment about the reliability of the Hybrid CB proposed as solution for the CB of JT-60SA QPC.

Other tests are planned to be performed with the Hybrid CB prototype in the next future, in order to better characterize the current commutation up to the prototype nominal value of 10 kA.

5.5 Conclusions

The design of the JT-60SA QPCs has been a complex and articulated task that I carried out inside the JT-60SA Project Team. It required the fulfillment of detailed analyses on the complete system of magnet circuits, that I performed by means of a complete model of the poloidal circuits of JT-60SA. Based on this model, the analyses of plasma disruption and QPC intervention allowed me to identify the peak currents in the poloidal coils, necessary for the design of the circuit components. Besides the present results, the model represents a useful tool for further studies and analyses of different operating conditions.

The main issues of the QPC, connected to the necessity of designing a system able to carry high dc current values with reduced power losses and to reliably interrupt it with reapplied voltage of some kilo-volts, have been solved with the hybrid mechanical static solution, that I deeply studied and sized and whose feasibility I proved by means of experimental tests.

Finally I developed and successfully tested a 10 kA prototype of the hybrid dc circuit breaker, whose experimental results with current values up to 7 kA proved the reliability of this hybrid solution.

The technical specifications for the JT-60SA QPCs based on the hybrid dc circuit breaker have been successfully submitted to the JT-60SA Project Team in November 2009, and the QPC Procurement Arrangement has been ratified by the Broader Approach Steering Committee in December 2009.

After the tender, the QPC Contract is expected to be assigned to industry in June 2010, and the QPC delivery in Japan is planned in 2014.

References

[1] “Energy, Powering Your World”, EFDA general booklet on energy, 60 pages, 2002

[2] http://www.jet.efda.org/

[3] http://www-fusion-magnetique.cea.fr/

[4] http://www-jt60.naka.jaea.go.jp/english/index-e.html

[5] http://www.iter.org

[6] S. Konishi, S. Nishio, K. Tobita, “DEMO plant design beyond ITER”, Fusion Engineering and Design, 63-64 (2002), pp. 11-17

[7] D. Maisonnier, “European DEMO design and maintenance strategy”, Fusion Engineering and Design, 83 (2008), pp. 858-864

[8] D. Maisonnier, I. Cook, P. Sardain, R. Andreani, L. Di Pace, R. Forrest et al., Final Report of the European Power Plant Conceptual Study, 2005, EFDA-RP-RE-50, available online http://www.efdfa.org.

[9] D. Maisonnier, D. Campbell, I. Cook, L. Di Pace, L. Giancarli, J. Hayward, et al., Power Plant Conceptual Studies in Europe, Nucl. Fusion 47 (2007) 1524–1532.

[10] The "King Report" - Conclusions of the Fusion Fast Track Experts Meeting held on 27 November 2001, chaired by Prof. Sir David King.

[11] “Agreement between the European Atomic Energy Community and the Government of Japan for the Joint Implementation of the Broader Approach Activities in the Field of Fusion Energy Research”, Official Journal of the European Union, 21.9.2007, L 246/34

[12] M. Matsukawa et al., “Status of JT-60SA tokamak under the EU-JA Broader Approach Agreement”, Fusion Engineering and Design, 83 (2008), pp. 795-803

[13] K. Tsuchiya, K. Kizu, T. Ando et al., “Design of the superconducting coil system in JT-60SA”, Fusion Engineering and design, 82 (2007), pp. 1519-1525

[14] L. Novello, E. Gaio, R. Piovan, M. Takechi, S. Ide, M. Matsukawa, "Overcurrents in JT-60SA Poloidal Circuits due to Plasma Disruption and Quench Protection Circuit Intervention", submitted to Fusion Engineering and Design, January 2010

[15] E. Durand, "Magnetostatique", Masson & Cie Editeurs, 1968

[16] Vector Fields: Software for Electromagnetic Design, "TOSCA", Cobham Group Company, 2005, http://www.vectorfields.com

[17] R.R. Khayrutdinov, V.E. Lukash, "Studies of Plasma Equilibrium and Transport in a Tokamak Fusion Device with the Inverse-Variable Technique", J. Comp. Phys. 109 (1993), pp. 193-201.

[18] Comsol Multiphysics: http://www.comsol.com

[19] E. Gaio, L. Novello, R. Piovan: "Conceptual design of the Quench Protection Circuits for the JT-60SA Superconducting Magnets", Fusion Engineering and Design, Volume 84, Issues 2-6, June 2009, Pages 804-809

[20] T. Bonicelli, A. De Lorenzi, D.Hrabal, R. Piovan, E. Sachs, E. Salpietro, and S.R. Shaw, "The European development of a full scale switching unit for the ITER switching and discharging networks", Fus. Eng. and Des. Special Issue, 75, 193, (2005)

[21] T. Rummel, O. Gaupp, G. Lochner, and J.Sapper, "Quench protection for the superconducting magnet system of WENDELSTEIN 7-X", Ieee Transactions On Applied Superconductivity, Vol. 12, No. 1, March 2002

[22] H. Chikaraishi, S. Tanahashi, S. Yamada, J. Yamamoto, 0. Motojima, et al., "Quench protection system using a novel d.c. circuit breaker for LHD", Fusion Engineering and Design 41 (1998) 259-264

[23] L. Xu, X. Liu, J. Jiang, Y. Liao, "The design of quench protection of EAST toroidal field power supply system", Fusion Engineering and Design 81 (2006) 2549–2554

[24] I. Song, C. Choi, and M. Cho, "Quench Protection System for the Superconducting Coil of the KSTAR Tokamak", IEEE Transactions on Applied Superconductivity, Vol. 17, No. 1, March 2007

[25] J. H. Schultz, E. Chaniotakis, R. D. Pillsbury Jr., P. W. Wang, J. Citrolo, C. Neumeyer, M. Caplin, W. V. Hassenzahl, "Superconducting magnet Protection System for the Tokamak Physics Experiment", IEEE Transactions on Magnetics, vol. 30, No. 4, July 1994

[26] ABB IGCT 5SHY-35L4512 Datasheet. Available on-line: http://www.abb.com

[27] ABB IGCT 5SHY-42L6500 Datasheet. Available on-line: http://www.abb.com

[28] B. Oedegard, T. Stiasny, E. Carrol, and M. Rossinelli, "An application specific asymmetric IGCT", Proceed. of PCIM 2001 Conference, Chicago, USA

[29] V. Toigo, L. Zanotto, E. Gaio et al., "Components and System Tests on the RFX Toroidal Power Supply", Fusion Engineering and Design, vol.75-79, pp. 55-59, November 2005

[30] J.-M. Meyer, A. Rufer, "A DC hybrid circuit breaker with ultra-fast contact opening and integrated gate-commutated thyristors (IGCTs)", IEEE Transactions on Power Delivery, vol.21, no.2, pp. 646-651, April 2006

[31] A. Weber, T. Dalibor, P. Kern, B. Oedegard, J. Waldmeyer and E: Carroll, "Reverse blocking IGCTs for Current Source Inverters" Proceed. of PCIM 2000 Conference, Nurenberg, DE

[32] N. Mohan, T.M. Undeland, and W.P. Robbins, Power Electronics, 2nd ed., John Wiley & Sons Inc, USA, 1989, pp. 730-743

[33] P. L. Mondino, T. Bonicelli, V. Kuchinskiy, A. Roshal, "ITER R&D: Auxiliary Systems: Coil power Supply Components", Fusion Engineering and Design, vol. 55, no. 2, pp. 325-330, July 2001

[34] R. Piovan, E. Gaio, and L. Novello, "Performance Analysis of a Hybrid IGCTs-Mechanical Dc Circuit Breaker for Quench Protection of Superconducting Magnets", in IEEE 22nd Symposium on Fusion Engineering,. 17-21 June 2007

[35] ABB Is-Limiter, Datasheet, Available on-line: http://www.abb.com

[36] http://www.ipr.res.in/sst1/SST-1.html